DEUTSCHES ELEKTRONEN-SYNCHROTRON DESY

HIGH ENERGY e^+e^- INTERACTIONS

by

G. Wolf

NOTKESTRASSE 85 · 2 HAMBURG 52

To be sure that your preprints are promptly included in the HIGH ENERGY PHYSICS INDEX , send them to the following address (if possible by air mail) :

DESY
Bibliothek
Notkestrasse 85
2 Hamburg 52
Germany

DESY 81-086
December 1981

High Energy e^+e^- Interactions*

G. Wolf

Deutsches Elektronen-Synchrotron, DESY, Hamburg

Content

* Lectures given at the 1981 Cargèse Summer Institute on Fundamental Interactions and at the 1981 International School of Elementary Particle Physics, Kupari-Dubrovnik.

1. Introduction

Electron-positron annihilation is a fascinating part of particle physics. Unlike in hadronic collisions the final states produced in e^+e^- annihilation possess well defined quantum numbers - those of the mediating current. Furthermore, at high energies, the current couples directly to the fundamental constituents of matter. In fact, all reactions observed in the nonresonant region follow from the same underlying process, pair creation of pointlike charged spin-1/2 fermions (either charged leptons or quarks). For production by the electromagnetic current - which is by far the dominant contributor at present energies - the cross sections for these processes can be calculated. As a result, e^+e^- annihilation is ideally suited to search for new charged leptons, new quarks or any other type of particle that is charged and pointlike. It is also a good place to search for new currents. If they couple to e^+e^- they lead to a breakdown of QED. First evidence for the presence of the weak neutral current has been seen just recently at PETRA. The angular distribution for muon pair production when combining the data from all PETRA experiments shows a distinct forward-backward asymmetry.

High energy e^+e^- annihilation has also become a testing ground for theories of strong interactions. The acceleration of quarks in $q\bar{q}$ formation, $e^+e^- \to q\bar{q}$, becomes so large that quarks have a fair chance to radiate energetic noncollinear field quanta that can be detected. The three-jet events observed at PETRA have given strong support to QCD where such events follow from bremsstrahlung of gluons. The rate of three-jet production provides a direct measurement of the strong coupling strength α_s.

Electron-positron interactions offer also the opportunity to study photon photon scattering. Experiments have just started to explore this field and many of the data obtained are still very preliminary. Nevertheless, the indications are that a wealth of new physics is waiting for discovery.

These lectures concentrate on electron-positron interaction data obtained above the upsilon family, $W \gtrsim 12$ GeV. They also include material presented only after the school at the Bonn Conference. No attempt is made to cover all experimental data, rather some topics are selected which appear to be of particular interest. More information on e^+e^- interactions at high energies can be found in recent review articles (see e.g. Wiik & Wolf 1979, Wolf 1980, Renard 1981), and in rapporteur reports from the Lisbon and Bonn conferences (Berger 1981, Duinker 1981, Holder 1981, Marshall 1981, Branson 1981, Braunschweig 1981, Bürger 1981, Felst 1981, Fournier 1981, Hollebeek 1981, Litke 1981, Wedemeyer 1981).

2. PETRA and PEP

2.1 PETRA

Most of the experimental data available at present were obtained at the DESY storage ring PETRA (Fig. 1) which was commissioned in autumn 1978. PETRA has four short and four long straight sections with a total circumference of 2.3 km. Two of the long straight sections are used for the accelerating structures. The maximum total c.m. energy W attained is 36.8 GeV. It is planned to increase in 1982 the maximum energy to 41 GeV by doubling the RF-power and to 46 GeV in 1983 by doubling the number of cavities. The maximum luminosity at W = 30 GeV in 1979 and 1980 was around $5 \cdot 10^{30} cm^{-2} s^{-1}$ which lead to an integrated luminosity of 100 - 150 nb^{-1} per day. At the end of 1980, by installing additional quadrupoles in the interaction region (minibeta scheme), the luminosity was increased by a factor of three to $1.7 \cdot 10^{31} cm^{-2} s^{-1}$ and 400 - 600 nb^{-1}/day. This gives roughly 100 hadronic annihilation events per day and experiment.

Five large detectors were constructed and took data, CELLO, JADE, MARK J, PLUTO and TASSO. CELLO and PLUTO share the same interaction pit in a push-pull fashion. PLUTO was taking data in 1979, CELLO in 1980 and in the first half of 1981. All detectors have almost complete solid angle coverage for charged particles and photons, and, except for MARK J, use a solenoidal magnet filled with cylindrical drift and proportional chambers for charged particle tracking. The MARK J detector is a calorimeter.

2.2 PEP

The SLAC storage ring PEP (see Fig. 2) has been put into operation in the summer of 1980. It has a total circumference of 2.2 km and a maximum design c.m. energy of W = 36 GeV. There are six interaction regions and seven approved experiments: MARKII, MAC, Free Quark Search, Monopole Search, DELCO, HRS and TPC. First preliminary results from the first four experiments were reported at the Bonn Conference (Hollebeek 1981, Litke 1981).

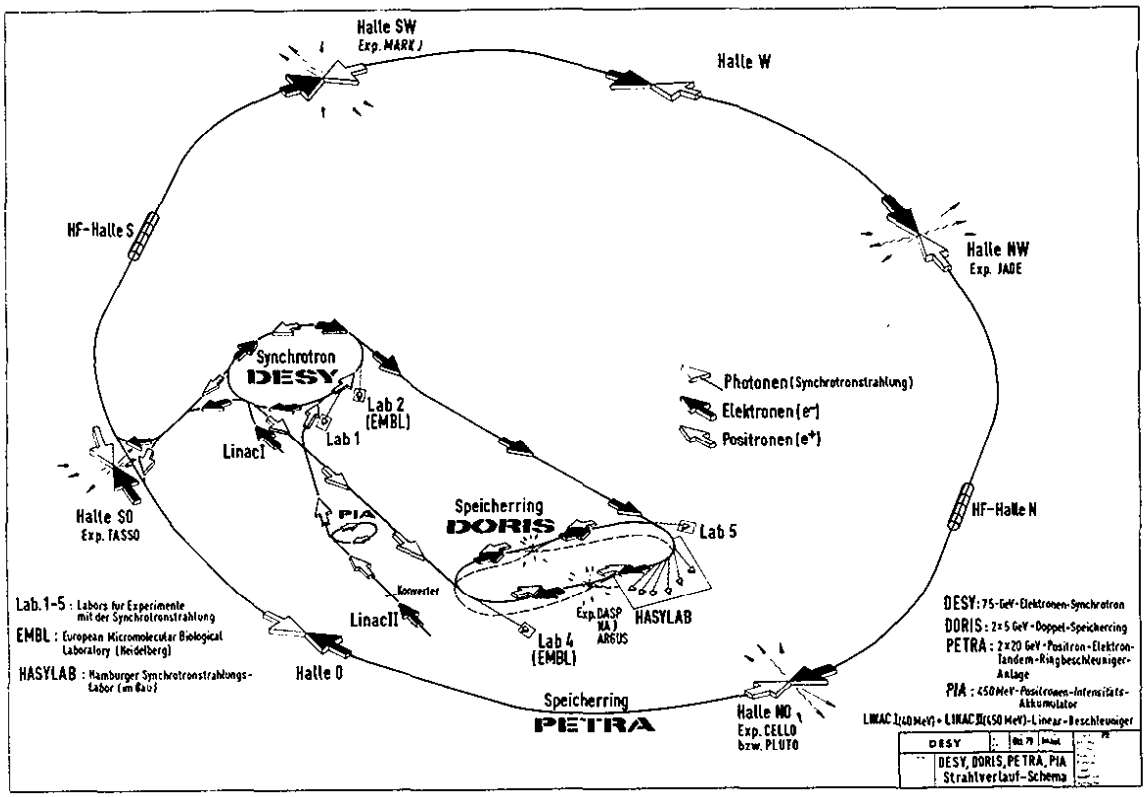

Fig. 1 Layout of the DESY accelerator complex

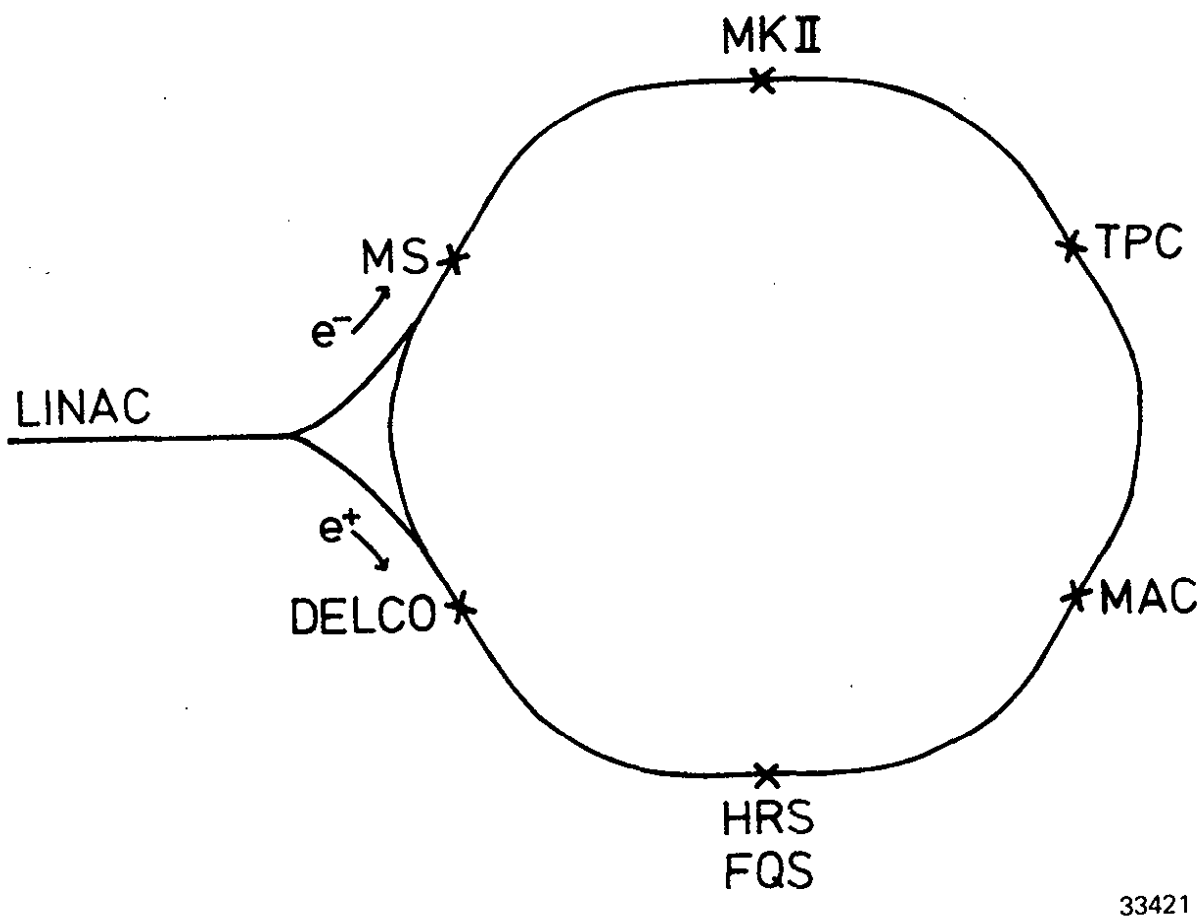

Fig. 2 The SLAC storage ring PEP

3. The structure of leptons

Muon pair production,

$$e^+e^- \to \mu^+\mu^- \tag{1}$$

is the simplest of all QED reactions and the prototype of almost all e^+e^- annihilation processes at high energies. It proceeds via time-like photon exchange (Fig. 3):

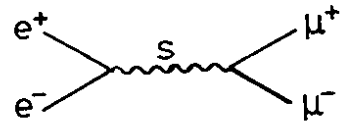

Fig. 3 Muon pair production

The differential cross section reads

$$\frac{d\sigma}{d\Omega} = \frac{\alpha^2}{4s}\,\beta_\mu \left\{(1 + \cos^2\Theta) + (1 - \beta_\mu^2)\,\sin^2\Theta\right\} \tag{2}$$

where $s = W^2$, $\beta_\mu = p_\mu/E_\mu$. For $p_\mu \approx E_\mu$

$$\frac{d\sigma}{d\Omega} = \frac{\alpha^2}{4s}\,(1 + \cos^2\Theta)$$

The integrated cross section is given by

$$\sigma_{\mu\mu} = \frac{4\pi}{3}\,\frac{\alpha^2}{s} = \frac{87.6\ \text{nb}}{s} \qquad (s \text{ in } \text{GeV}^2) \tag{3}$$

At W = 30 GeV the muon pair cross section is of the order of 0.1 nb. An integrated luminosity of 500 nb^{-1}/day will yield a maximum detectable event rate of 50 per day.

If electron or muon are extended objects a deviation from the QED prediction will be observed. This deviation can only depend on the mass squared s of the virtual photon and can be parametrized by a cut-off parameter Λ,

$$\sigma = \sigma_{QED}\,\left(1 \mp \frac{s}{s - \Lambda_\pm^2}\right)^2 \tag{4}$$

Clearly, the higher the energy, the deeper one can probe for a structure of electron and muon. The parametrization (4) includes also corrections to the photon propagator or the exchange of heavy photon-like objects.

Other second order QED processes which were studied to test QED are:

Bhabha scattering (Fig. 4a,b): $e^+e^- \to e^+e^-$

Two photon annihilation (Fig. 4c,d): $e^+e^- \to \gamma\gamma$

τ-pair production: $e^+e^- \to \tau^+\tau^-$

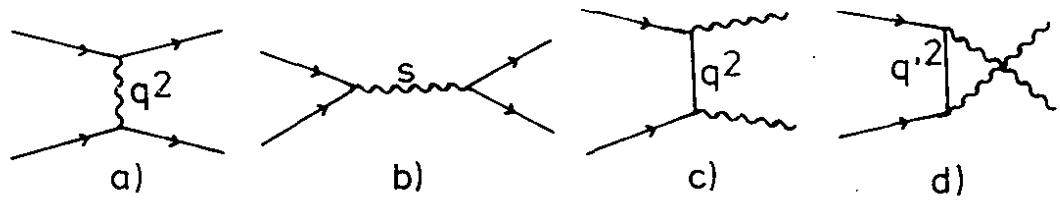

Fig. 4 The space like (a) and time-like (b) diagrams for Bhabha scattering and the diagrams for two-photon annihilation (c,d)

Besides the electron structure, Bhabha scattering tests the photon propagator in the space-like and time-like region. Two-photon annihilation is sensitive to contributions from a seagull term (Fig. 5a) and from excited electrons (Fig. 5b). All four processes have the same s-dependence, $d\sigma/d\Omega \sim s^{-1}$. Fig. 5 summarizes their differential cross sections as predicted by QED.

Fig. 5 Seagull term (a) and excited electron exchange (b) for $e^+e^- \to \gamma\gamma$

For a recent review see Dittmann & Hepp (1981).

The experimental data have to be radiatively corrected before a comparison with QED can be made:

$$\frac{d\sigma}{d\Omega}^{corr} = \frac{d\sigma}{d\Omega}^{meas} (1 - \delta) \qquad (5)$$

The corrections account for photon emission, for electromagnetic modifications of the vertices and for vacuum polarization due to leptons and hadrons (see e.g. Berends and Kleiss 1981).

Possible contributions from weak neutral currents will be discussed in the next chapter.

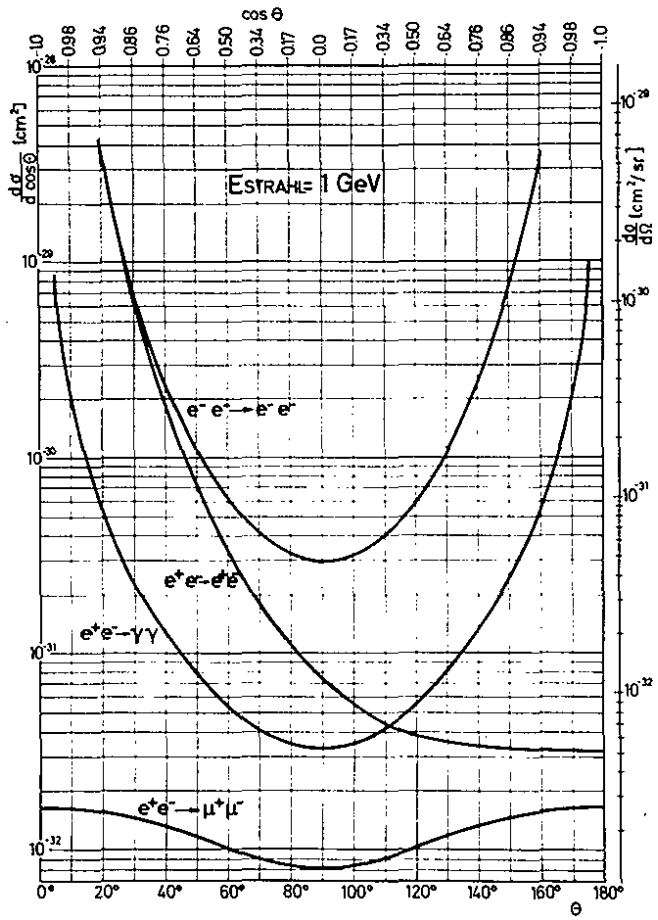

Fig. 6 Differential cross sections for $e^-e^- \to e^-e^-$, $e^+e^- \to e^+e^-$, $e^+e^- \to \gamma\gamma$ and $e^+e^- \to \mu^+\mu^-$ for a beam energy of 1 GeV.

Fig. 7 displays the total cross section data on μ pair production. They are seen to agree rather well with the QED prediction (solid line). Agreement with QED is also observed for Bhabha scattering (Fig. 8), for two-photon annihilation (Fig. 9) and for τ pair production (Fig. 10a).

Table I summarizes the 95 % confidence lower limits on the cut-off parameter Λ. The lower limits on Λ are found to be in the range from 100 to 200 GeV. Bearing in mind that we made the implicit assumption that whatever modifies the photon propagator or the lepton-lepton photon vertex has the coupling strength e the results of table 1 can be rephrased by saying that QED has been tested down to distances of $1 - 2 \cdot 10^{-16}$ cm and/or that e,μ and τ are pointlike down to this distance.

Table 1. QED cut-off parameters: 95 % confidence lower limits in GeV. From Branson (1981) and Hollebeek (1981)

Experiment	$e^+e^- \to e^+e^-$		$\mu^+\mu^-$		$\tau^+\tau^-$		$\gamma\gamma$	
	Λ_+	Λ_-	Λ_+	Λ_-	Λ_+	Λ_-	Λ_+	Λ_-
CELLO	83	155			139	120	43	48
JADE	112	106	142	126	111	93	47	44
MARK J	128	161	194	153	126	116	55	38
PLUTO	80	234	107	101	79	63	46	-
TASSO	140	296	127	136	104	189	34	42
MARKII							50	41

The study of τ pair production provided first measurements on the τ lifetime. Fig. 10b shows a typical $\tau^+\tau^-$ event with one τ decaying into a μ and the other one into three charged particles. Using the latter tracks one can triangulate the decay vertex and obtain the τ lifetime T from the distance between beam position and decay vertex. The expected flight path at W = 30 GeV is typically 700 μ. The TASSO group (Brandelik et al. 1980a and Woodworth 1981) found

$$\langle T_\tau \rangle = -0.25 \pm 3.5 \cdot 10^{-13} \text{ sec}$$

and a 95 % C.L. upper limit of $5.7 \cdot 10^{-13}$ sec. A more precise value was obtained by the MARKII group (Hollebeek 1981). Fig.10c shows their τ decay length distribution. There is an excess of τ's with positive decay lengths. From this distribution a τ lifetime of

$$\langle T_\tau \rangle = 4.9 \pm 1.8 \cdot 10^{-13} \text{ sec}$$

is deduced. Based on the assumption that the $\tau - \nu_\tau$ coupling to the weak

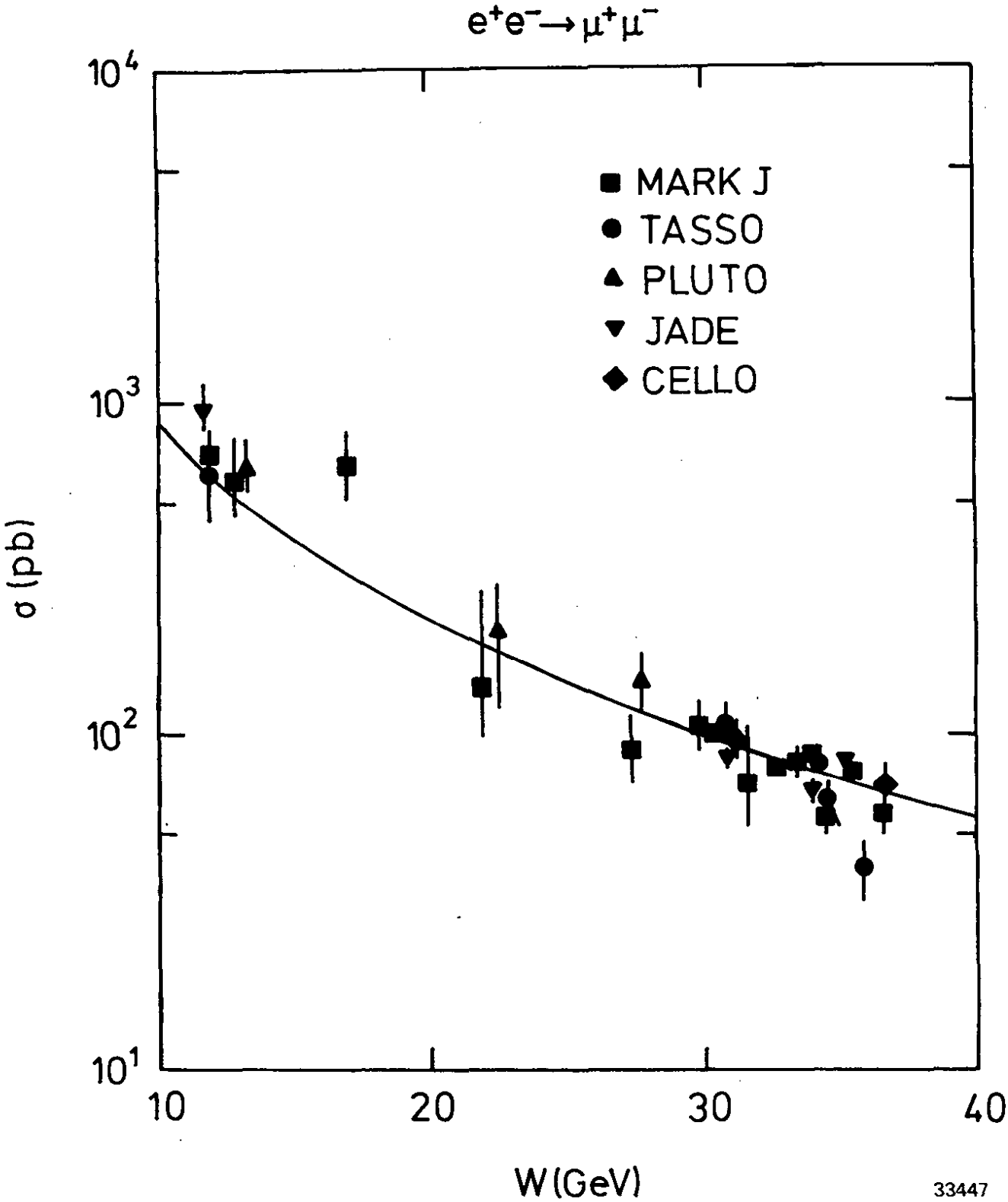

Fig. 7 The total cross section for $e^+e^- \rightarrow \mu^+\mu^-$. The solid curve shows the QED prediction $\sigma_{\mu\mu} = \frac{4\pi\alpha^2}{3s}$. From Branson (1981).

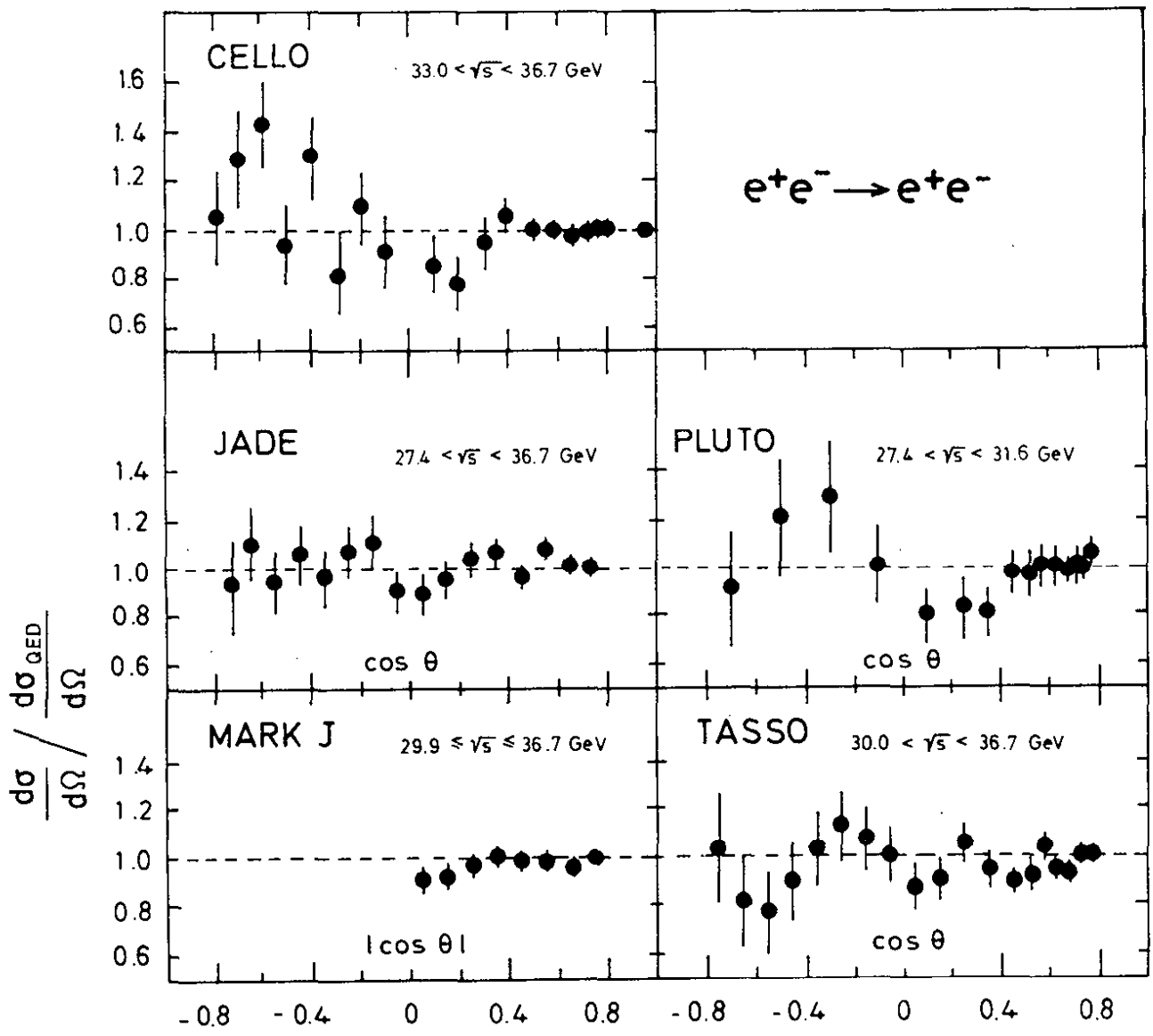

Fig. 8 Differential cross section for the reaction $e^+e^- \to e^+e^-$ divided by the QED prediction. The data are corrected for radiative effects and hadronic vacuum polarization. From Dittmann & Hepp (1981).

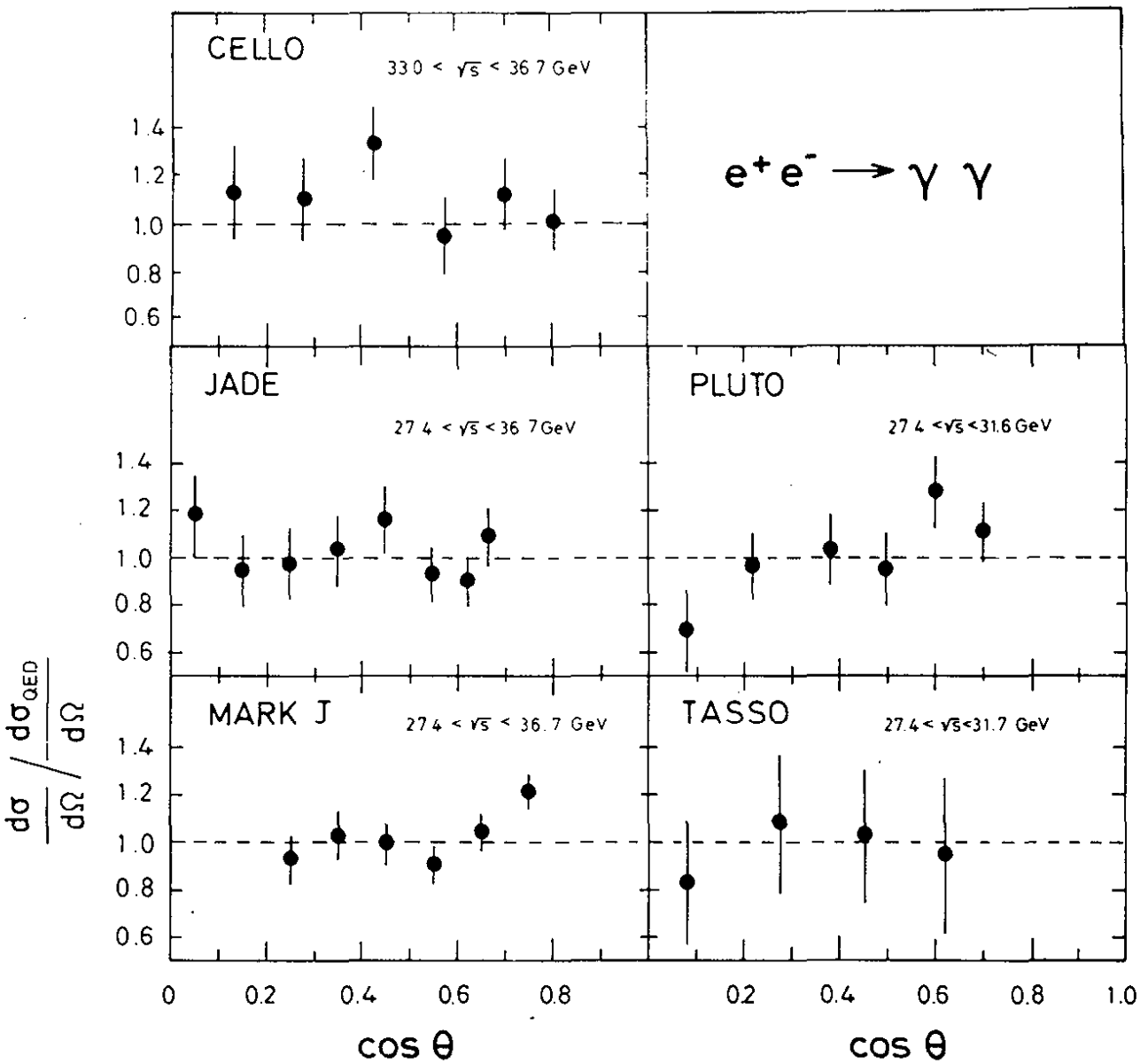

Fig. 9 Differential cross section for the reaction $e^+e^- \to \gamma\gamma$ divided by the QED prediction. The data are corrected for radiative effects. From Dittmann & Hepp (1981).

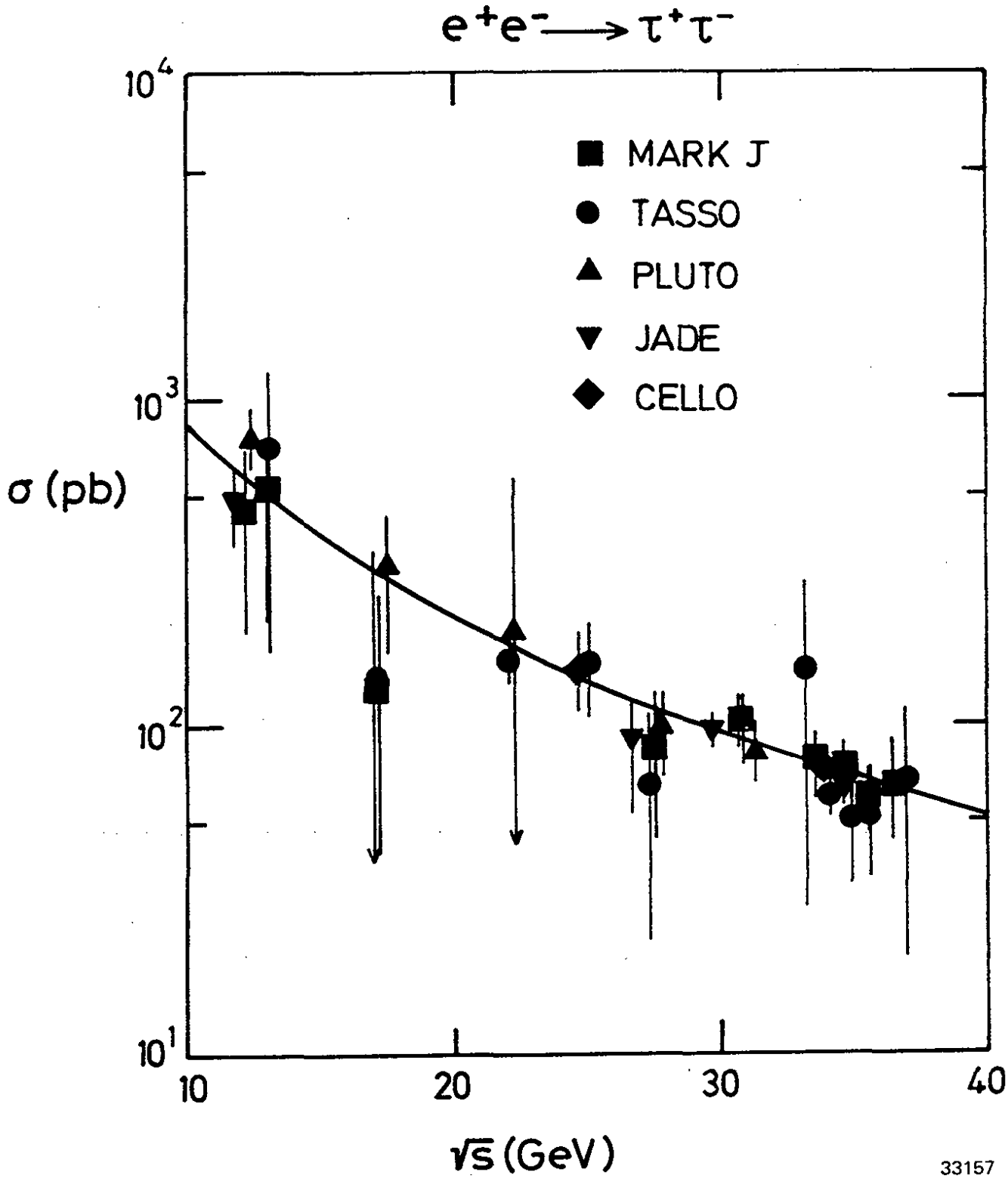

Fig. 10a The total cross section for $e^+e^- \to \tau^+\tau^-$. The solid curve shows the QED prediction. From Branson (1981).

charged current is of the same strength as for e - ν_e, theory predicts $<T_\tau> = 2.8\cdot10^{-13}$ sec, which is in agreement with the data.

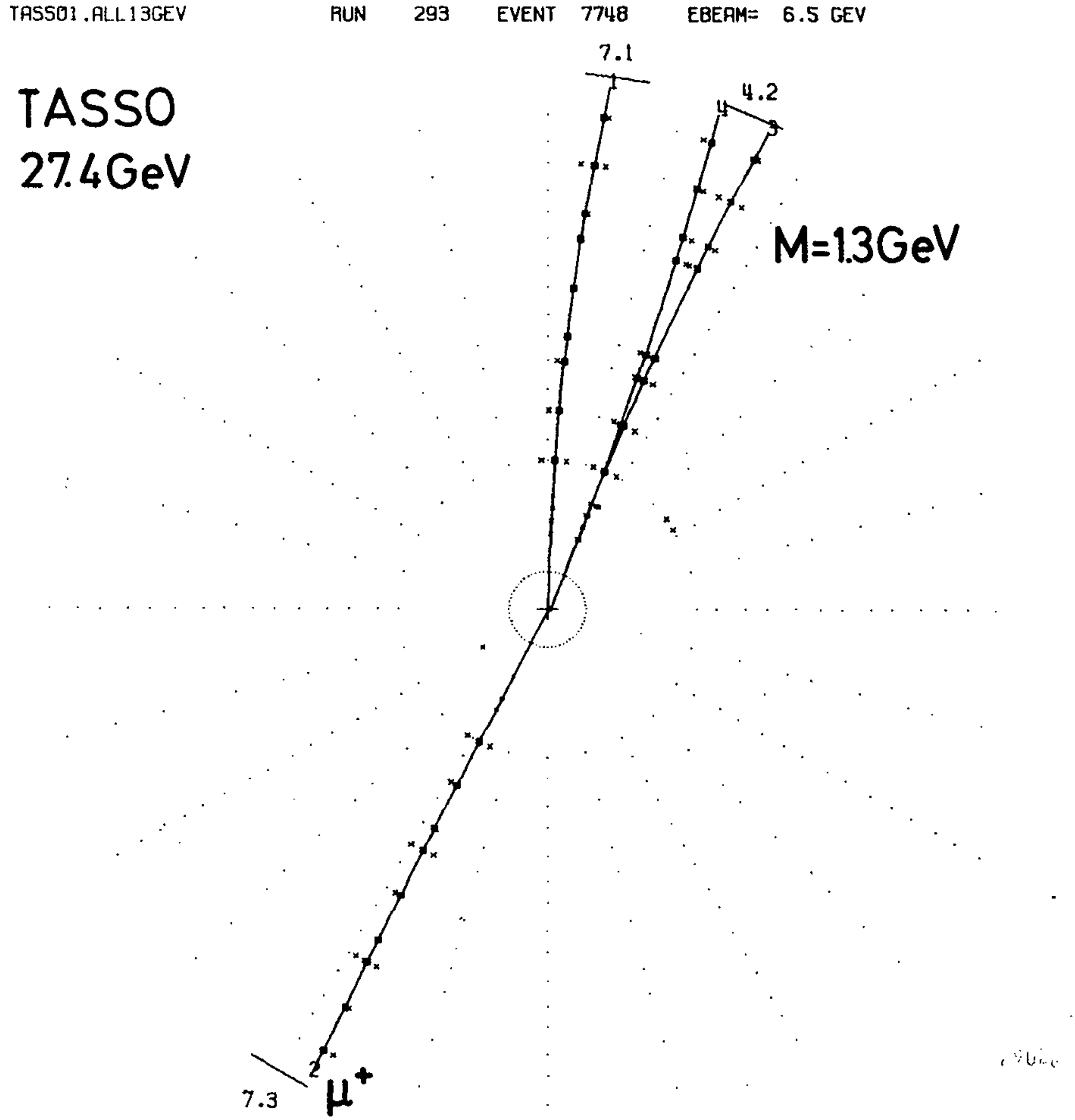

Fig. 10b Candidate for τ pair production, as observed by TASSO at 13 GeV.

$e^+e^- \rightarrow \tau^+ \tau^-$

$\tau^+ \rightarrow \mu^+\nu\nu$, $\tau^- \rightarrow \nu$ + 3 charged

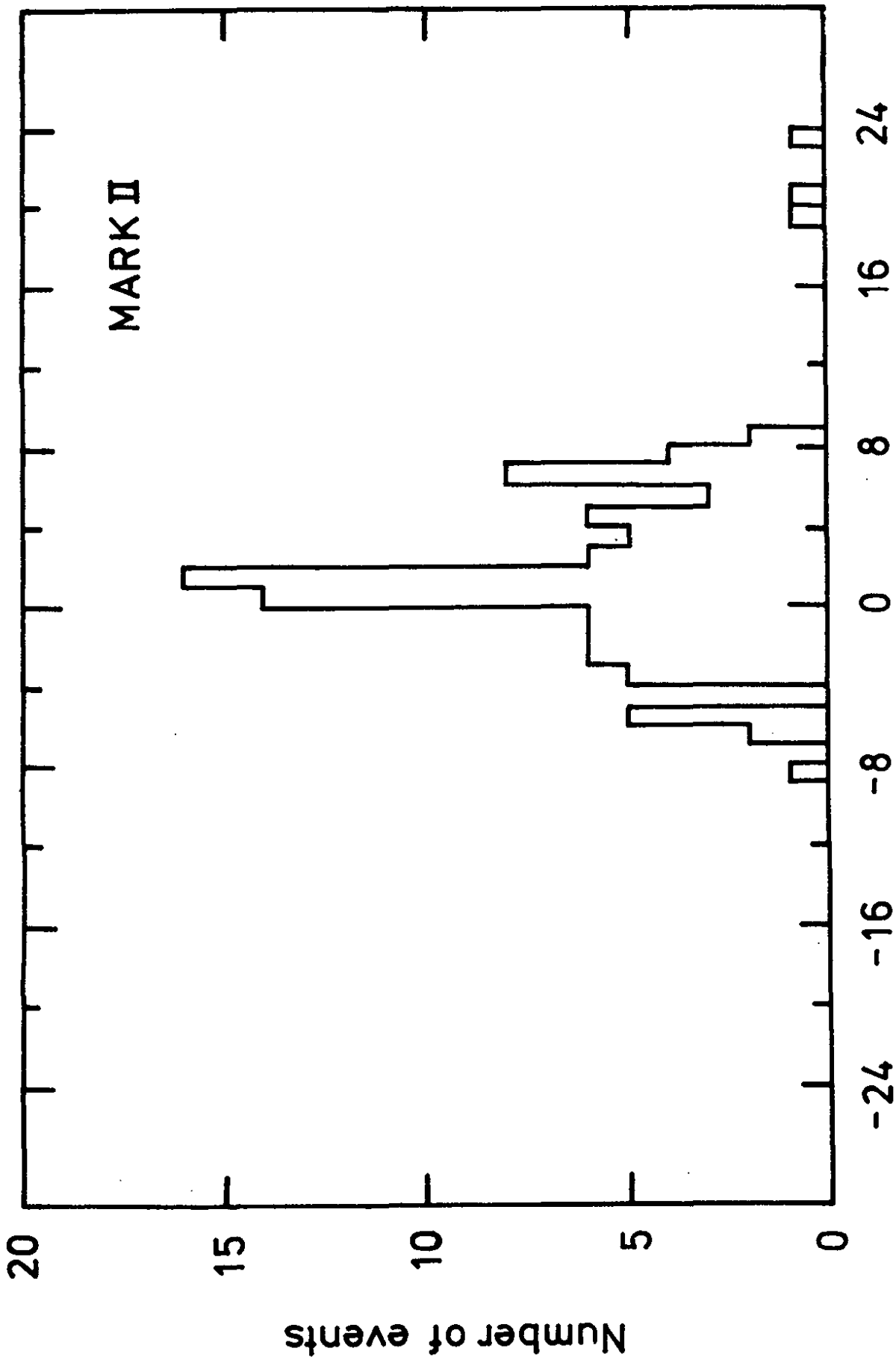

Fig. 10c The decay length distribution for τ's measured by MARK II. From Hollebeek (1981).

4. Weak neutral current contributions to lepton pair production.

The standard theory predicts neutral weak current contributions via Z^0 exchange to lepton pair production, $e^+e^- \to \ell^+\ell^-$ (see e.g. Fig. 11).

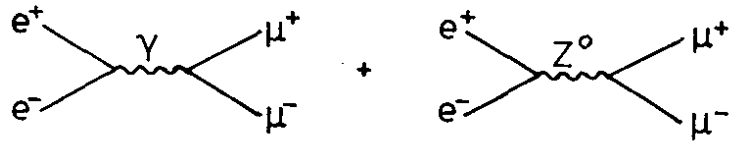

Fig. 11 The electromagnetic and weak contributions to μ pair production

The matrix element for the diagrams in Fig. 11 is given by (see e.g. Hepp and Dittmann 1981)

$$M = -\frac{4\pi\alpha}{s}\bar{\ell}\gamma_\mu\ell\bar{e}\gamma^\mu e - \left(\frac{G_F/(2\sqrt{2})}{\frac{s}{m_z^2} - 1 + i\frac{\Gamma}{m_z}}\right)\bar{\ell}\gamma_\mu(v + a\gamma_5)\ell\bar{e}\gamma^\mu(v + a\gamma_5)e \qquad (6)$$

where $v \equiv 2g_V$, $a \equiv 2g_A$, g_V, g_A are the vector and axial vector couplings, $G_F = 1.02\cdot10^{-5}/m_p^2$ GeV^{-2}, m_z, Γ_z are the Z^0 mass and width. In writing eq.(6) lepton universality, i.e. g_V and g_A to be the same for e and μ, was assumed.

It is convenient to define

$$D \equiv \frac{G_F}{8\sqrt{2}\pi\alpha}\,\frac{s}{s/m_z^2 - 1} \equiv g\cdot\frac{s}{s/m_z^2 - 1} \qquad (7)$$

where $\Gamma_z << m_z$ was assumed and $g = 4.5\cdot10^{-5}$ GeV^{-2}. At PETRA/PEP energies where $s << m_z^2$

$$D \approx -g\cdot s \qquad (8)$$

For W = 35 GeV, $D \approx -0.065$. The differential and total cross sections for $\gamma + z^0$ exchange read:

$$\frac{d\sigma}{d\Omega} = \frac{\alpha^2}{4s}\left[(1 + \cos^2\Theta)\,\{1 + 2v^2D + (v^2 + a^2)^2\,D^2\} + 4\cos\Theta\,\{a^2D + 2v^2a^2\,D^2\}\right] \qquad (9)$$

$$\sigma(\gamma + z^0) = \sigma_{\mu\mu}(\gamma)\left[1 + 2v^2D + (v^2 + a^2)^2D^2\right] \qquad (10)$$

The Z^0 contribution leads to a deviation from the total cross section predicted by QED and to a forward-backward asymmetry due to the presence of a $\cos\Theta$ term.

In the standard model (Glashow 1961, Salam 1962, Weinberg 1967) the size of these effects can be calculated. For all leptons:

$$g_A = -0.5 \qquad g_V = -0.5\ (1 - 4\sin^2\Theta_W) \tag{11}$$

Taking the current value for Θ_W from the neutrino nucleon data, $\sin^2\Theta_W = 0.228$, one finds $g_V \approx 0$. The weak contribution to $\sigma_{\mu\mu}$ expected at present energies is therefore very small,

$$\sigma_{\mu\mu}(\gamma + z^0) \approx \sigma_{\mu\mu}\ (1 + a^4D^2) \approx 1.003\cdot\sigma_{\mu\mu}$$

and cannot be detected with the available statistics.

The forward-backward asymmetry is given by

$$A = \frac{d\sigma/d\Omega(\Theta < 90^0) - d\sigma/d\Omega(\Theta > 90^0)}{d\sigma/d\Omega(\Theta < 90^0) + d\sigma/d\Omega(\Theta > 90^0)}$$

$$= \frac{3}{2}\ \frac{a^2D + 2v^2a^2D^2}{1 + 2v^2D + (v^2 + a^2)^2D^2} \tag{12}$$

which in the standard model reduces to

$$A \approx 1.5\ D$$

At W = 35 GeV the expected asymmetry is sizeable, A = -0.10, and should be observable with a few thousand muon pair events.

In extracting A from the data one has to correct $d\sigma/d\Omega$ for radiative effects which also produce a forward-backward asymmetry. Fig. 12 depicts some of the QED diagrams of order α^2 to α^4 which have to be included in the calculation (see e.g. Berends, Gaemers and Gastmans 1973).
The occurrence of a forward-backward asymmetry can qualitatively be understood by noting that the muon pairs produced from some of the diagrams have negative C parity - in particular from the lowest order diagram (a), but also from (b), (d) - (f) - while other diagrams such as (g), (h) and the box diagrams (i), (j) produce C = + μ pairs. The interference between the C = - and C = + diagrams will produce a forward-backward asymmetry. Its size depends on the experimental conditions; e.g. different cuts in the acollinearity angle ζ between the muons or in the muon energies E_μ alter the relative contributions

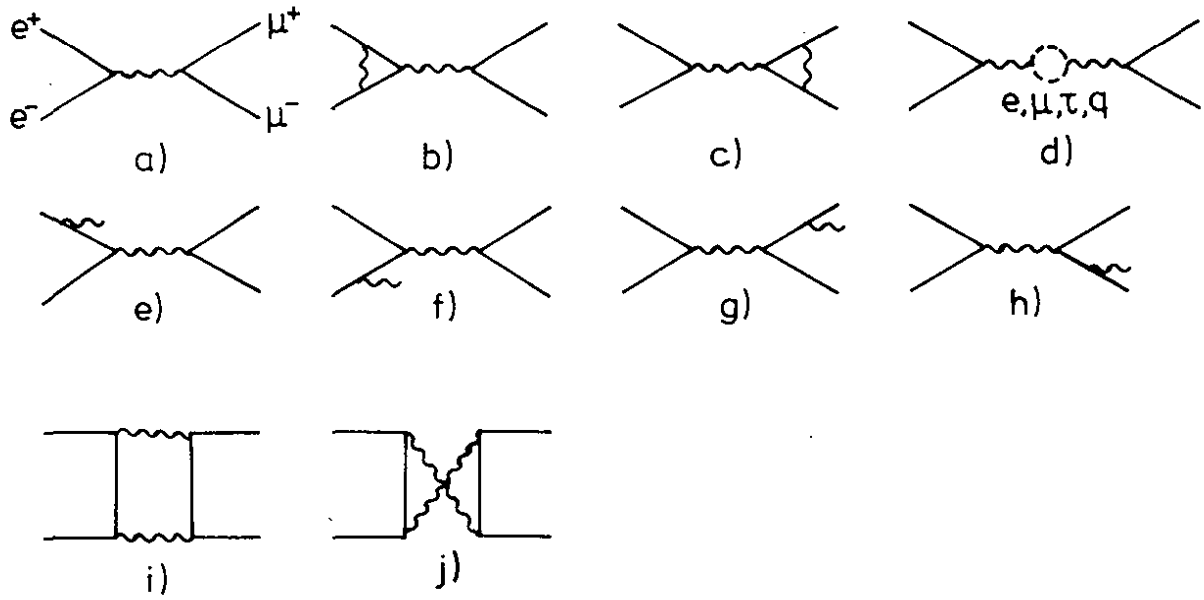

Fig. 12 QED diagram contributing to muon pair production.

of (e) - (h) and therefore the amount of interference. Fig. 13 shows as an example the radiative corrections δ, defined as

$$\frac{d\sigma^{corr}}{d\Omega} = \frac{d\sigma^{meas}}{d\Omega} \quad (1 - \delta)$$

as a function of $\cos\Theta$ for the choice $\xi \leq 20^{o}$ and $E_{\mu} \geq 0.5\ E_{beam}$. For a typical acceptance of $|\cos\Theta| < 0.8$ the forward-backward asymmetry due to radiative effects is +1.5 %, i.e. it is small and has the opposite sign from that expected for the weak contribution. As a test of the radiative corrections Fig. 14 presents the acollinearity angle distribution for Bhabha scattering. The agreement between data and theory is impressive.

Fig. 15 shows the radiatively corrected differential cross section for muon pair production as measured at an energy of W = 33.5 GeV by the JADE group (Bartel et al. 1981a). The data indicate an angular asymmetry: less μ^{+} than μ^{-} are emitted in the direction of the incoming e^{+}.

Table 2 summarizes the measured and expected asymmetry values for the five PETRA experiments. The total number of muon pairs that enter Table 2 is about 2700. The average over all PETRA experiments yields

$$\overline{A}_{\mu\mu} = -7.7 \pm 2.4\ \%$$

at a mean $\overline{s} = 1100\ GeV^{2}$. This is the first evidence for a weak neutral current contribution in $e^{+}e^{-}$ annihilation.

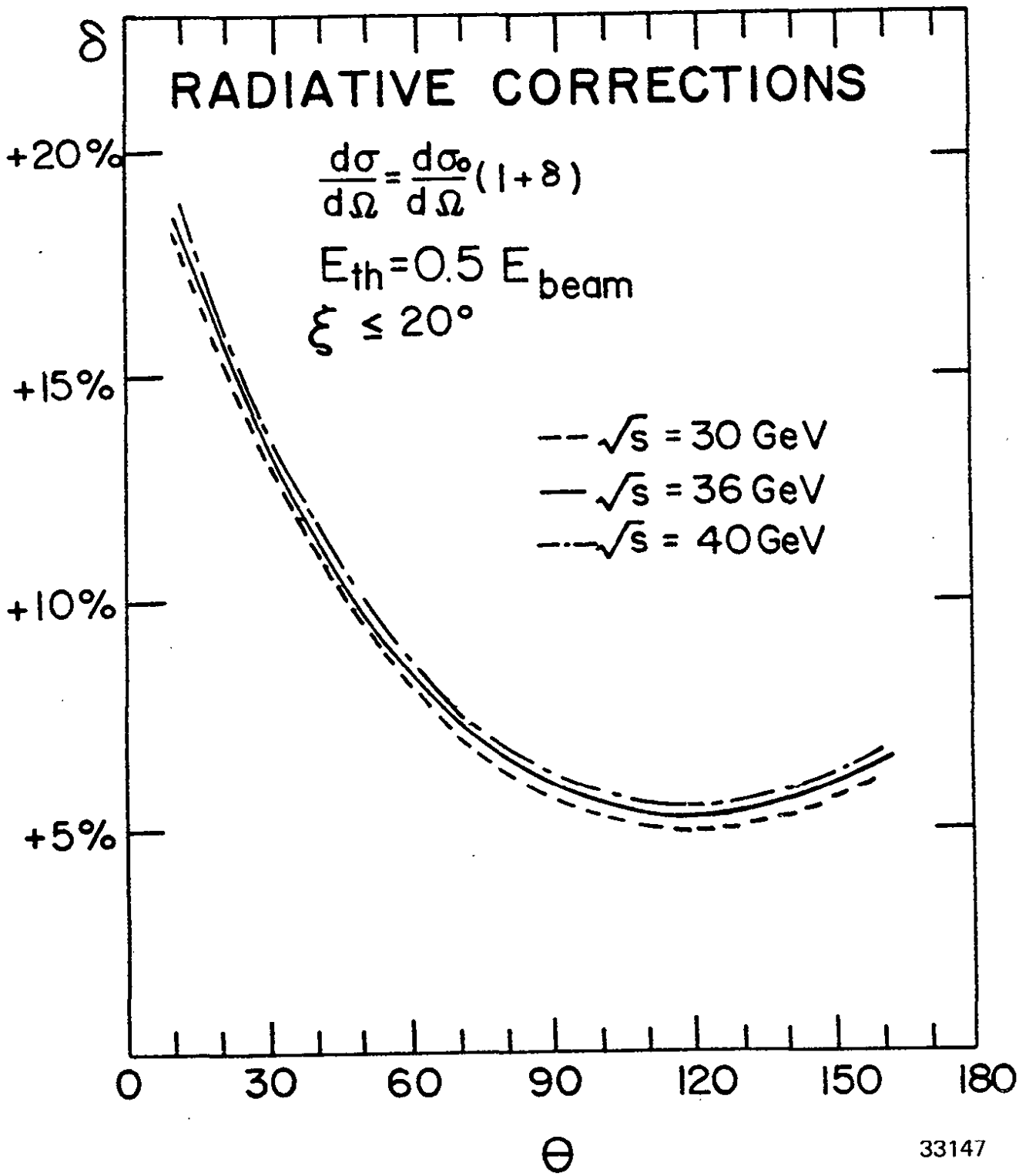

Fig. 13 The radiative corrections δ (see text) for μ pair production as a function of production angle Θ for an acollinearity angle $\xi \leq 20^{\circ}$ and μ energy $E_{\mu} \geq 0.5\ E_{beam}$ for c.m. energies of 30, 36 and 40 GeV.

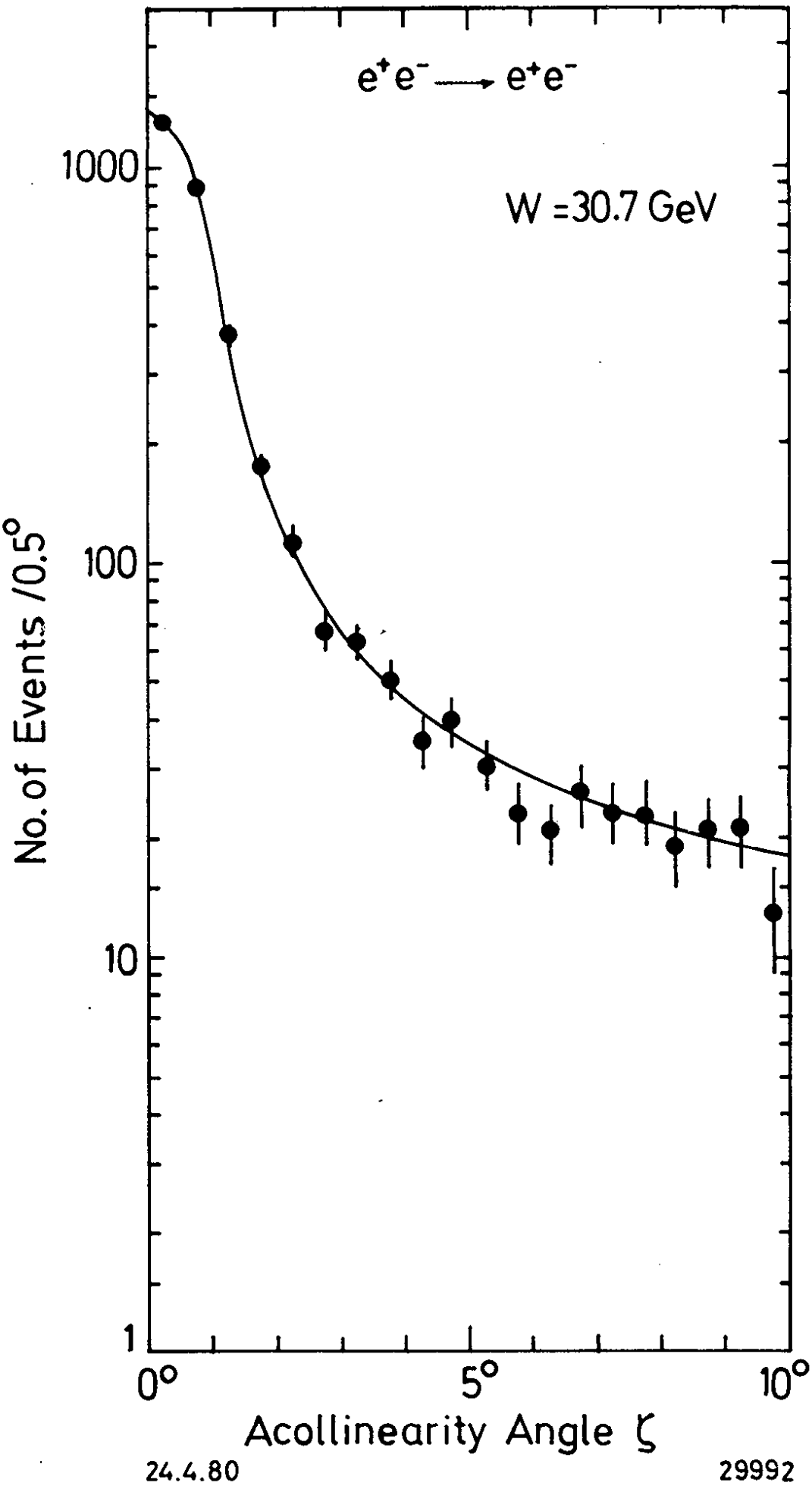

Fig. 14 Distribution of the acollinearity angle ζ in the Bhabha scattering at W = 30.7 GeV as measured by TASSO

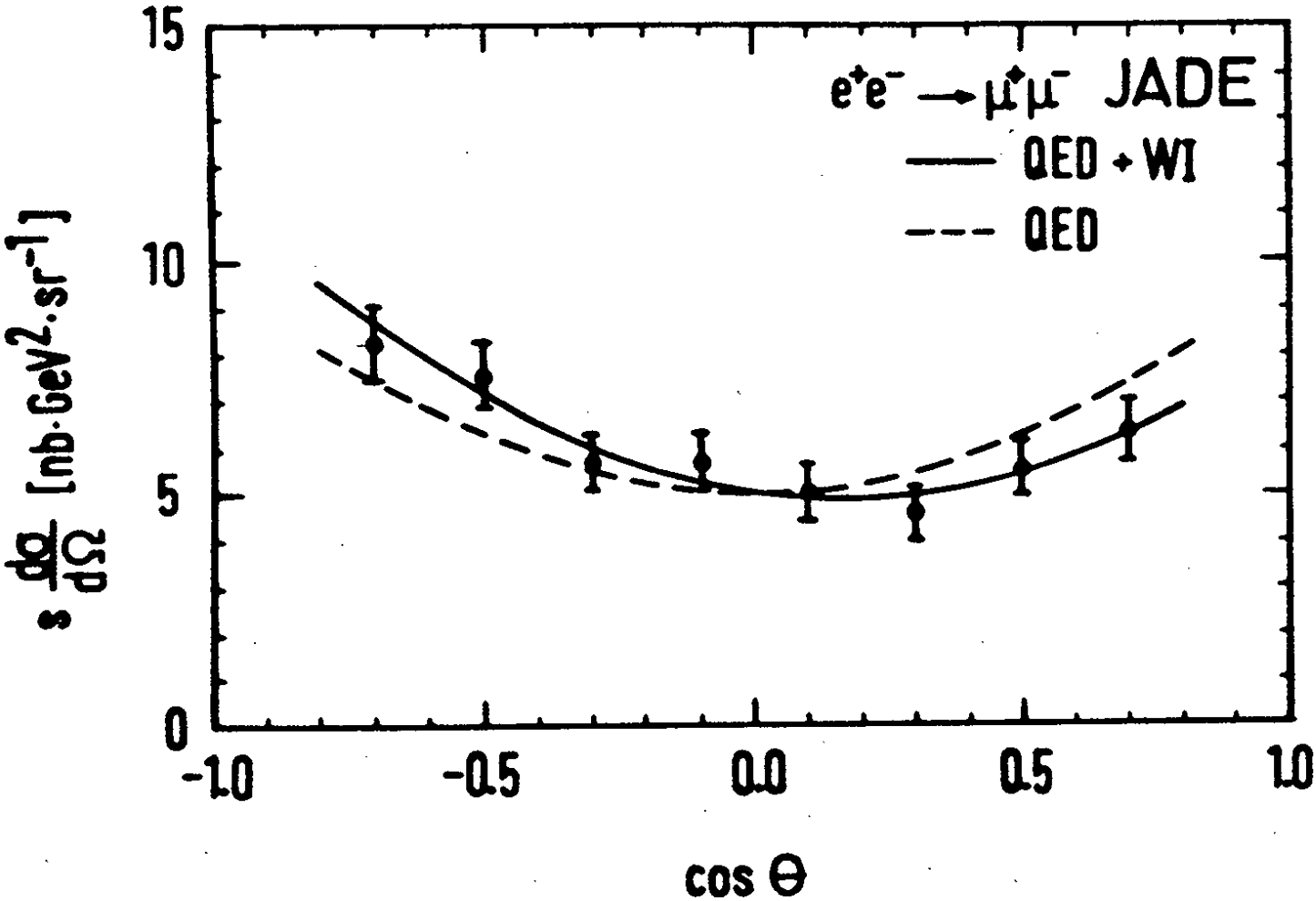

Fig. 15 Differential cross section for μ pair production of an average anergy of 33.5 GeV. The curves show the QED prediction (dashed) and the QED plus weak neutral current contributions (solid). From Bartel et al. (1981a).

The observed size of A agrees with the standard model prediction, $A_{theor} = -7.8$ %. It leads to the following value for the axial vector coupling:

$$|g_A| = 0.50 \begin{matrix} + 0.07 \\ - 0.09 \end{matrix}$$

Table 2. The muon pair asymmetry as measured at PETRA. For TASSO $A_{\mu\mu}$ has been extrapolated to $|\cos\Theta| \leq 1$. For the other experiments $A_{\mu\mu}$ integrated over the detector acceptance, typically $|\cos\Theta| < 0.8$, is given. The theoretically expected asymmetry values were calculated from the standard model. From Branson (1981).

experiment	s (GeV^2)	$A_{\mu\mu}^{meas}$ (%)	$A_{\mu\mu}^{theor}$ (%)
CELLO	900 - 1340	$-1.3 \begin{matrix} + 8 \\ - 10 \end{matrix}$	-5.8
JADE	900 - 1340	- 11 ± 4	-7.8
MARK J	900 - 1340	-3 ± 4	-7.1
PLUTO	900	+7 ± 10	-5.8
TASSO	900 - 1340	-11.3 ± 5.0	-8.7

The asymmetries measured at PEP (Hollebeek 1981) for W = 29 GeV are -4.0 ± 3.5 % (MARKII) and (-0.9 ± 5.2 ± 1.5 %) (MAC).

Fig. 16 compares the measured $A_{\mu\mu}$ value with the asymmetry predicted by the standard model for $s = 1100$ GeV^2 and $s = 1600$ GeV^2 as a function of the Z^0 mass. The present data limit m_Z only from below, $m_Z > 49$ GeV with 95 % C.L. Much higher statistics and preferrably higher energies are required to distinguish between a four fermion interaction ($m_Z = \infty$) and a theory with a finite Z^0 mass. The standard model with $\sin^2\Theta_W = 0.228$ predicts $m_Z = 89$ GeV.

As discussed above the size of the cross sections for lepton pair production is sensitive to the vector coupling (g_V) and therefore to $\sin^2\Theta_W$. The fact that no deviations from QED were observed provides rather tight limits on $\sin^2\Theta_W$. The average over all PETRA experiments yields

$$\sin^2\Theta_W = 0.24 \pm 0.07$$

at $\bar{s} = 1100$ GeV^2. The nontrivial result is that $\sin^2\Theta_W$ appears to be the same at this mass squared as measured in νN scattering at Q^2 of 50 - 100 GeV^2.

The data can also be used to put limits on weak models with more than one Z^0 and/or W doublet. More information can be found in (Branson 1981).

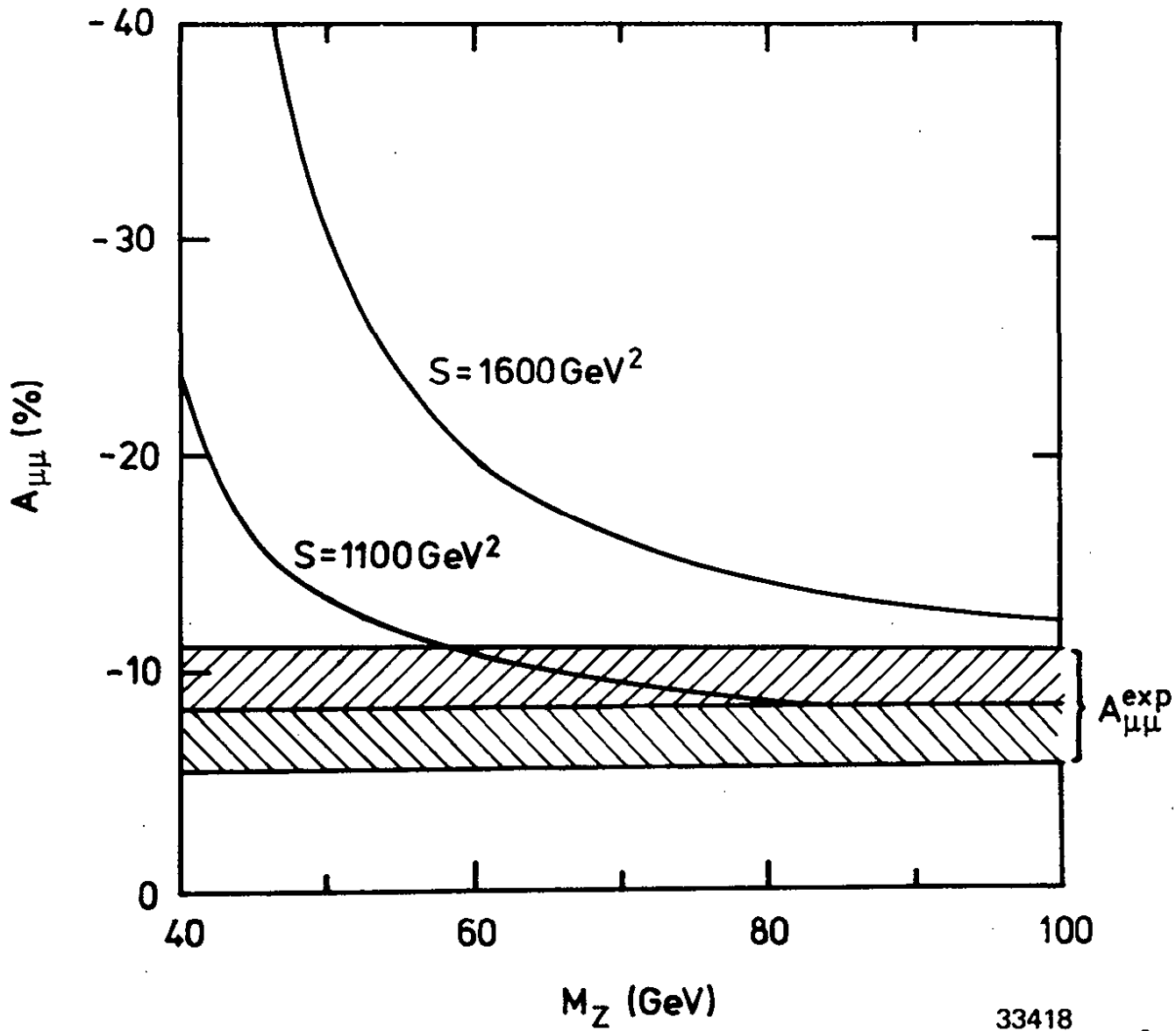

Fig. 16 The asymmetry $A_{\mu\mu}$ measured by the PETRA experiments at s = 1100 GeV^2 (dashed band). The curves show the expected asymmetry as a function of the Z^o mass for s = 1100 GeV^2 and s = 1600 GeV^2.

5. Search for new particles.

As mentioned above an electron-positron storage ring is an ideal place to search for new particles. Any charged and pointlike particle will be produced with a sufficiently large cross section. For spin 1/2 fermions the pair production cross section is given by the expression for μ pair production (eq.(2)). For charged pointlike scalars the cross section has a different rise near threshold and its asymptotic value is one quarter of $\sigma_{\mu\mu}$ since the spin is zero:

$$\frac{d\sigma}{d\Omega}(e^+e^- \to H^+H^-) = \frac{\alpha^2}{8s}\beta^3 \sin^2\Theta$$

and $$\sigma(e^+e^- \to H^+H^-) = \frac{\beta^3}{4}\sigma_{\mu\mu} \qquad (13)$$

The PETRA experiments conducted intensive searches for a great variety of new particles. So far the findings have been negative. Some of these results put stringent limits on new symmetry schemes. The discussion of these results will follow the review by Bürger (1981).

5.1 Excited leptons

The existence of excited leptons (e*,μ*,τ*) will give the ground state leptons a structure. As discussed in section 3 the lepton pair data rule out a structure down to 10^{-16} cm. The presence of an excited electron could be seen directly in two-photon annihilation, $e^+e^- \to \gamma\gamma$, where it adds a contribution described by diagram 5b. The deviation of the cross section from the QED prediction can be written as

$$\frac{d\sigma}{d\Omega}(e^+e^- \to \gamma\gamma) = \frac{d\sigma}{d\Omega}_{QED}\left(1 + \frac{s}{2\Lambda^4}\sin^2\Theta\right) \qquad (14)$$

where $\Lambda = m_{e^*} \cdot \sqrt{\alpha/\alpha^*}$, m_{e^*} is the mass of the excited electron, α^* its coupling to electron and photon. As shown by Fig. 9 there is no evidence in the data for any deviation from QED. Assuming $\alpha^* = \alpha$ the experimental lower limit on m_{e^*} is 50 GeV (see Tab.3).

Table 3. Lower limits (95 % C.L.) on the mass m_{e*} of a possible excited electron, assuming $\alpha^* = \alpha$. From Bürger (1981).

experiment	W(GeV)	m_{e*}(GeV)
CELLO	35	>43
JADE	35	47
MARK J	35	58
PLUTO	31	46
TASSO	35	34
MARKII	29	50

Next we consider excited muons which could be produced either pairwise,

$$e^+e^- \to \mu^{*+}\mu^{*-} \tag{15}$$

or together with a μ,

$$e^+e^- \to \mu^*\mu \tag{16}$$

For spin 1/2 μ^* the cross section for (16) can be written as

$$\frac{d\sigma}{d\Omega}(e^+e^- \to \mu^*\mu) = \lambda^2\alpha^2 \frac{(s + m_{\mu^*}^2)^2}{s^3} \left\{(s + m_{\mu^*}^2) - (s - m_{\mu^*}^2)\cos^2\Theta\right\} \tag{17}$$

where the $\mu^*\mu\gamma$ vertex factor is $2\lambda e\sigma_{\mu\nu}$. The MARK J group searched for the reaction (15) in $\mu^+\mu^-\gamma\gamma$ final states. A μ^* with a mass $m_{\mu^*} < 10$ GeV is ruled out by the data. MARK J and JADE studied events of the type $\mu^+\mu^-\gamma$ to look for reaction (16). The $\mu\gamma$ mass distribution (Fig. 17) as measured by JADE agrees well with QED and shows no evidence for a narrow μ^*. The data are sensitive to μ^* masses up to 30 GeV provided the coupling λ is sufficiently large. If m_{μ^*} is arbitrarily fixed to $m_{\mu^*} = 16$ GeV the data limit the cross section to $\sigma_{\mu^*\mu} < 0.0075 \cdot \sigma_{\mu\mu}$ with 90 % C.L. (see Fig. 18).

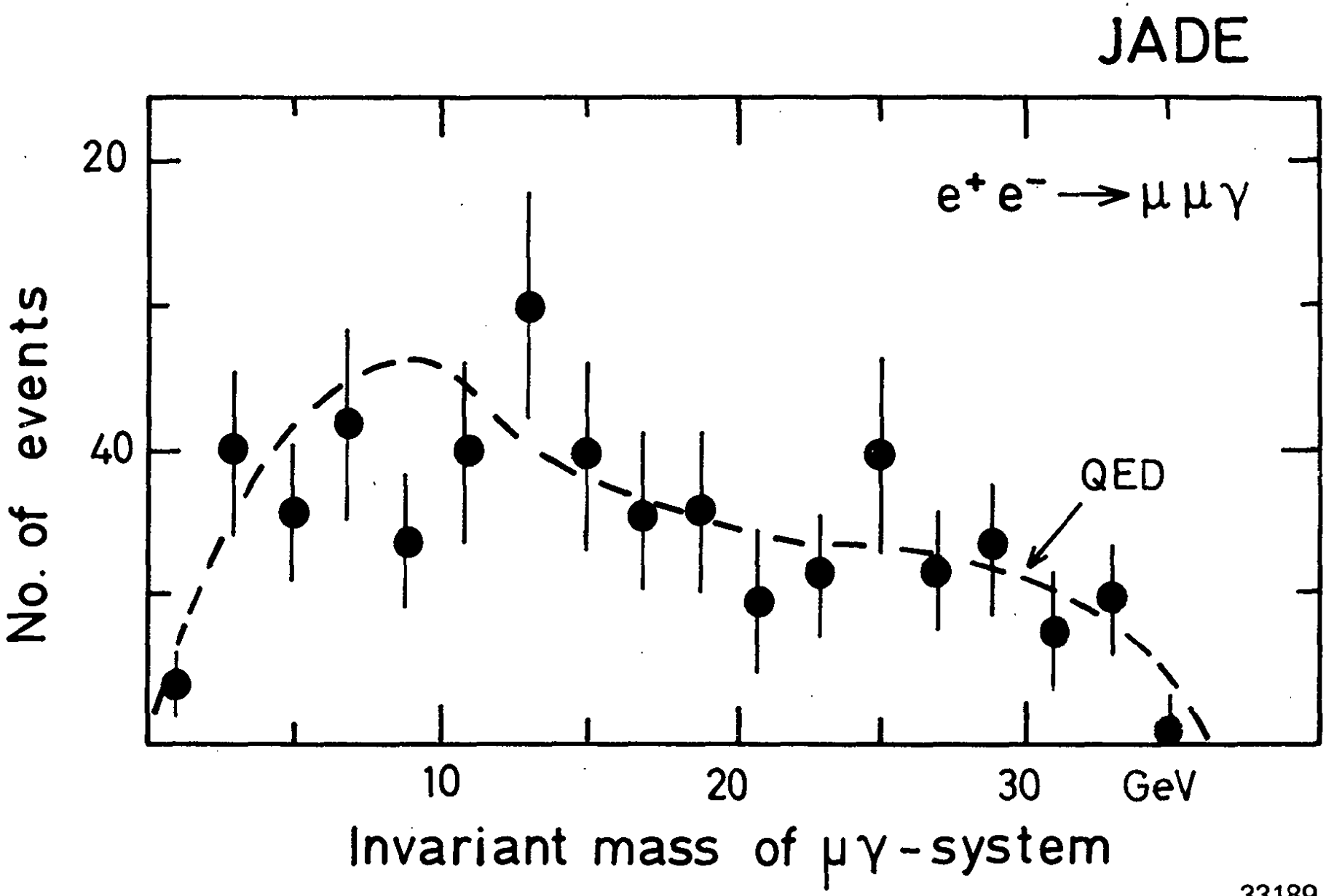

Fig. 17 The reaction $e^+e^- \rightarrow \mu^+\mu^-\gamma$ at W = 22 - 37 GeV as measured by JADE. Events were selected with $E_\gamma > 1$ GeV, $M_{\mu\mu} > 1$ GeV, angle between γ and μ larger than 15° and angle sum $>350^\circ$. From Bürger (1981).

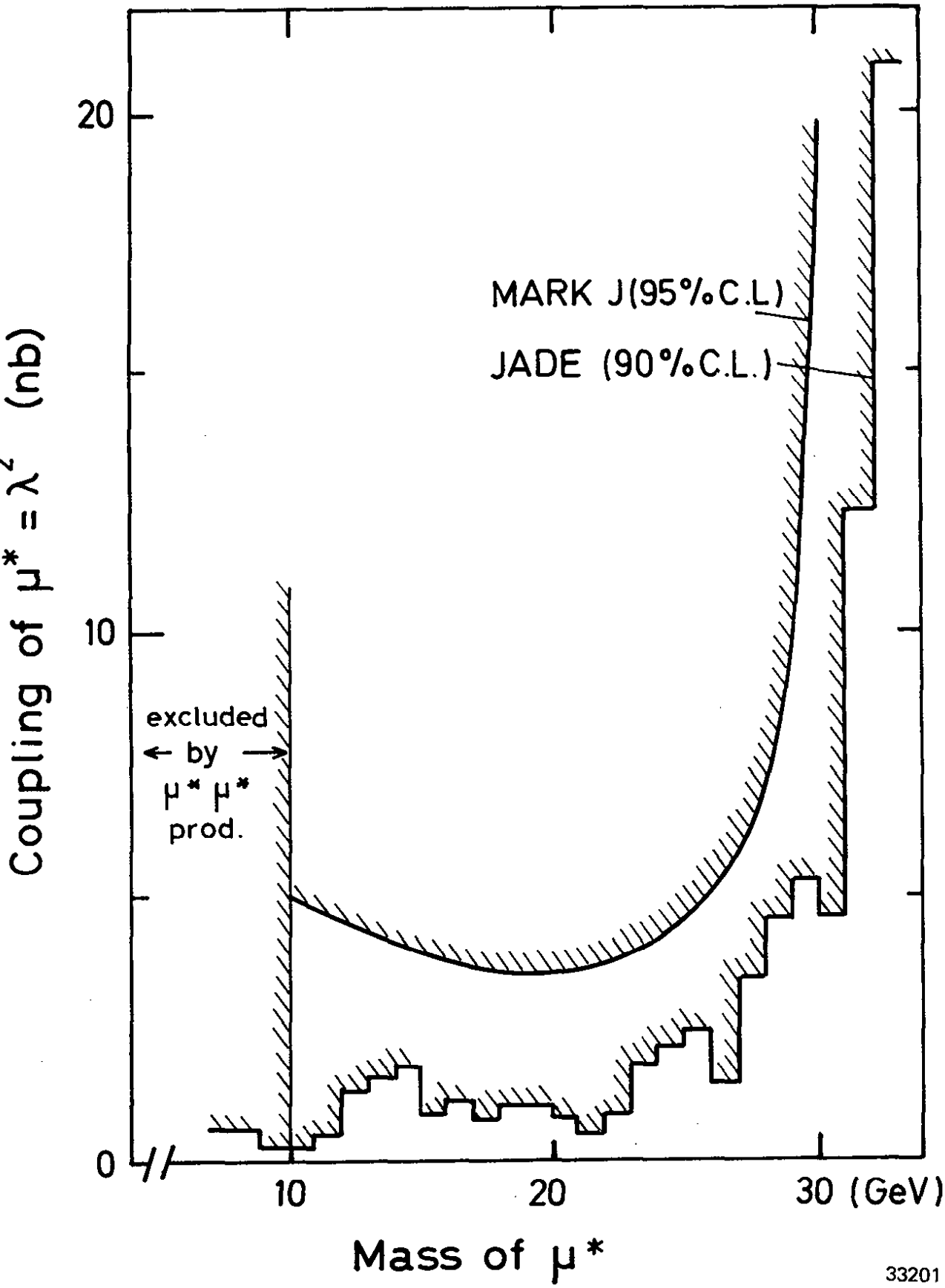

Fig. 18 Upper limit on the coupling constant λ^2 versus the μ^* mass. From Bürger (1981).

5.2 Search for a heavy sequential lepton.

We know presently of three generations of leptons, (e,ν_e), (μ,ν_μ) and (τ,ν_τ). Whether there should be a fourth one, (L,ν_L), or even more is an open question. The cross section for pair production of L,

$$e^+e^- \to L^+L^-$$

is given by eq.(4).

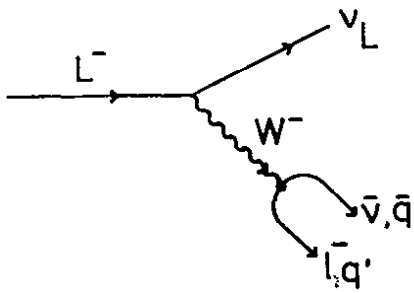

Fig. 19 Diagram for L decay into leptonic and semileptonic final states.

The possible decay modes of L (see Fig. 19) are either leptonic, $L^- \to \nu_L \bar{\nu}_e \ell^-$ or semileptonic, $L^- \to \nu_L \bar{q}q'$ and can be computed in the standard weak theory following the same lines used in the case of the τ (see e.g. Bjorken & Llewellyn-Smith 1973). Neglecting mass effects and possible enhancements one expects all leptonic and semileptonic channels to have the same branching ratio (note: the $\bar{q}q'$ channels count three times because of the colour factor), hence for a lepton of mass 15 GeV, $B(L^- \to \nu_L e^- \bar{\nu}_e) = 1/9$. The possible decay channels lead to characteristic event signatures which readily identify L^+L^- production. Table 4 summarizes the various event topologies studied by different experiments. No evidence was found and the existence of a heavy sequential lepton is excluded for lepton masses below 18 GeV.

Table 4. Mass limits on a new heavy sequential lepton. From Bürger (1981).

experiment	95 % lower limit on M_L (GeV)	event signature
MARK J Barber et al. (1980a)	16	single muon recoiling against many hadrons
TASSO Brandelik et al.(1981a)	15.5	single charged part. recoiling against many hadrons
PLUTO Berger et al.(1981a)	14.5	single muon recoiling against many hadrons
JADE	18.1	two acollinear jets

5.3 Neutral heavy leptons

The existence of heavy neutrinos was discussed in connection with the atomic experiments on parity violation (see e.g. Harari 1977). A possible candidate is the E^0 which has the same lepton number as the electron. It can be produced by W exchange (see Fig. 20a) via

$$e^+e^- \rightarrow \bar{E}^0\nu \tag{18}$$

and will decay in the standard way (Fig. 20b), i.e. leptonically ($E^0 \rightarrow e^-e^+\nu_e$ with a branching ratio of 11 %) and semileptonically ($E^0 \rightarrow e^-\bar{q}q'$). The cross section for reaction (18) assuming V-A coupling is given by Bletzacker & Nieh (1977) (see also Bjorken & Llewellyn-Smith 1973).

$$\frac{d\sigma}{d\Omega} = \frac{G_F^2}{32\pi^2} \frac{(1 - \frac{M^2}{s})^2}{(1 - \frac{q^2}{M_W^2})^2} \left\{ 2s(1 + \cos\Theta) - (s - M^2)\sin^2\Theta \right\} \tag{19}$$

where M is the mass of E^0 and q^2 the square of the momentum transfer between e^+ and $\bar{E}^0$. The predicted cross section is surprisingly large, for W = 35 GeV $\sigma(\bar{E}^0\nu) \simeq 3$ pb which is roughly 4 % of $\sigma_{\mu\mu}$.

For E^0 masses not too close to the c.m. energy W reaction (18) leads to events with particles in only one hemisphere (Fig. 20c). The JADE group has searched for such events and found none. Fig. 21 compares their upper limit with the number of events predicted for V-A and V+A coupling. Assuming V-A (V+A) coupling E^0 masses below 17 GeV (20 GeV) can be excluded.

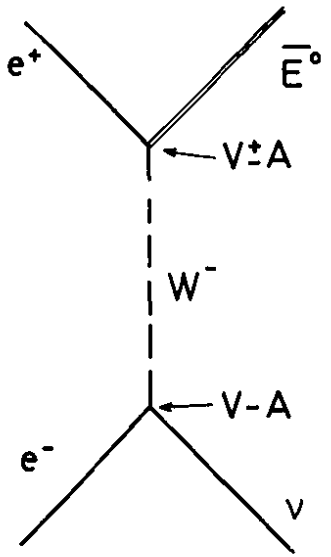

a) Production

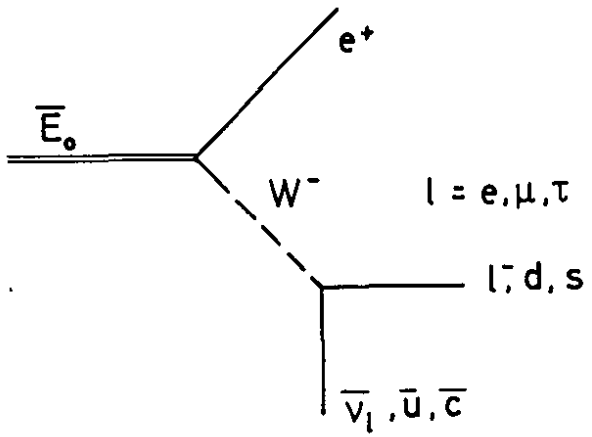

b) Decay

Neutral heavy electron

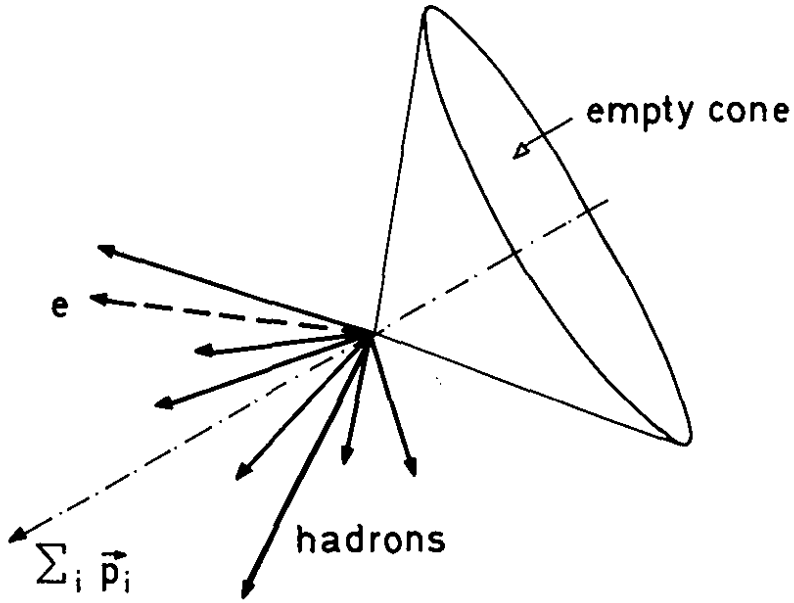

Event signature for
neutral heavy electron

33194

Fig. 20

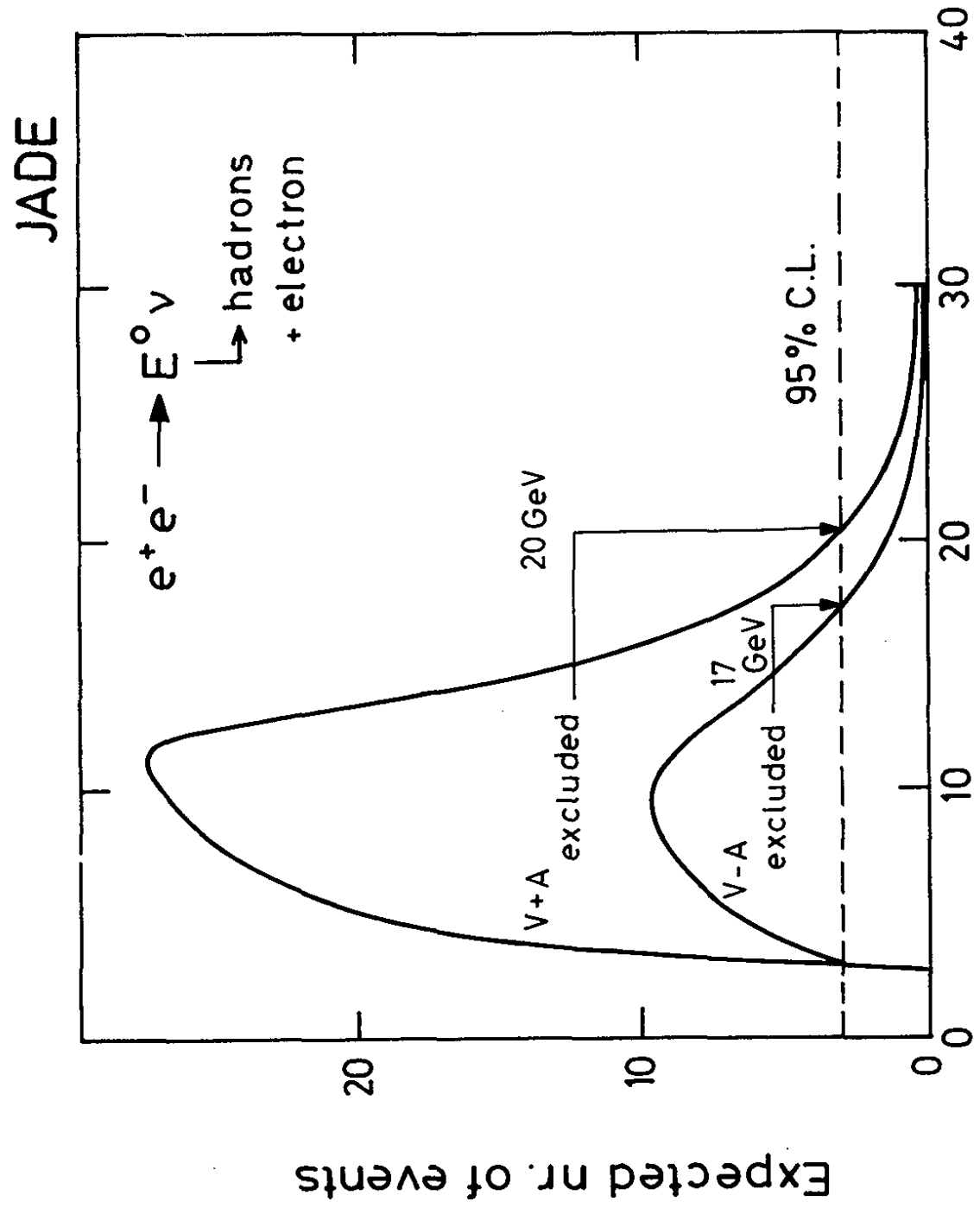

Fig. 21 The reaction $e^+e^- \rightarrow \bar{E}^o \nu$: Comparison of expected number of events as a function of E^o mass with observed upper limit. From Bürger (1981).

5.4 Supersymmetric scalar leptons

In supersymmetry the fundamental constituents of matter: leptons, quarks, quanta of fields with spin J have supersymmetric partners with spin J ± 1/2 (see e.g. Gol'fand & Likhtman 1971, Volkov & Akulov 1973, Wess & Zumino 1974, Fayet & Ferrara 1977, Farrar 1987)

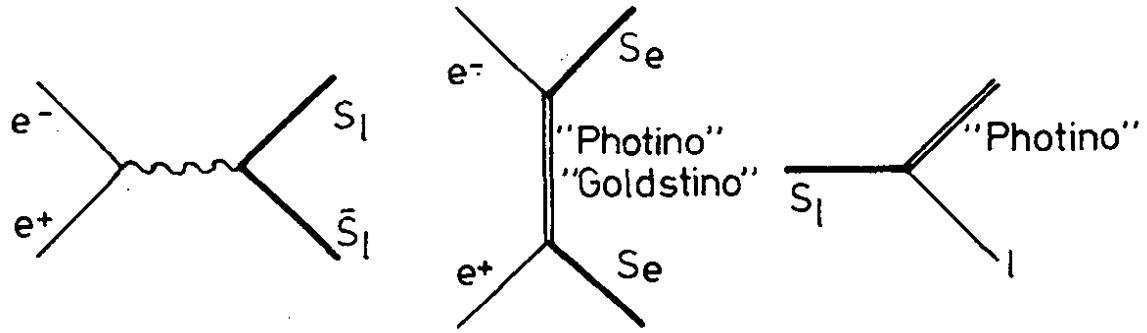

Fig. 22 Production and decay of scalar leptons

In particular, there should exist scalar electrons (S_e) and muons (S_μ) as supersymmetric partners of e and μ. They can be produced in e^+e^- interactions by photon exchange with a cross section given by eq.(13);scalar electrons can also be produced by the exchange of a space-like photino or goldstino (Fig. 22a) (see Farrar and Fayet 1980). The photino is the supersymmetric partner of the photon and the goldstino is associated with the breaking of the symmetry. Both have J = 1/2. The S_e and S_μ are expected to be short lived and to decay by photino emission, $S_e \rightarrow \ell$ + photino (Fig. 22b). The photino behaves like a neutrino in its interaction with matter.

Production of scalar leptons (S_e and S_μ) was searched for by several experiments analysing events with two acoplanar leptons:

$$e^+e^- \rightarrow \ell^+\ell^- + \text{missing momentum}$$

Background from events of the type $e^+e^- \rightarrow e^+e^-\gamma$, $e^+e^- \rightarrow \tau^+\tau^- \rightarrow e^+e^-$ + ν's, $e^+e^- \rightarrow e^+e^-e^+e^-$ (and similarly for μ's) required special attention. No evidence was found for scalar leptons. As Table 5 shows scalar electrons (muons) are excluded for masses between 2 (5.5 GeV) and 16 (15) GeV.

Table 5. Mass limits on scalar leptons.

Experiment	Mass range excluded by experiment (GeV) S_e	S_μ
JADE (Cords 1980)	>16	
MARK J (Barber et al. 1980)		3 - 15
PLUTO (Spitzer 1980)	>13	
CELLO	2 - 16.6	5.5 - 15

5.5 Free quarks

Using the dE/dx information in the central drift chamber the JADE group (Bartel et al. 1980) searched for free quarks produced in pairs, and together with ordinary hadrons:

$$e^+e^- \to q\bar{q} \tag{20}$$

$$e^+e^- \to q\bar{q} + \text{hadrons} \tag{21}$$

at energies between 27 and 37 GeV. The ionization loss dE/dx for quarks with charge Q = 2/3 (1/3) will be 1/4 (1/9) of that for a charge Q = 1 particle provided the velocity is the same. The detection efficiency for Q = 2/3 (1/3) quarks lies between 0.15 - 0.36 (0.11 - 0.27) depending on the quark mass. Fig. 23 shows the mean energy loss dE/dx for charged particles measured as a function of the apparent momentum P/Q. Basically all particles lie in one of the regions expected for e, π, k, p, d or t. The p, d and t points result mainly from beam gas scattering. In the region where Q = 2/3 or 1/3 particles can clearly be separated from the known particles no events are found. Fig. 24 shows the upper limits for free quark production in (20) and (21) as a function of the quark mass. There are two different curves for inclusive quark production (21) based on different assumptions of the quark momentum distribution. Also shown in Fig. 24 are the upper limits obtained by MARKII (Weiss et al.1981) at lower energies and by the free quark search experiment at PEP (Litke 1981). The upper limits are roughly 10^{-2} - 10^{-4} below the cross section for muon pair production.

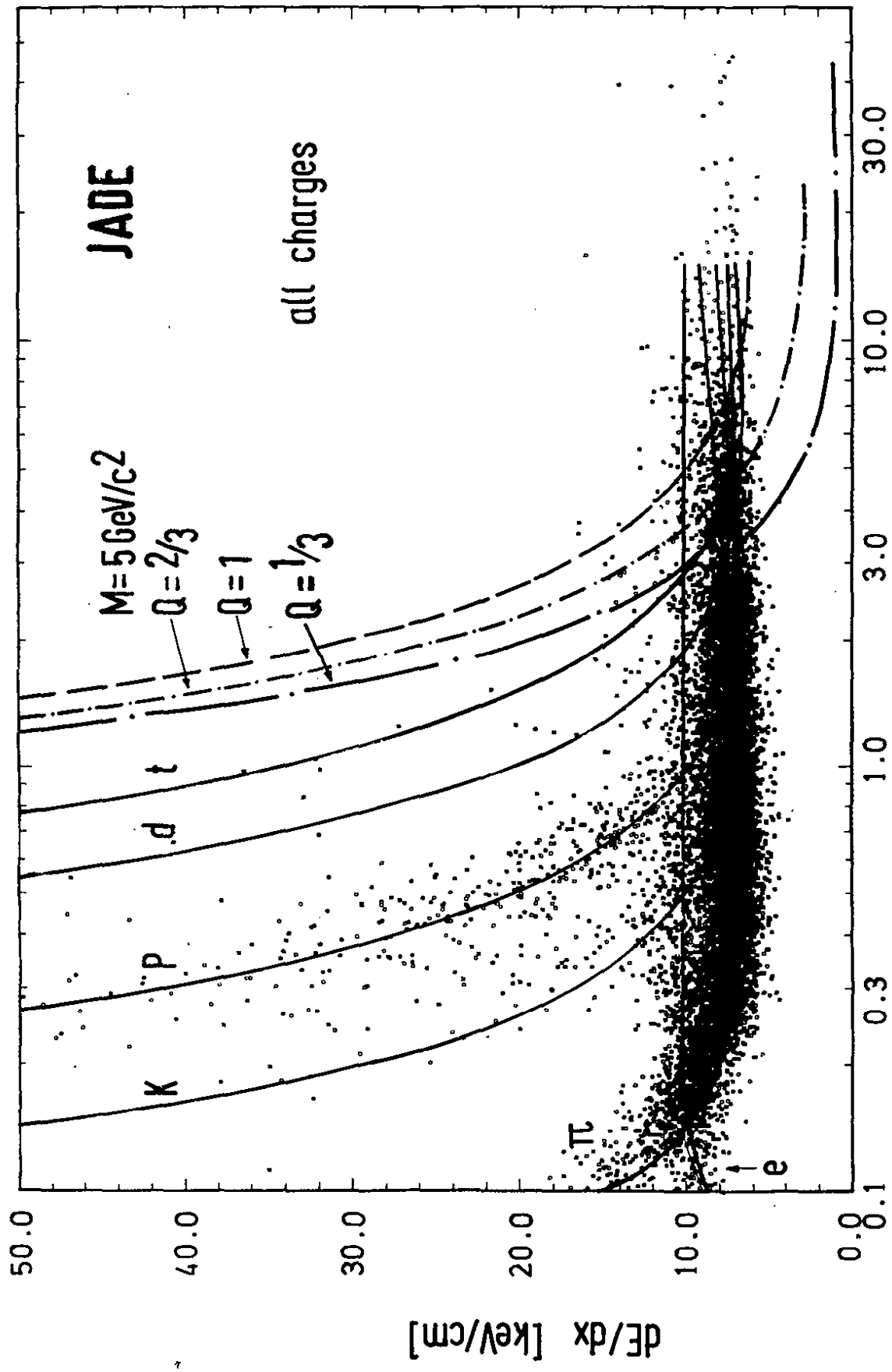

Fig. 23 Mean Energy loss dE/dx as a function of the apparent momentum P/Q where Q is the particle charge. From JADE.

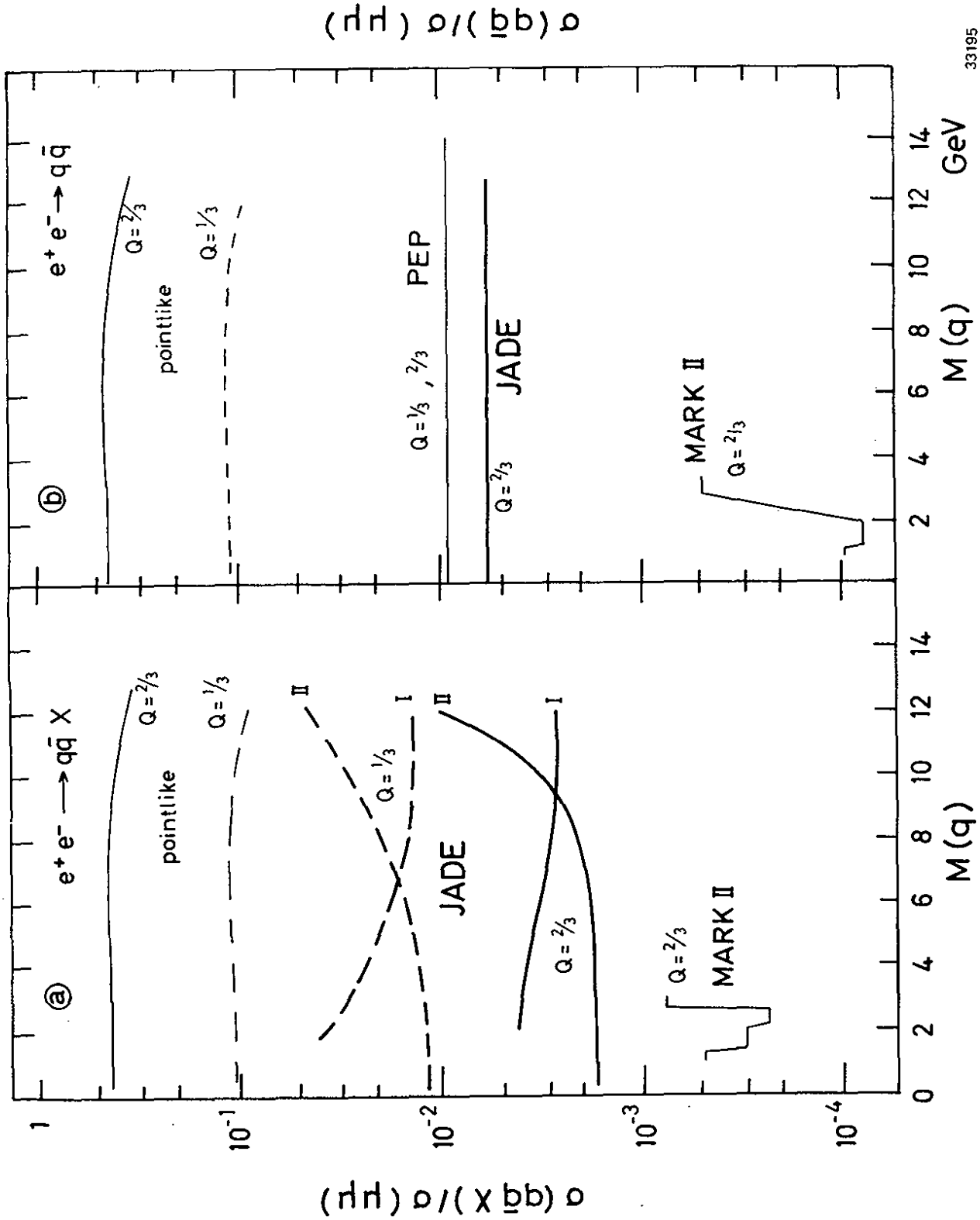

Fig. 24 Upper limits on the inclusive and exclusive production of free quarks as a function of the quark mass. From Bürger (1981).

In summary, as the title of this section: "Search for ..." suggested, no evidence has been found yet for excited electrons or muons, for new heavy leptons, for neutral heavy leptons, for supersymmetric scalar leptons, nor for free quarks. The upper limits obtained exclude for most of these particles mass values below ~16 - 20 GeV.

6. Jet formation in e^+e^- annihilation.

6.1 The quark parton model

In the quark parton model e^+e^- annihilation into hadrons,

$$e^+e^- \rightarrow \text{hadrons}$$

proceeds in two steps (see Fig. 25). First, e^+ and e^- annihilate into a photon which then materializes into quark(q) and antiquark($\bar{q}$). In the second step q and $\bar{q}$ fragment into hadrons. The first step is almost identical to the production of a pair of muons.

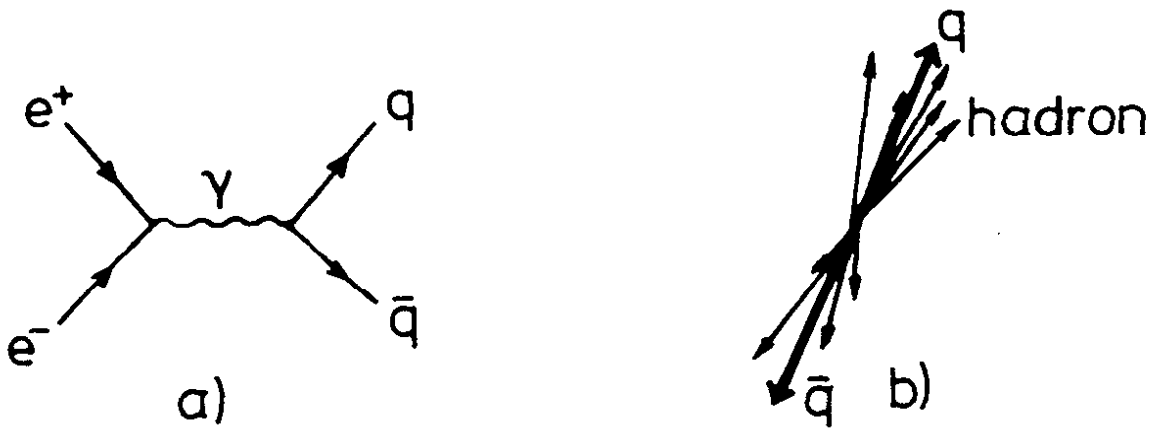

Fig. 25 e^+e^- annihilation in the quark model

The quark model description of e^+e^- annihilation into hadrons has been extensively tested and has been found in surprising agreement with experiment. The evidence for the model rests on the following observations:

1) The total cross section

The total cross section is readily calculated. The cross section for producing a free $q\bar{q}$ pair is the same as for producing a $\mu^+\mu^-$ pair except that the quark charge e_q replaces the muon charge of unity. Assuming that the produced $q\bar{q}$ pairs turn into hadrons with unit probability one finds

$$R \equiv \sigma_{tot}/\sigma_{\mu\mu} = 3 \sum_{q=u,d,s\ldots} e_q^2 \qquad (22)$$

where the factor of three accounts for the fact that quarks come in three colours. At energies above W = 10 GeV where all five known quarks: u,d,s,c,b can be pair produced the predicted value of R is

$$R = 3 \left\{ \left(\frac{2}{3}\right)^2 + \left(\frac{1}{3}\right)^2 + \left(\frac{1}{3}\right)^2 + \left(\frac{2}{2}\right)^2 + \left(\frac{1}{3}\right)^2 \right\} = \frac{11}{3}$$

Fig. 26 shows R up to the highest energy measured at PETRA, W = 36.6 GeV (Felst 1981). The error bars indicate the statistical uncertainties. The systematic errors are typically of the order of 7 - 10 %. The outstanding features of R are spikes due to the excitation of vector states, $\rho,\ldots,$ $J/\psi,\ldots,$ $\Upsilon\ldots$ and the fact that in between these families of vector states and above R is rather constant. The data above 1.5 GeV indicate two steps. Between 1.5 and 3.8 GeV R is approximately 2 - 2.5. Near charm threshold (at 4 GeV) R rises sharply to reach a new level around 4 which persists up to 36.6 GeV and which is in striking agreement with the quark model prediction of 11/3 (see curve in Fig. 26).

The high energy data on R can be used to test the pointlikeness of quarks (Söding & Wolf 1981). In terms of the quark electric and magnetic formfactors G_E, G_M the ratio R is given by

$$R = 3 \sum e_q^2 \left\{ \frac{2m_q^2}{s} |G_E(s)|^2 + |G_M(s)|^2 \right\} \qquad (23)$$

where m_q is the quark mass and $m_q^2 \ll s$ has been assumed. If $G_E \sim G_M$ and all quarks have the same form factor we find:

$$R/R_o = |G_M(s)|^2 \qquad (24)$$

with $R_o = 3 \sum e_q^2$. With the ansatz

$$G_M(s) = (1 - s/M^2)^{-1} \qquad (25a)$$

treating R_o as a free parameter and including the systematic uncertainties of σ_{tot} the data yield for $W \geq 17$ GeV, $M > 124$ GeV with 95% C.L. If quarks are composites of 3 subquarks G_M may have a dipole behaviour:

$$G_M(s) = (1 - s/M_D^2)^{-2} \qquad (25b)$$

For this case the fit gives $M_D > 176$ GeV with 95 % C.L. Converting the M parameters into a length we conclude that quarks behave pointlike down to distances of $\sim 1 \cdot 10^{-16}$ cm.
An analysis in terms of the cut-off parameter Λ yields $\Lambda_+ = 190$ GeV, $\Lambda_- = 285$ GeV (Branson 1981).

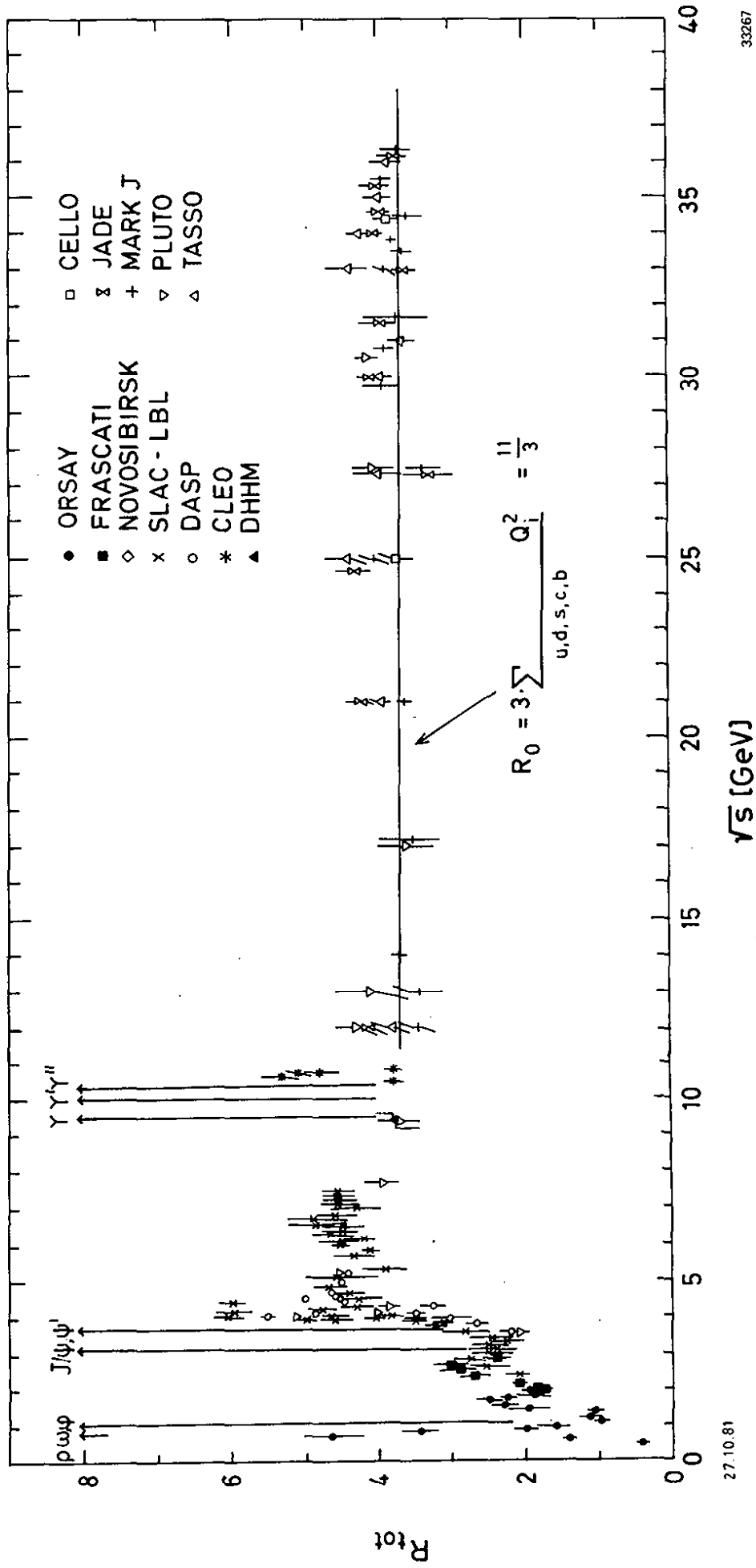

Fig. 26 The ratio R of the total cross section for e^+e^- annihilation into hadrons to the μ pair cross section, $\sigma_{\mu\mu} = \frac{4\pi\alpha^2}{3s}$. From Felst (1981).

2) The occurrence of jets

The quark-parton model predicts the occurrence of jets: at high energies the hadrons will be collimated around the direction of the primary $q\bar{q}$ pair. This can be understood in the following way. Consider a hadron emitted by a quark with longitudinal and transverse momentum components $p_{\parallel}$ and p_T relative to the quark direction of flight (Fig. 27). If the average p_T is energy inde-

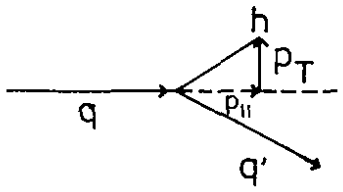

Fig. 27 Hadron emission by a quark

pendent and the average particle multiplicity <n> grows only slowly with energy then for high energies

$$\langle p_{\parallel} \rangle \approx \langle p \rangle \approx \frac{W}{\langle n \rangle} \tag{26}$$

and $$\frac{\langle p_T \rangle}{\langle p_{\parallel} \rangle} \sim W^{-1}. \tag{27}$$

The produced hadrons will be emitted more and more closely to the primary quark direction as the energy increases. The mean half opening angle of the jet cones is given by $\langle \delta \rangle \approx \frac{\langle p_T \rangle}{\langle p_{\parallel} \rangle}$; thus the jet cones shrink roughly $\sim W^{-1}$. (Actually, in a realistic calculation of the quark model using the fragmentation functions of Field and Feynman (1978) one finds $\langle \delta \rangle \sim W^{-1/2}$).

The presence of a two-jet structure is commonly tested in terms of sphericity, S (Bjorken and Brodsky 1970) and thrust, T (Brandt et al. 1964, and Fahri 1977):

$$\begin{aligned} S &= 3/2 \ \text{Min} \ (\Sigma p_{Ti}^2)/(\Sigma p_i^2) \qquad 0 \leq S \leq 1 \\ T &= \text{Max} \ (\Sigma |p_{\parallel i}|)/(\Sigma p_i) \qquad 0.5 \leq T \leq 1 \end{aligned} \tag{28}$$

Sphericity measures approximately the square of the jet cone half opening angle,

$$S \approx 3/2 \ \langle \delta^2 \rangle$$

Extreme jettiness ($\delta = 0$) leads to $S = 0$ and $T = 1$ while for spherical events $S \to 1$ and $T \to 0.5$.

The two-jet structure of hadronic events produced by e^+e^- annihilation was first observed in 1975 by the SLAC-LBL group (Hanson et al. 1975). Fig. 28 shows the energy dependence of the average sphericity as measured at DORIS and PETRA. At low energies, $W \lesssim 4$ GeV, the observed $\langle S \rangle$ values are close to those predicted by phase space, $\langle S \rangle \approx 0.4$. Above 5 GeV $\langle S \rangle$ decreases rapidly with increasing W, i.e. the particles become more and more collimated in clear distinction to a phase space behaviour. A power law, $\langle S \rangle = 0.8\ W^{-1/2}$ describes the data well. The jet cone half opening angle as inferred from $\langle S \rangle$ shrinks from $\sim 31^\circ$ at W = 4 GeV to $\sim 17^\circ$ near 36 GeV.

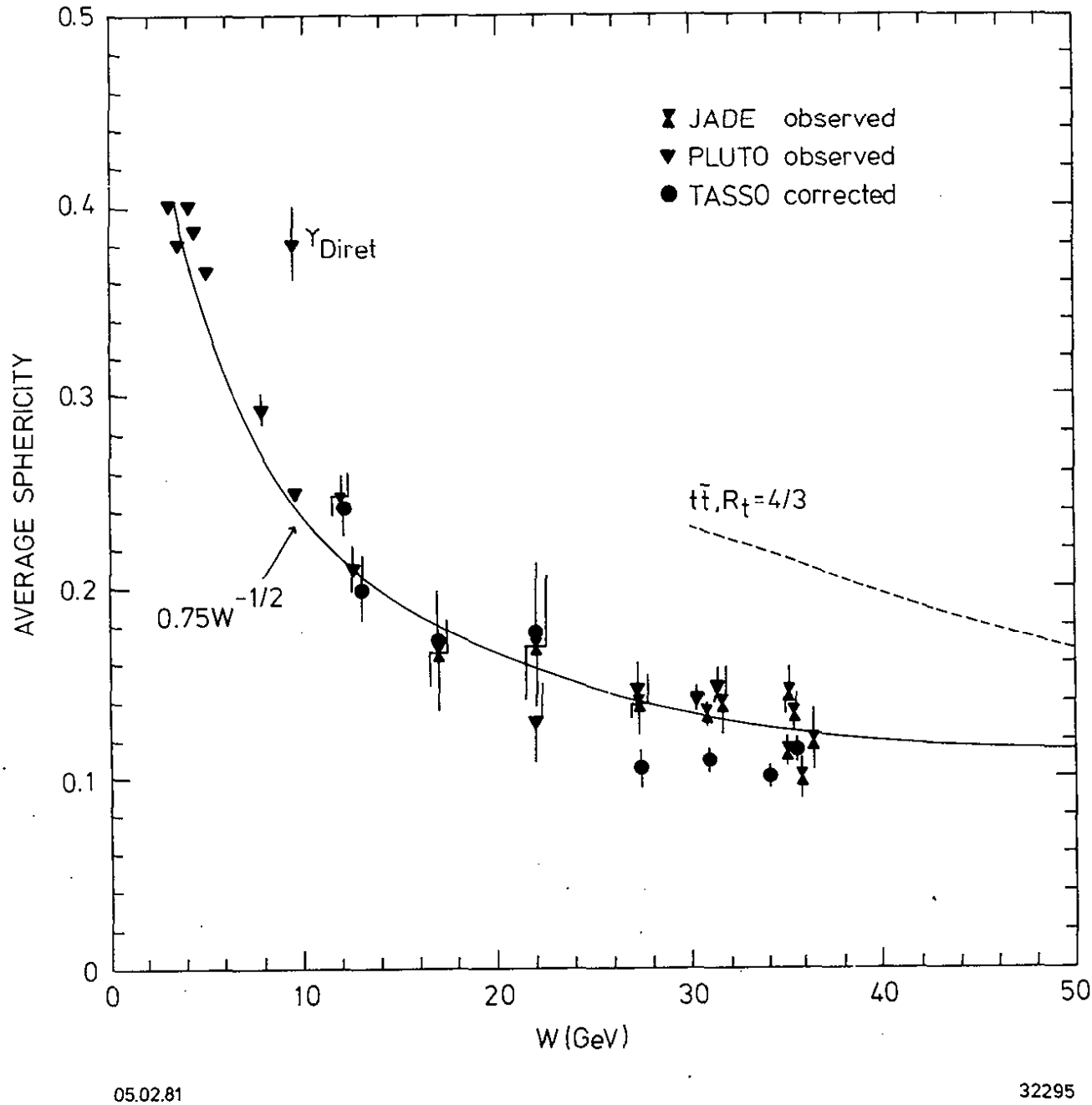

Fig. 28 The average sphericity as measured by the JADE, PLUTO and TASSO groups (see Cords 1980).

Fig. 29 shows a typical two-jet event at W = 35 GeV.

3) The jet angular distribution

The angular distribution of the jet axis relative to the beam axis is of the form (Schwitters et a. 1975)

$$W(\cos\Theta_{jet}) \sim 1 + \cos^2\Theta_{jet}$$

in agreement with what is expected for production of a pair of spin 1/2 particles. For comparison spin 0 particles would lead to $W(\cos\Theta_{jet}) \sim 1 - \cos^2\Theta_{jet}$. Fig. 30 shows a measurement of $W(\cos\Theta_{jet})$ for two-jet events at high energies (W = 30 - 36 GeV). The agreement with the $1 + \cos^2\Theta_{jet}$ form (solid curve) is good.

4) Long range charge correlations

The back-to-back produced quarks have opposite charge. Since in the standard picture of quark fragmentation the primary quark is found predominantly in one of the fast particles, one expects a correlation between the charges of leading particles in opposite jets. Besides this long range correlation also a short range charge correlation is expected since neighbouring particles in the jet cascade should have preferrentially opposite charges. First evidence for long range correlations was presented by the TASSO group (Brandelik et al. 1981b). The effect was established in two ways, from a study of the weighted jet charges and from charge correlations measured as a function of rapidity along the jet axis. The first method goes back to a suggestion by Field and Feynman (1978) who proposed to use the momentum weighted jet charge

$$q_{jet}(\gamma) = \sum_{i=1}^{n_{jet}} e_i \, x_i^{\gamma} \qquad (29)$$

as a measure of the charge of the parton that initiated the jet. In eq.(29) the charge of the i'th particle e_i in the jet is weighted with a power γ of its fractional momentum $x_i = p_i/p_{beam}$; n_{jet} is the number of particles in the jet. According to current ideas on fragmentation a fast particle has a larger probability to contain the primary parton as a constituent than a slow one. Therefore the weighted charge $q_{jet}(\gamma)$ for positive exponents γ is expected to be more strongly correlated to the primary parton charge than the unweighted jet charge $Q_{jet} = q_{jet}(0)$. It is convenient to take out the strong γ dependence of q_{jet} by introducing the quantity q'_{jet}:

$$q_{jet}(\gamma) \rightarrow q'_{jet}(\gamma) = \frac{\sum x_i^{\gamma}}{\sum x_i^{2\gamma}} \, q_{jet}(\gamma) \qquad (30)$$

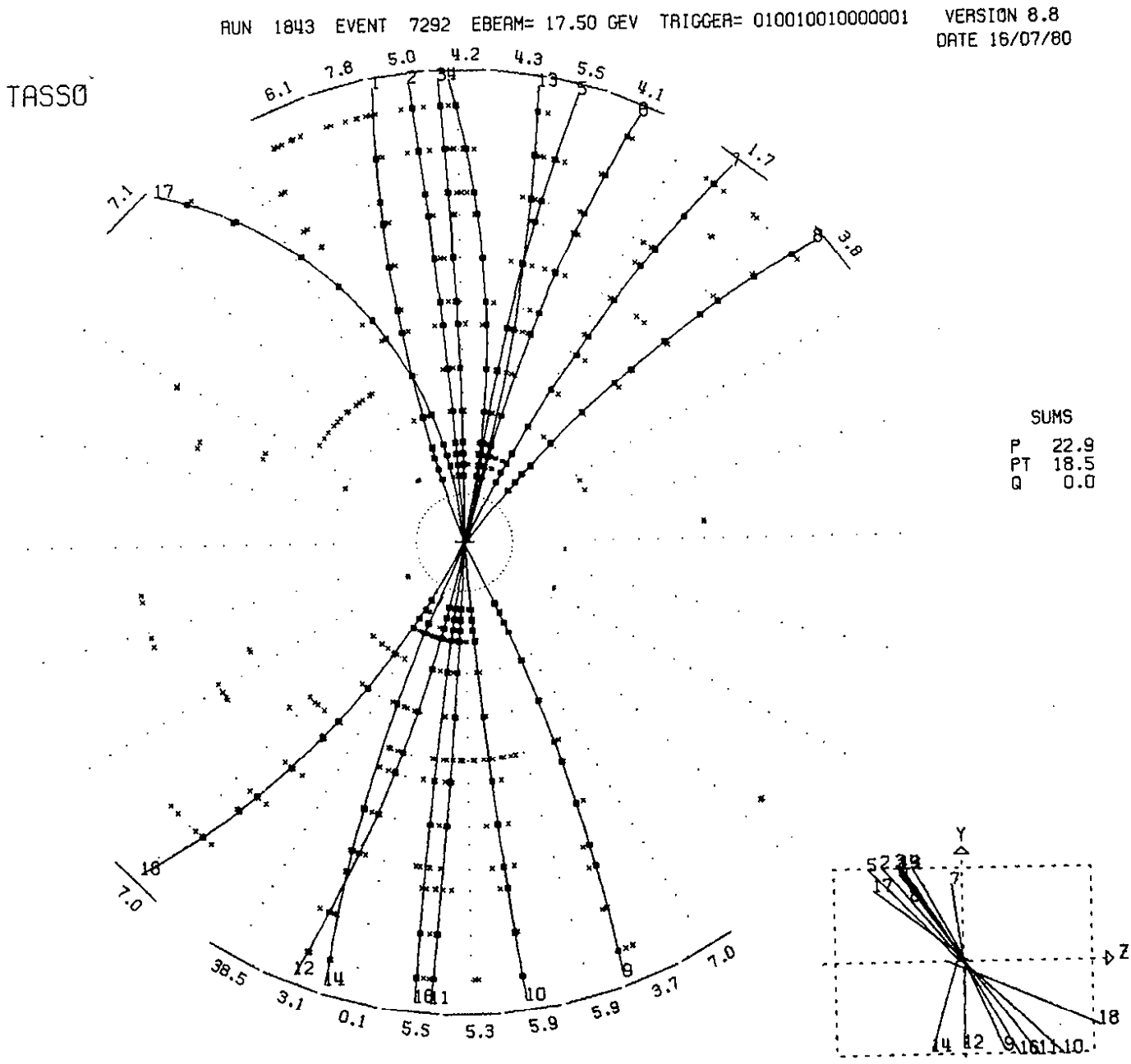

Fig. 29 A two-jet events as observed at W = 35 GeV in the TASSO detector.

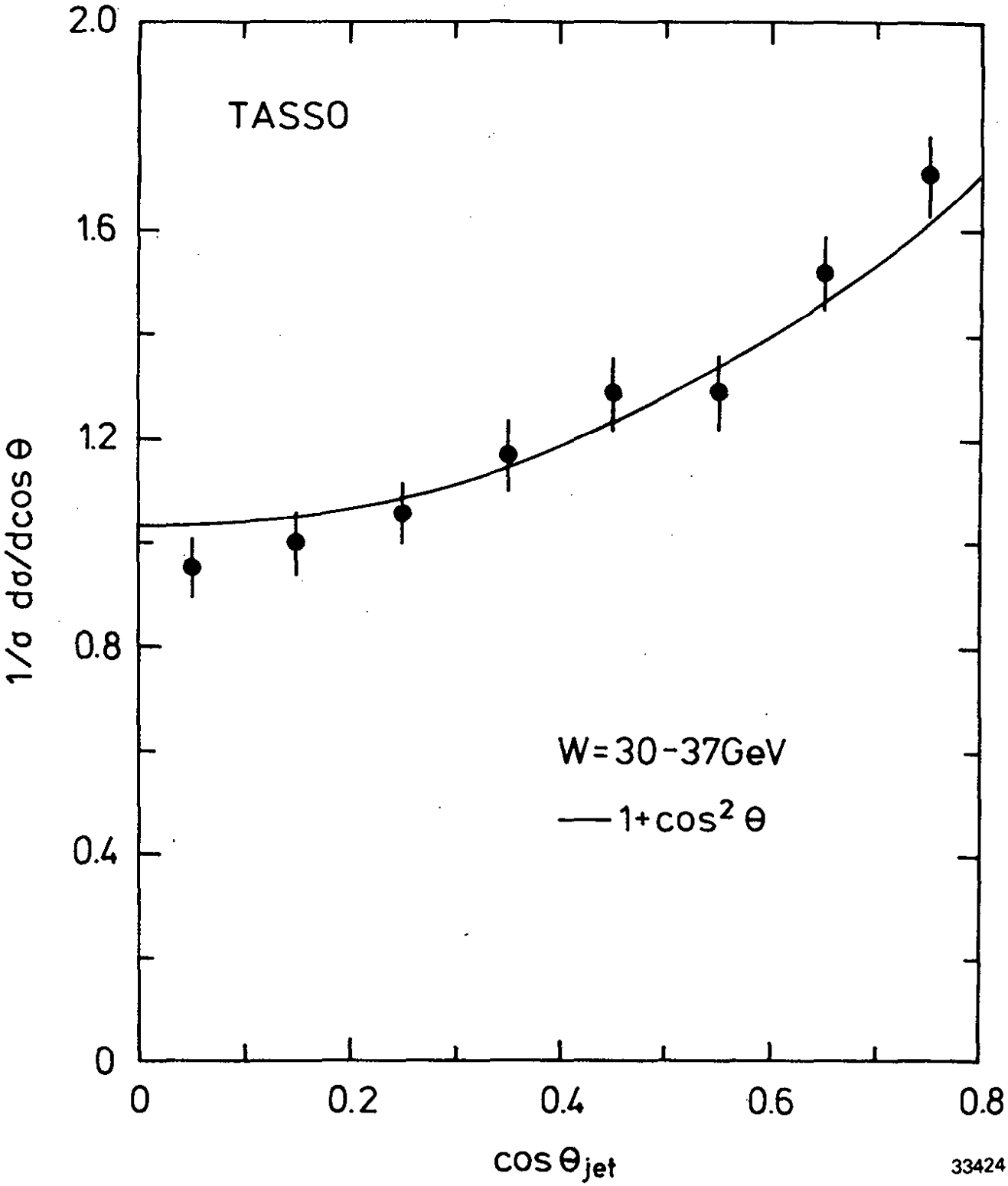

Fig. 30 Angular distribution of the jet axis for two-jet events as measured by TASSO at W = 30 - 37 GeV.

Consider now the average product of weighted charges

$$P'(\gamma) = - \langle q_1'(\gamma)\, q_2'(\gamma) \rangle \qquad (31)$$

of the two jets in an event where < > denotes the average over the event sample. Fig. 31a shows $P'(\gamma)$ for all two-jet events at W = 27.4 - 36.7 GeV. The data show a small but positive value for $P'(\gamma)$. However, this could be a trivial consequence of charge conservation: if there is a net positive charge in one jet there has to be a net negative charge of the same magnitude in the opposite jet. The contribution of charge conservation to $P'(\gamma)$ was determined by randomly redistributing in each jet the observed particle charges amongst the particles of the jet. This yields $P'^{rand}(\gamma)$ which is shown by the solid curve. For $\gamma \leq 1$ it is seen to be of almost the same size as $P'(\gamma)$, i.e. most of the value of $P'(\gamma)$ is a result of charge conservation. This is no longer so if one requires each jet to have at least one particle with fractional momentum $x > x_0 = 0.35$ (see Fig. 31b). In this case $P'(\gamma)$ is clearly larger than P'^{rand} which shows that the fastest particles in opposite jets know about their relative charge.

We shall discuss the study of charge correlations with respect to the rapidity y in a rather superficial manner. For the mathematical details the reader is referred to the paper of Brandelik et al. (1981). The analysis is illustrated in Fig. 32, where y is defined in terms of the particle energy and longitudinal momentum $p_{\parallel}$ relative to the jet axis, $y = 0.5\, \ell n\, [(E + p_{\parallel})/(E - p_{\parallel})]$. We consider now a reference particle with charge $e_i(y')$ at position y' and ask where is its charge compensated. The answer is given by the charge compensation probability which, roughly speaking, is defined by

$$C(y,y') = \frac{N^{+-}(y,y') + N^{-+}(y,y') - N^{++}(y,y') + N^{--}(y,y')}{N(y')} \qquad (32)$$

where $N^{+-}(y,y')$ is the two-particle density for having a positive particle in the internal $y, y + \Delta y$ and a negative particle in $y', y' + \Delta y$; similar definitions hold for N^{-+}, N^{++} and N^{--}. $N(y')$ measures the particle density at $y', y' + \Delta y'$.

Consider an idealized two-jet event (Fig. 32c) with the fastest particles in jet 1 and jet 2 being positive and negative, respectively, and exactly one positive and one negative particle in all other y intervals. If the fastest particle in jet 1 (position y' in Fig. 32d) is chosen as the reference particle, C is zero everywhere except for the interval containing the fastest particle in the

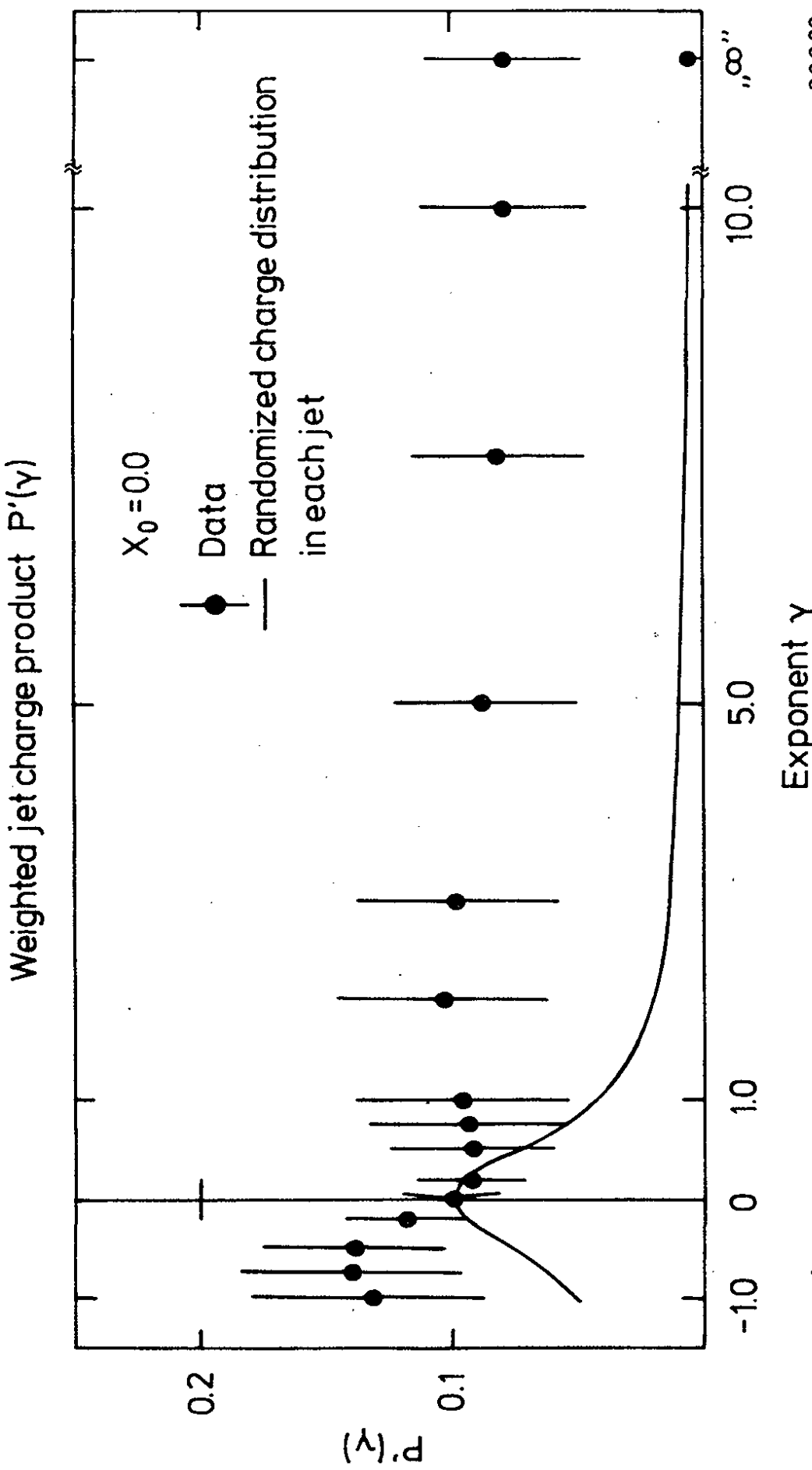

Fig. 31a The momentum-weighted jet charge product P'(γ) as a function of the exponent γ for events having in each jet at least one particle with fractional momentum $x > x_0$. The solid line shows the expectation for a charge distribution randomized in each jet. From TASSO (Brandelik et al. 1981b).

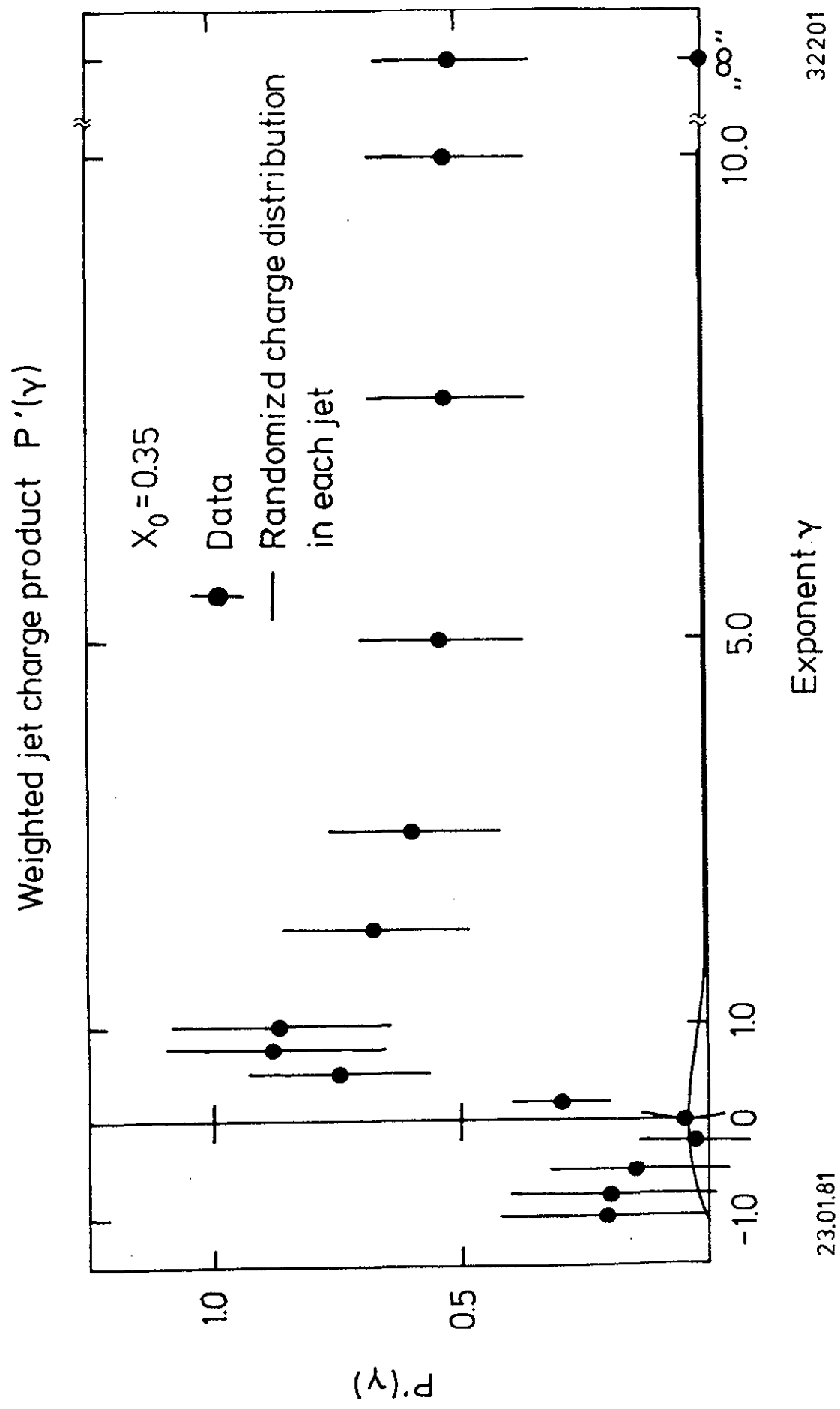

Fig. 31b Same as Fig. 31a for $X_o > 0.35$

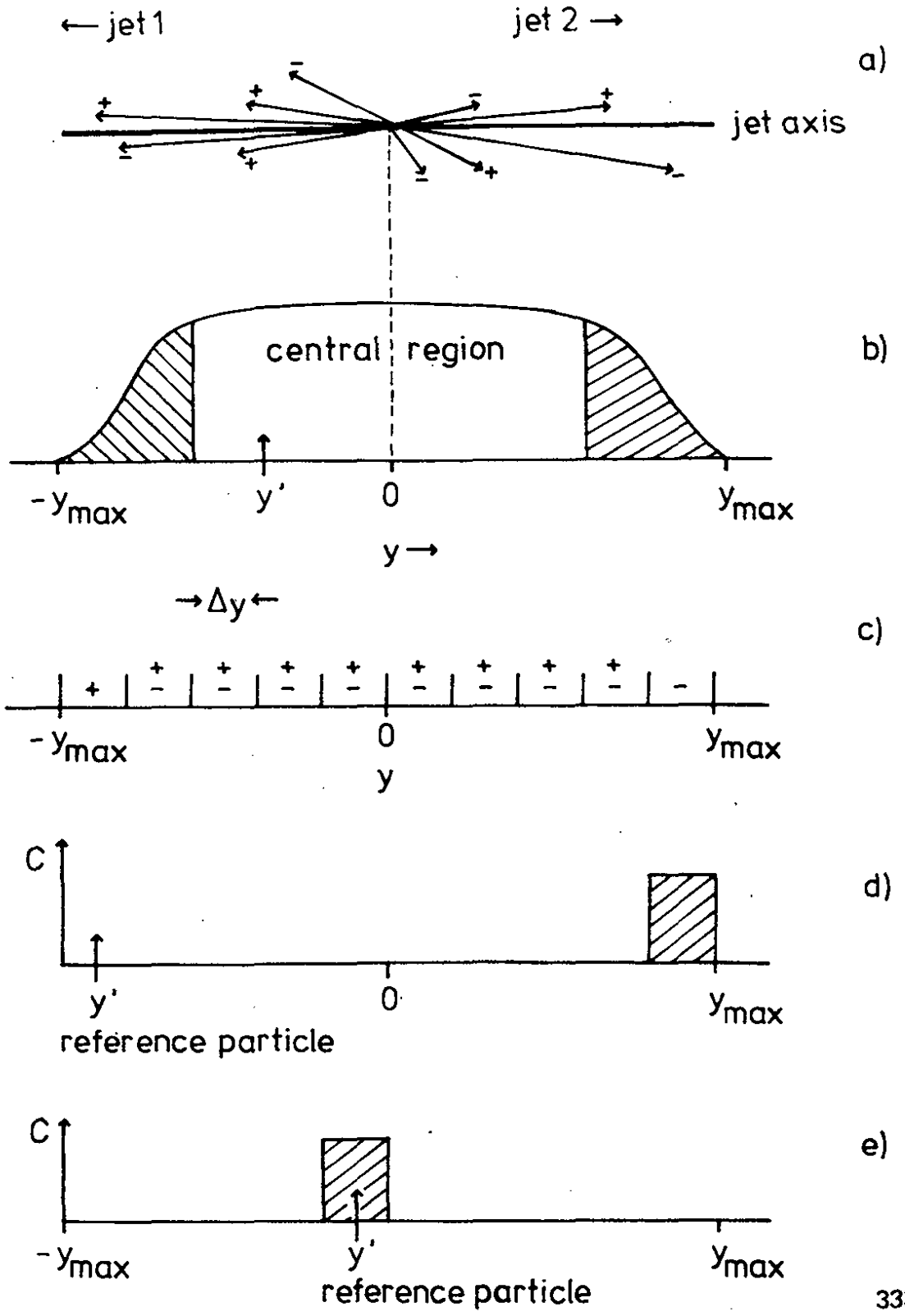

Fig. 32 Illustration of the charge correlation studies
a) particle vectors in a two-jet event
b) rapidity distribution; y' indicates the position of the reference particle
c) idealized charge distribution along the rapidity axis. For this case (d) shows the value of the charge compensation C if the reference particle is at y' in the fragmentation region of jet 1 and (d) in the central region.

opposite jet. This is called a long range correlation. If, on the other hand, the reference particle is in the central region (y' near zero, see Fig. 32e) we have a short range correlation: C is nonzero at y = y' and zero everywhere else.

Fig. 33 shows the properly defined charge compensation probability $\tilde{\Phi}_r(y,y')$ as a function of y for various positions y' of the reference particle, indicated by the shaded area. Also shown is $\tilde{\Phi}_r^{rand}$ which is obtained when the charges are distributed randomly amongst the charged particles of an event (open circles). In contradistinction to $\tilde{\Phi}_r^{rand}$, $\tilde{\Phi}_r$ shows a clear peak centered near the position y' of the reference particle which moves with y' as y' is moved from the central region to the fragmentation region of one jet. This is evidence for the presence of short range charge correlations also observed in hadron-hadron collisions (Drijard et al. 1979, 1980).

When moving out to higher values of |y'| $\tilde{\Phi}_r$ exhibits, besides the peak at $y \approx y'$, an increasing skewness, showing finally for $-2.5 > y' > -5.5$ a long tail in the opposite jet, $y > 0$. This demonstrates the presence of long range charge correlations. The probability that the charge of a particle at $y' < -2.5$ is compensated in the opposite jet at $y > 1$ is found to be $(15.4 \pm 2.6)\%$. The observed long range correlation proves that the primary partons which produce the particlejets are charged, in agreement with the assumption that these partons are quarks.

The strong evidence for the quark parton model make e^+e^- annihilations into hadrons a good place to test strong interaction theories, in particular, Quantum Chromodynamics (QCD). Before comparing QCD with the data we remind the reader of some of the ingredients of QCD.

6.2 Elements of QCD

QCD (Nambu 1966, Fritzsch & Gell-Mann 1972, Fritzsch et al. 1973, Weinberg 1973, Gross & Wilczek 1973) describes the interaction between quarks. The force is provided by the exchange of gluons (see Fig. 34a) in much the same way proton and electron are bound in the hydrogen atom by photon exchange (Fig. 34b).

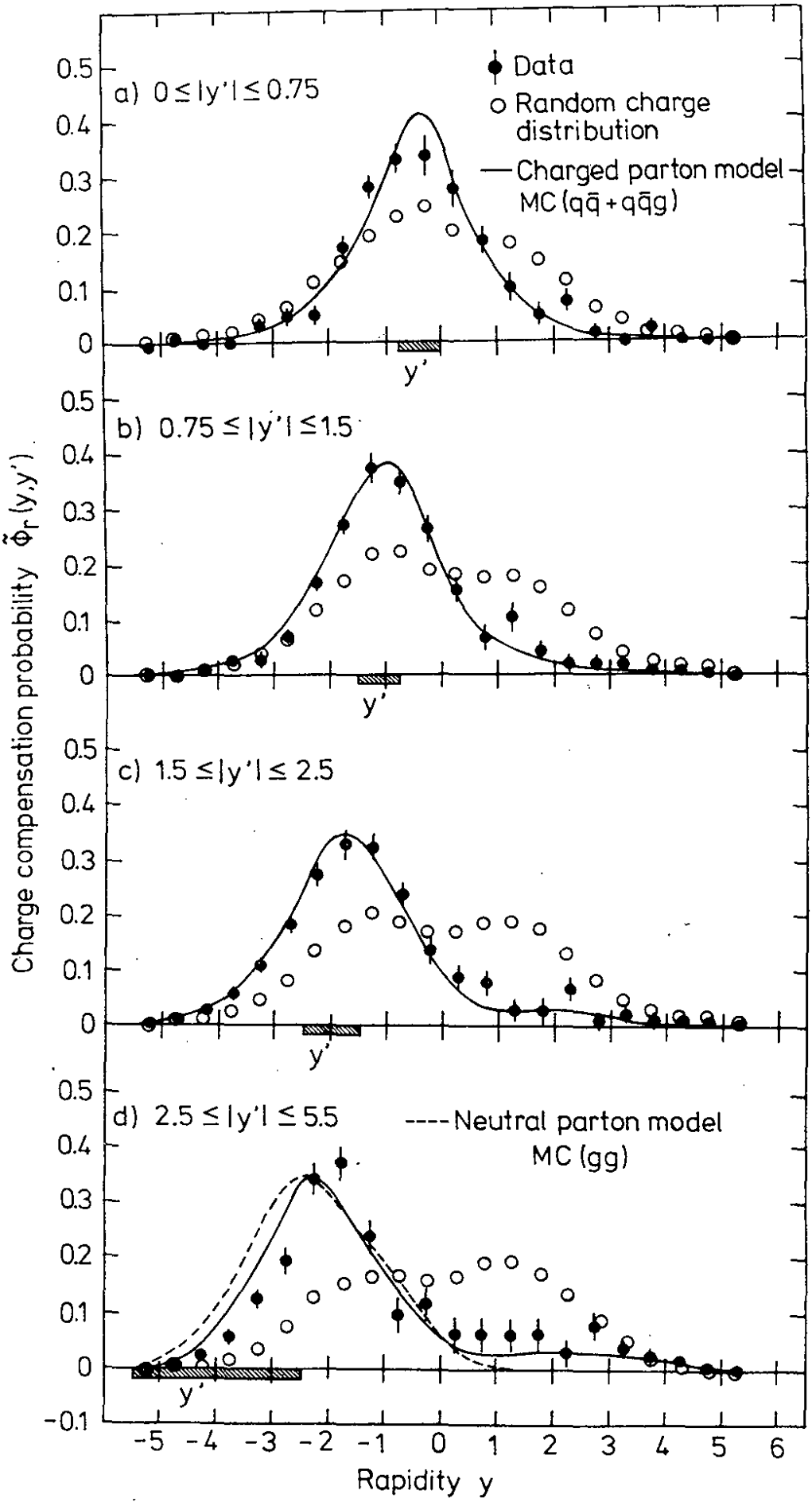

Fig. 33 Charge compensation probability $\tilde{\Phi}_r(y,y')$ as a function of rapidity y for a particle produced at y', as measured by TASSO (Brandelik et al.1981b). The open circles show the expectation for a charge distribution randomized over the whole event, $\tilde{\Phi}_r^{rand}(y,y')$. The solid line shows the prediction of model MC($q\bar{q}$ + qqg), the dashed line the prediction of a neutral parton model MC(gg).

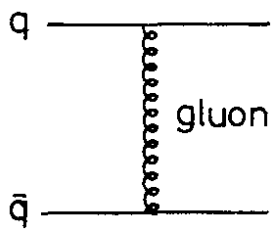

Fig. 34a $q\bar{q}$ system bound by gluon exchange

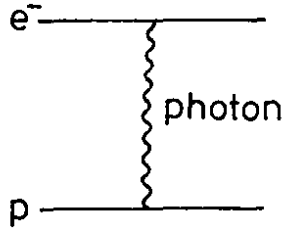

Fig. 34b electron and proton bound in the hydrogen atom by photon exchange

The properties of gluons are:

- mass $m = 0$
- spin, parity $J^P = 1^-$
- gluons are colour octet states. There are 8 different gluons. They interact with the colour charges of the quarks (see Fig.35).

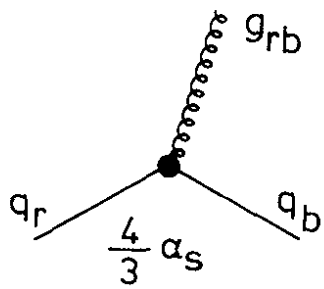

Fig. 35 Quark-gluon interaction

- The gluon quark coupling strength α_s is independent of the quark type (or flavour), i.e. α_s is the same for u, d, s, ...
- In contrast to photons, which are electromagnetically neutral, gluons carry colour charge. As a result gluons can interact with themselves which leads to the presence of three- and four gluon vertices (Fig.36) in the theory.

Fig. 36 Three- and four-gluon vertices

- The coupling strength α_s is not constant (running coupling constant). In lowest order

$$\alpha_s = \frac{12\pi}{(33-2N_f)\,\ell n\, Q^2/\Lambda^2} \tag{33}$$

where N_f is the number of different quark types, Q^2 the characteristic momentum transfer and Λ is the QCD scale parameter. The Q^2 behaviour of α_s is sketched in Fig. 37. The coupling strength decreases with increasing Q^2 consistent with asymptotic freedom. That is to say, for small distances (large Q^2) between quarks α_s becomes small and the quarks behave as free. For low Q^2 or large distances ($Q^2 \to \Lambda^2$) α_s will become of order one and confinement may arise: quarks never become free; in this regime perturbation theory becomes invalid.

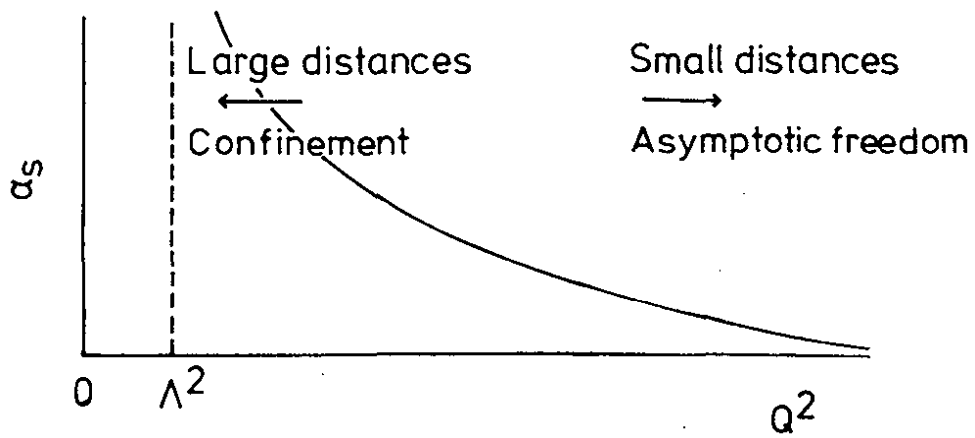

Fig. 37 Qualitative behaviour of the strong coupling strength α_s

The most stringent tests of QCD are provided by large Q^3 processes where perturbative methods can be used. Examples are deep inelastic lepton nucleon scattering and e^+e^- annihilation at high energies. We shall concentrate on the latter field with the emphasis on R and jet production.

6.3 QCD modifications to R

The predictions of the quark parton model are modified by the emission of gluons (see Fig. 38). For R the QCD

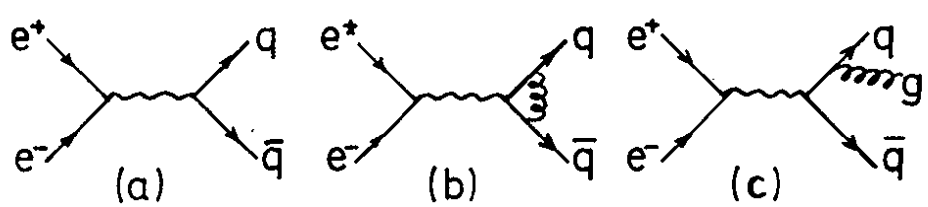

Fig. 38 Quark parton diagram and lowest order QCD diagrams for $e^+e^- \to q\bar{q}$, $q\bar{q}g$

corrected expression is

$$R = 3 \sum_q e_q^2 \left\{1 + \frac{\alpha_s}{\pi} + C_2 \left(\frac{\alpha_s}{\pi}\right)^2 + \ldots\right\} \qquad (34)$$

The corrections have been computed up to second order (Dine & Sapirstein 1979, Chetyrkin et al. 1979, Celmaster & Gonsalves 1979). In the $\overline{MS}$ scheme

$$C_2 = 1.99 - 0.12\, N_f$$

where N_f is the number of quark flavours.

After a careful examination of the theoretical problems at low energy ($W < 2$ GeV) Eidelman et al. (1979) deduced from low energy σ_{tot} data a value of $\Lambda \approx 0.1$ GeV. QCD fits to the intermediate energy region (4 to 7 GeV) have been performed by Barnett et al. (1980). We compare the QCD expression to the data measured above 20 GeV. This energy region is well above heavy quark thresholds; furthermore, higher twist effects should be negligible. The average over all PETRA experiments gives

$$\bar{R} = 3.91 \pm 0.04 \text{ (stat.)} \pm 0.3 \text{ (syst.)}$$

for $\bar{W} = 33$ GeV. After corrections for weak neutral current contributions (which amount to $\Delta\bar{R}_{weak} = 0.03$ for $\sin^2\theta_W = 0.228$) one obtains $\alpha_s = 0.16 \pm 0.03$ (stat.) ± 0.26 (syst.). In Fig. 39 the QCD prediction for $\Lambda = 0.3$ GeV is compared to the data (note that only statistical errors are shown). The agreement is good. Unfortunately, the large systematic uncertainty of R prevents a precise determination of α_s. Still, the data show that the second order contribution is smaller than the first order one, i.e. $C_2\left(\frac{\alpha_s}{\pi}\right)^2 < \frac{\alpha_s}{\pi}$ suggesting that the perturbative calculation is reliable.

For a detailed discussion of possible weak contributions to R see Bartel et al. (1981b), Barber et al. (1981a) and Branson (1981).

6.4 Gluon bremsstrahlung

At high e^+e^- energies the acceleration of the quarks in $q\bar{q}$ formation becomes so large that the quarks have a fair chance to radiate a hard gluon. This offers the possibility to observe gluons directly (Polyakov 1975, Ellis et al. 1976, De Grand et al. 1977, Hoyer et al. 1979, Kramer et al. 1978, 1979, 1980).

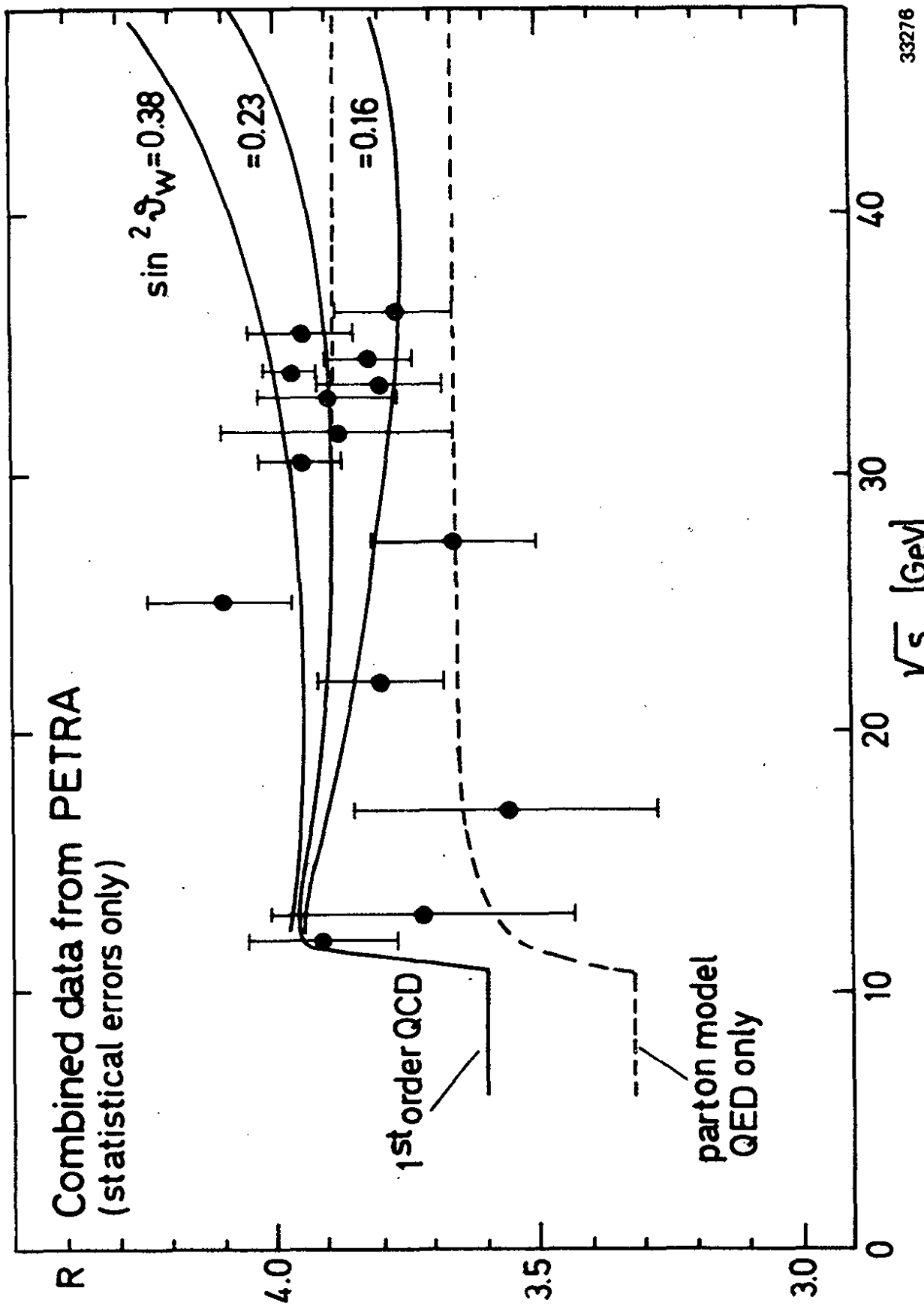

Fig. 39 The ratio R for the high energy region. The data points are averages over the PETRA experiments. The dashed curve indicates the quark parton prediction corrected for quark mass effects. The solid curves show the QCD prediction with Λ = 0.3 GeV for different values of $\sin^2\Theta_W$. From Felst (1981).

Denoting by x_1, x_2 the fractional energies of the quarks, $x_i = 2E_i/W$, the cross section for gluon emission (see diagram in Fig. 40),

$$e^+e^- \to q\bar{q}g \tag{35}$$

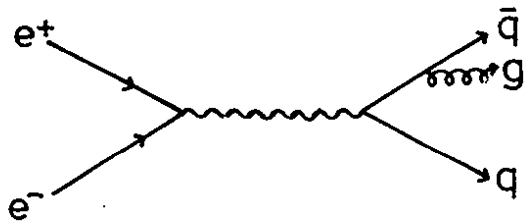

Fig. 40 First order QCD diagram for $e^+e^- \to q\bar{q}g$

is given by (Ellis et al. 1976, De Grand et al. 1977):

$$\frac{d\sigma(q\bar{q}g)}{dx_1 dx_2} = \frac{2\alpha_s}{3\pi}\sigma_o \frac{x_1^2 + x_2^2}{(1-x_1)(1-x_2)} \tag{36}$$

where $\sigma_o = 3\sigma_{\mu\mu}\sum e_q^2$. The energy and angular distribution of the radiated gluon is equal to that of bremsstrahlung photons. For small gluon energies K and angles θ (see Fig. 41)

$$\frac{d\sigma(q\bar{q}g)}{dK d\theta} \sim \frac{\alpha_s}{K\sin\theta} \tag{37}$$

Fig. 41 Illustration of the process $e^+e^- \to q\bar{q}g$

Since gluons are coloured we cannot observe them as free particles. Like quarks they materialize into a jet of hadrons. The emission of hard noncollinear gluons changes the event structure from back-to-back jets to a more complicated one. The most conspicuous effects predicted are (Ellis et al. 1976, De Grand et al. 1977)

1) Broadening of the transverse momentum (p_T) distribution of hadrons relative to a common jet axis with increasing c.m. energy W. The reason for this is

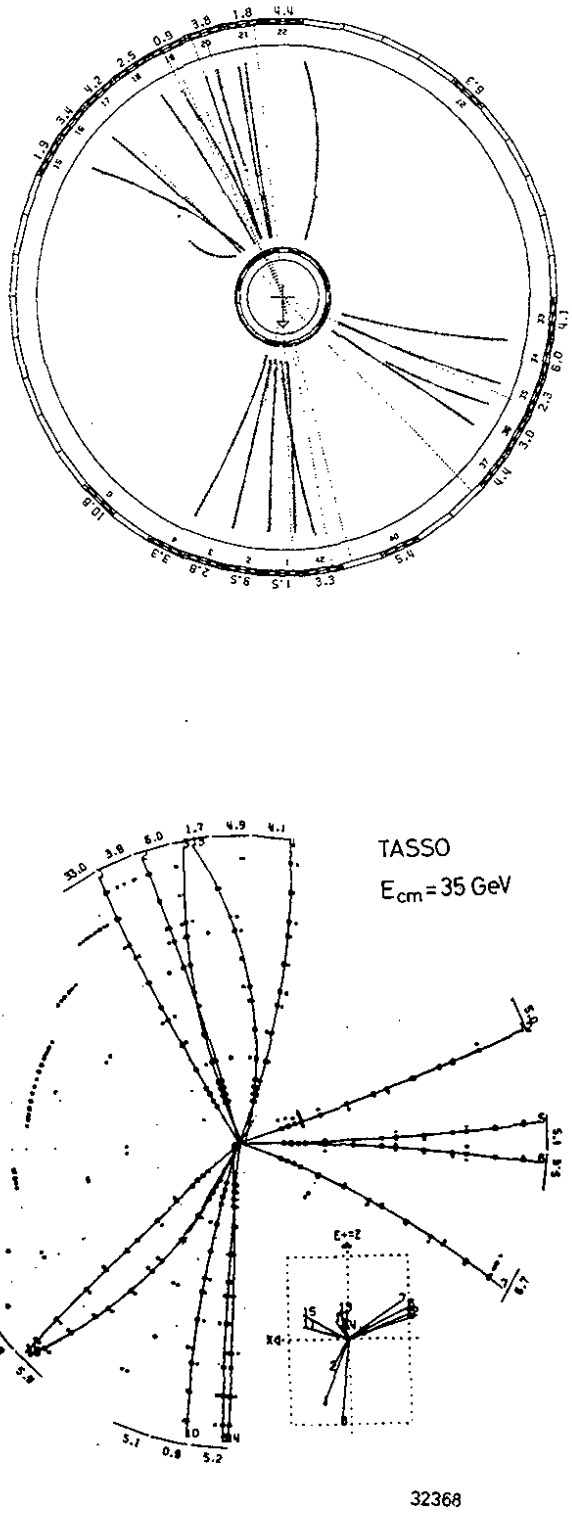

Fig. 42 Examples of three-jet events as observed in the TASSO and JADE detectors.

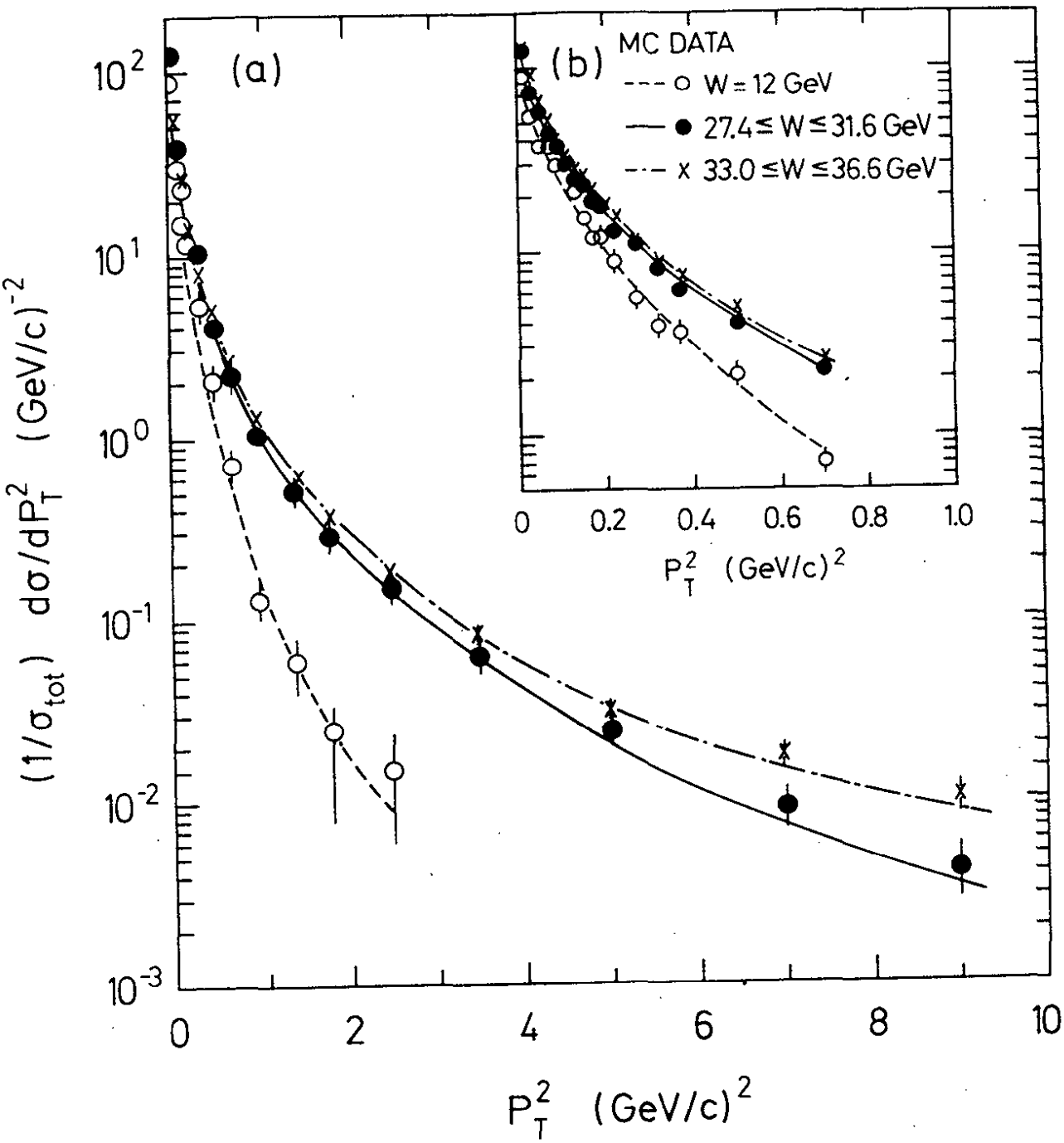

Fig. 43 Distribution of the square of the transverse momentum of charged particles with respect to the jet axis at 12, 27.4 - 31.6 and 35 - 36.6 GeV as measured by the TASSO group (Brandelik et al. 1979a, Brandelik et al. 1981b). The curves show the QCD prediction for $\alpha_s = 0.17$.

that the average transverse momentum of the gluon, K_T, grows with W like

$$\langle K_T \rangle \sim \alpha_s W \tag{38}$$

2) Presence of planar events since $q,\bar{q}$ and g lie in a plane.

3) Occurrence of events with a three-jet structure.

All three effects have been observed almost instantaneously when PETRA reached energies around 30 GeV in summer 1979 (Brandelik et al. 1979, Barber et al. 1979, Berger et al. 1979, Bartel et al. 1980b). Roughly 10 % of the hadronic events observed at W = 30 - 36 GeV are non two-jet events and half of these have a clear three jet structure. Two examples of three jet events are shown in Fig. 42.

In discussing the experimental evidence, we begin by showing in Fig. 43 the transverse momentum distribution $1/\sigma_{tot}\ d\sigma/dp_T^2$ of charged particles evaluated with respect to the jet axis for c.m. energies between 12 and 36 GeV (Brandelik et al. 1979, 1981c). The broadening of the p_T^2 distribution with rising energy is clearly borne out by the data. The 12 GeV distribution is well fitted by the $q\bar{q}$ model using a gaussian p_T distribution with σ_q = 0.3 GeV/c. To fit the high energy data with the same model σ_q had to be increased to 0.45 GeV/c.

One of the several methods devised to study event shapes and test for planar events starts from the momentum tensor (Bjorken & Brodsky 1970). The method is similar to the characterization of an extended body by its ellipsoid of inertia. The tensor is formed from the N measured particle momenta:

$$M_{\alpha\beta} = \sum_{j=1}^{N} p_{j\alpha}\, p_{j\beta} \qquad \alpha,\beta = x,y,z \tag{39}$$

Let $\hat{n}_1$, $\hat{n}_2$ and $\hat{n}_3$ be the eigenvectors of this tensor associated with the eigenvalues Λ_1, Λ_2 and Λ_3 which have been ordered such that $\Lambda_1 < \Lambda_2 < \Lambda_3$. The Λ_i give the sum of the squares of the momentum components with respect to the $\hat{n}_i$ axis:

$$\Lambda_i = \sum_j (p_j \hat{n}_i)^2 \tag{40}$$

The principal axis is the $\hat{n}_3$ direction which is identical to the jet axis. The event plane is spanned by $\hat{n}_2$ and $\hat{n}_3$; $\hat{n}_1$ defines the direction along which the sum of the momentum components is minimal (see Fig. 44).

Fig. 44 The momentum tensor ellipsoid and a 3 jet configuration

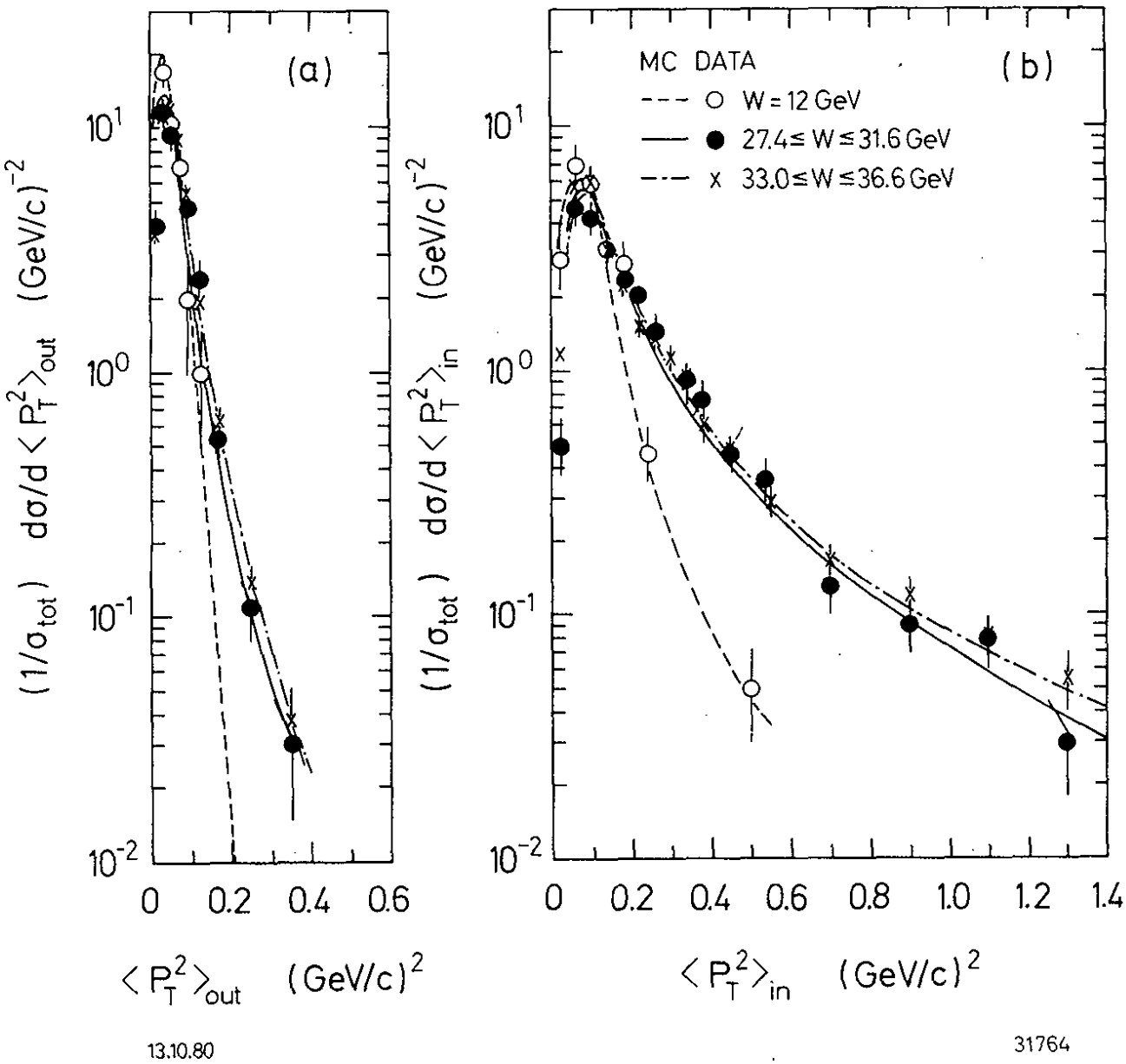

Fig. 45 Distribution of the mean transverse momentum squared per event for charged particles, normal to ($\langle p^2_{Tout}\rangle$) and in the ($\langle p^2_{Tin}\rangle$) event plane as measured by the TASSO group (Brandelik et al. 1979a, 1981b) at c.m. energies of 12, 27.4 - 31.6 and 33 - 36.6 GeV. The curves show the predictions for $\alpha_s = 0.17$.

The Λ_i measure the flatness (Λ_1), width (Λ_2) and length (Λ_3) of an event. In Fig. 45 the distribution of

$$\langle p_{out}^2 \rangle = \frac{1}{N} \sum (\vec{p}_j \cdot \hat{n}_1)^2 = \frac{\Lambda_1}{N} \tag{41}$$

(= square of momentum component normal to the event plane) is compared with that of

$$\langle p_{Tin}^2 \rangle = \frac{1}{N} \sum (\vec{p}_j \cdot \hat{n}_2)^2 = \frac{\Lambda_2}{N} \tag{42}$$

(= square of momentum component in the event plane and perpendicular to the jet axis). The data show little increase in $\langle p_{out}^2 \rangle$ from low (W = 12 GeV) to high energy (W = 30 to 36 GeV). There are basically no events with $\langle p_{Tout}^2 \rangle > 0.4$ (GeV/c)^2. The distribution of $\langle p_{Tin}^2 \rangle$, however, becomes much wider at high energies with a long tail of events with high $\langle p_{Tin}^2 \rangle$. The tail extends well beyond 1.2 (GeV/c)^2, i.e. for a fraction of the events $\langle p_{Tin}^2 \rangle >> \langle p_{Tout}^2 \rangle$. This demonstrates that the data contain a certain number of planar events (Brandelik et al. 1979, Berger et al. 1979, Bartel et al. 1980b). The same conclusion is reached when the energy flow around the jet axis is studied (Barber et al. 1979).

In order to test whether for planar events the particle momenta are distributed uniformly in the plane or collimated into three jets the TASSO group (Brandelik et al. 1979, 1980a) analysed all planar noncollinear events at W = 30 GeV as three jet events and determined the three jet axes. Fig. 46 shows the distribution of p_T^2 of the charged particles where the p_T of each particle was calculated with respect to the jet axis it had been associated with. The average transverse momentum is found to be about 0.3 GeV/c. The distribution is compared with the p_T^2 distribution of particles from events at W = 12 GeV analysed as two jets. The p_T^2 behaviour is found to be the same in both cases, i.e., the particles from planar events at high energies are collimated as closely around three coplanar axes as particles from lower energy events are collimated around a single jet axis.

The three jet structure of planar events can also be seen in the following way (Marshall 1981). The event is first analysed as a two-jet event. After summing the transverse momenta of particles in each jet, $\sum_{\text{jet}\alpha} p_{T_i}$, the narrow jet which has the smaller $\sum p_{T_i}$ is found.

Then, as illustrated in Fig. 47, the angular distribution of particles in the event plane is found with respect to the direction of the narrow jet. Θ is the

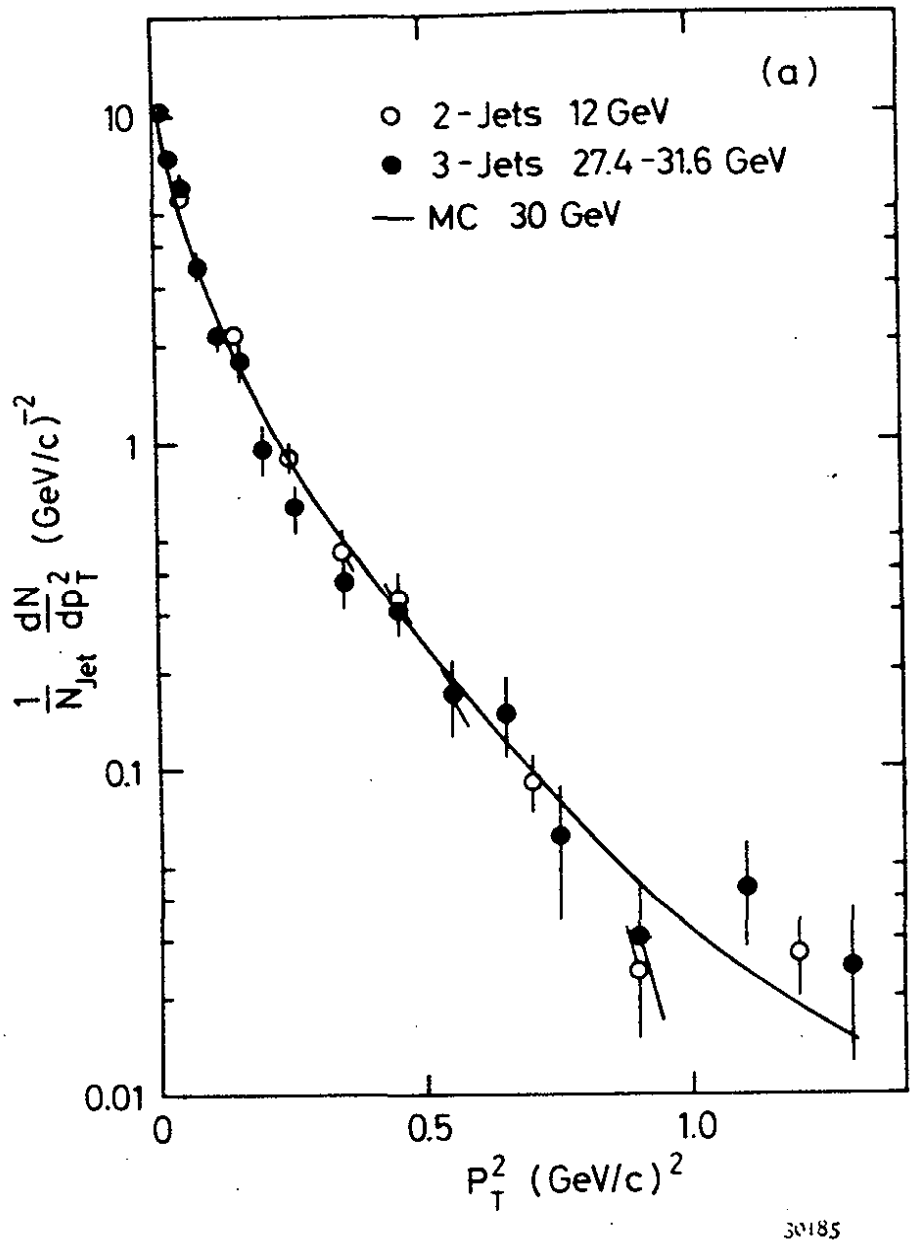

Fig. 46 Distribution of the square of the transverse momentum of charged hadrons from planar events with respect to the three axes found by the generalized sphericity method at W = 30 GeV (●). It is compared to the p_T^2 distribution relative to the sphericity axis for all events at W = 12 GeV analyzed as two jet events (o). The curve shows the QCD prediction for α_s = 0.17. The analysis was made by the TASSO group (Brandelik et al. 1980a).

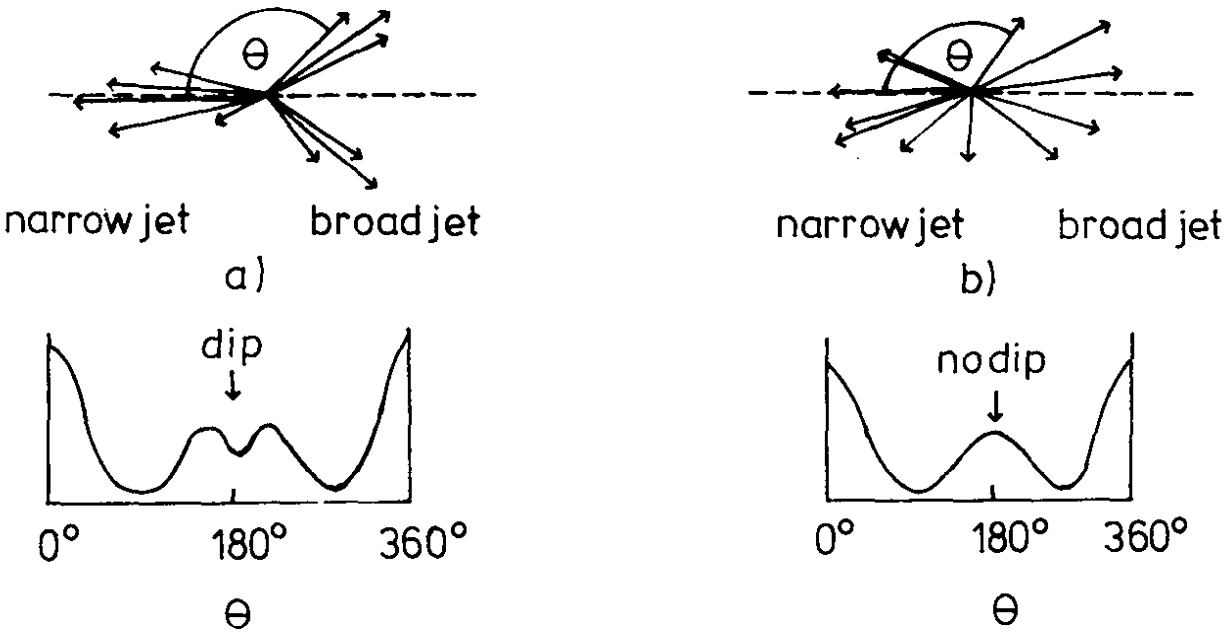

Fig. 47 Particle angular distribution in the event plane expected for three-jet production (a) and two-jet production (b).

angle between particle i projected into the event plane and the direction of the narrow jet. For a planar event with three-jet structure (Fig. 47a) no or only few particles will be found in the direction opposite to the narrow jet and the particle yield will show a dip at $\Theta = 180^{\circ}$. On the other hand, for a two-jet event (Fig. 47b) the angular distribution will show no dip at $\Theta = 180^{\circ}$. Fig. 48 shows the momentum weighted angular distribution for planar events. There is a narrow peak at $\Theta = 0^{\circ}$ which represents the particles in the narrow jet. In addition there is a broad distribution around $\Theta = 180^{\circ}$ which has a distinct dip at $\Theta = 180^{\circ}$ giving evidence to the three-jet nature of the events. The two bumps result from the two jets opposite the narrow jet.

6.5 Quantitative comparison of jet production with QCD

The observation of three-jet events is one of the great successes of QCD. It does, of course, not rule out other mechanisms as possible sources of these events. Therefore quantitative tests are called for. The quantitative comparison with QCD faces the problem that QCD predicts the parton distributions (e.g. for $q,\bar{q}$ and g in $e^+e^- \to q\bar{q}g$) but what can be observed experimentally are the particle jets. Since the hadronization process is not calculable in perturbative QCD one has to combine the QCD calculations with a model that describes quark and gluon fragmentation into hadrons. Most of the analyses have been done using the model of Field and Feynman (1978) where quark fragmentation into hadrons is treated as an iterative process: (see Fig. 49) a quark q fragments into a hadron h plus another quark q'.

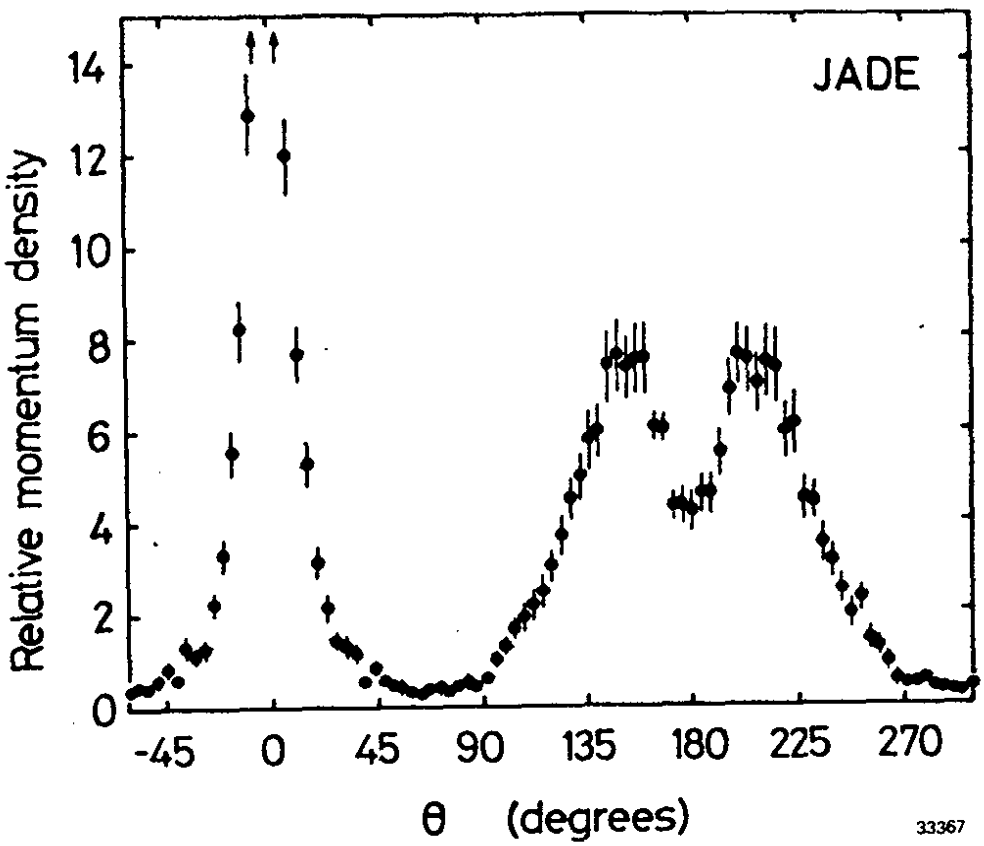

Fig. 48 The momentum weighted angular distribution of particles from planar events measured in the event plane $\Theta = 0^{o}$ is the direction of the narrow jet. From Marshall (1981).

Then q' fragments into h' plus q" and so on until the available energy/momentum is used up. The (three) fragmentation parameters

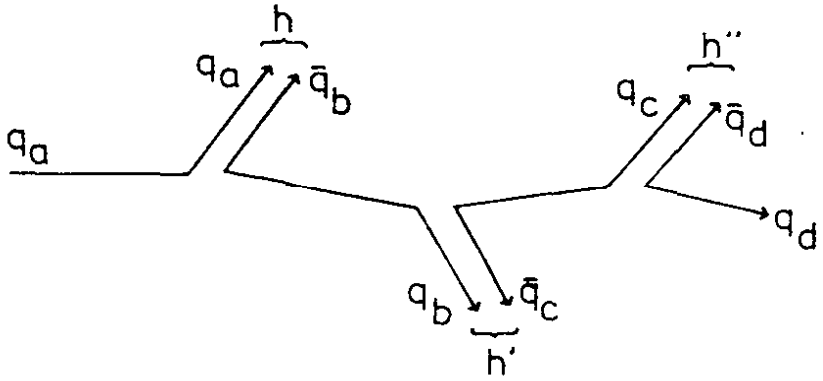

Fig. 49 Quark fragmentation into mesons in the Field-Feynman model

such as the average transverse momentum of the produced hadrons have to be determined from the data itself.

In the quantitative comparison of data with the QCD prediction, two elaborate Monte Carlo programs have played a major role, that of Hoyer et al. (1979) and an extension by Ali et al. (1980). The first one considers only contributions up to first order in α_s (first 3 diagrams in Fig. 50), the second one includes those second order terms that lead to four-jet events (diagrams at bottom of Fig. 50).

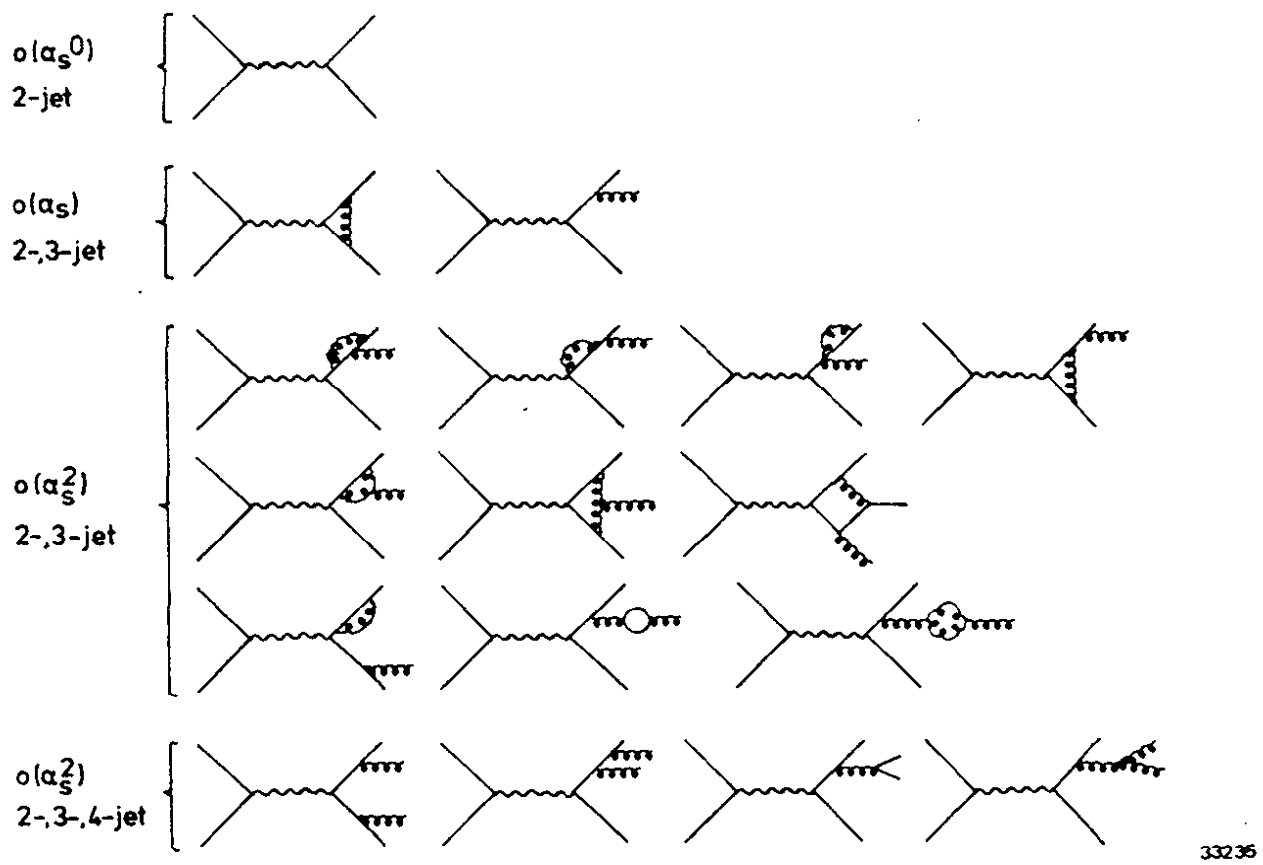

Fig. 50 Leading and next to leading order QCD diagrams for hadron production.

Both programs use the Field-Feynman scheme to describe quark fragmentation. In the analysis of the TASSO group (Brandelik et al. 1980a) the strategy followed was to determine first the fragmentation parameters and the strong coupling constant α_s, using as little of the measured information as possible (to be precise, the distributions at W = 30 GeV for $\langle p^2_{Tout}\rangle$, for the charge particle momenta and multiplicity) and then to use the remaining information for a quantitative check which then no longer involves any free parameter.* The fit yielded $\alpha_s = 0.17 \pm 0.02$ (stat.) $\pm$ 0.03 (syst.) at W = 30 GeV. The QCD predictions obtained in this way for p_T^2, $\langle p^2_{Tout}\rangle$, $\langle p^2_{Tin}\rangle$ and for the 3-jet p_T^2 are shown by the curves in Figs. 43, 45, 46. The agreement is excellent. In particular the strong c.m. energy dependence of the data for p_T^2 and $\langle p^2_{Tin}\rangle$ is well reproduced by QCD.

Similar conclusions have been reached by the other PETRA groups. Some of these results are presented in the Figs. 51 - 54.

6.6 The gluon spin

The angular correlation between $q,\bar{q}$ and gluon (see Fig. 65a) depends on the spin of the gluon. For vector gluons the first order cross section in terms of the scaled parton energies $x_i = 2E_i/W$ is given in eq. (36). From this the distribution of the angles Θ_i between the partons Θ_i can be calculated with the following relation:

$$x_i = \frac{2\sin\Theta_i}{\sin\Theta_1 + \sin\Theta_2 + \sin\Theta_3} \tag{43}$$

In order to see that the angular correlation between the jet axes is indeed sensitive to the spin of the gluon we also consider a theory with scalar gluons which lead to (Ellis et al. 1976):

$$\frac{d\sigma}{dx_1 dx_2} = \frac{\tilde{\alpha}_s}{3\pi}\,\sigma_o\,\frac{x_3^2}{(1-x_1)(1-x_2)} \tag{44}$$

where $x_3 = 2E_3/W$ for the gluon and $\tilde{\alpha}_s$ is the gluon quark coupling for the scalar case. The vector expression (eq. 36) has both collinear and infrared divergencies, whereas for the scalar case there is only a collinear divergence which leads to a somewhat weaker dependence on x_1. Unfortunately, the difference is largest when x_1 (or x_2) is near 1 where one approaches the two jet configuration, and where the quark and gluon jets become difficult to separate.

---

* A more thorough description of the treatment of hadronization can be found in Söding and Wolf (1981).

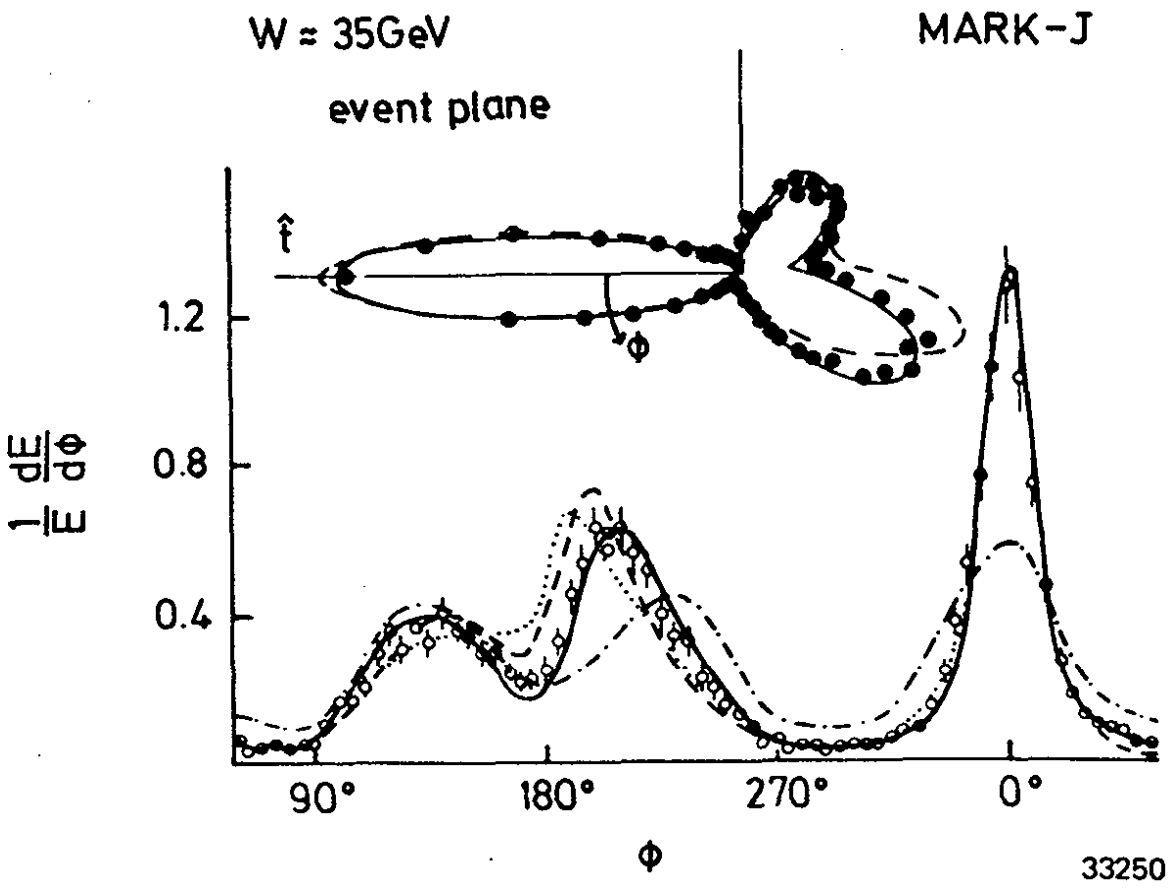

Fig. 51 Energy flow observed for planar events as a function of the azimuthal angle in the event plane relative to the thrust axis. From the MARK J group (Barber et al. 1981b). The curves show fits by i) a QCD calculation (full curve) with $\alpha_s = 0.18$; ii) a two-jet $q\bar{q}$ model with a Gaussian (dashed) or exponential (dotted) p_T distribution; iii) a pure phase space distribution (dashed-dotted curve).

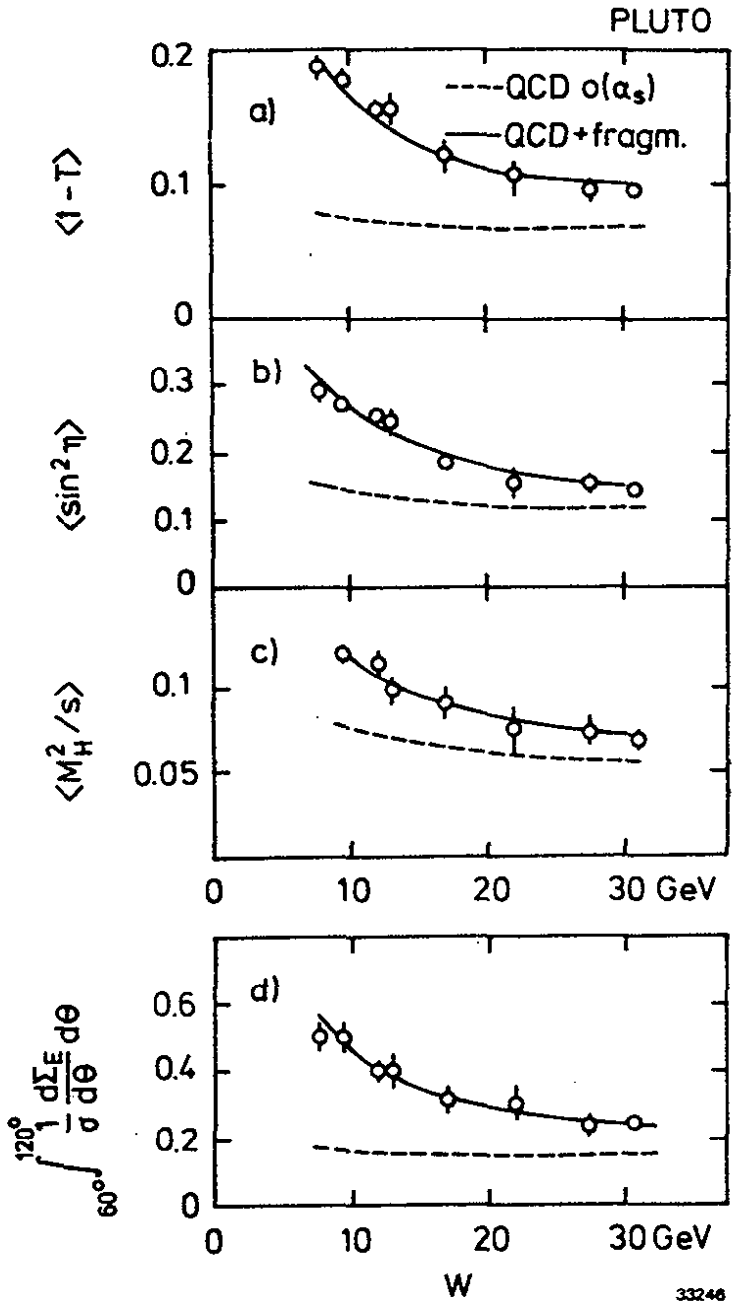

Fig. 52 W-dependence of average thrust, energy-weighted jet broadness, squared invariant mass of the "heavy" jet, and of the integral over the wide-angle part of the energy-energy correlation function in the reaction e^+e^- → hadrons measured by the PLUTO group (C.Berger et al. 1981b). The curves show the results of fits by a two-term formula $a/\ell n(W^2/\Lambda^2) + b/W$; the first term describes the logarithmic W-dependence of the $o(\alpha_s)$ QCD contributions (on the parton level), the second term approximates hadronization effects. From the size of the perturbative QCD terms one extracts $\alpha_s = 0.18 \pm 0.02$.

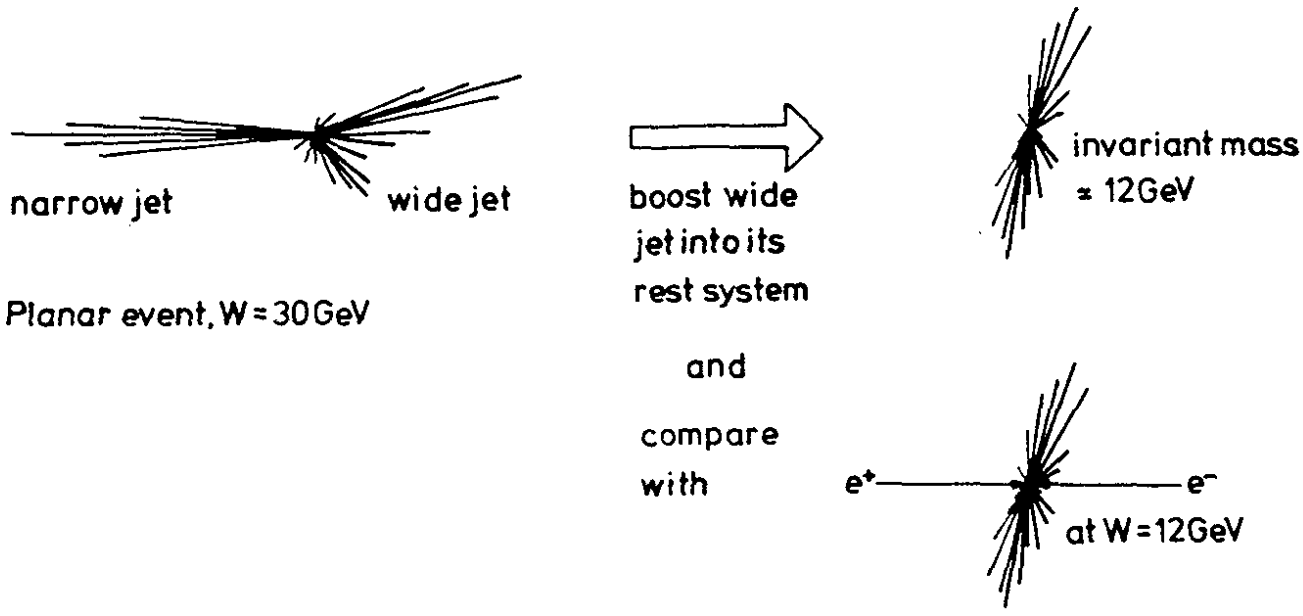

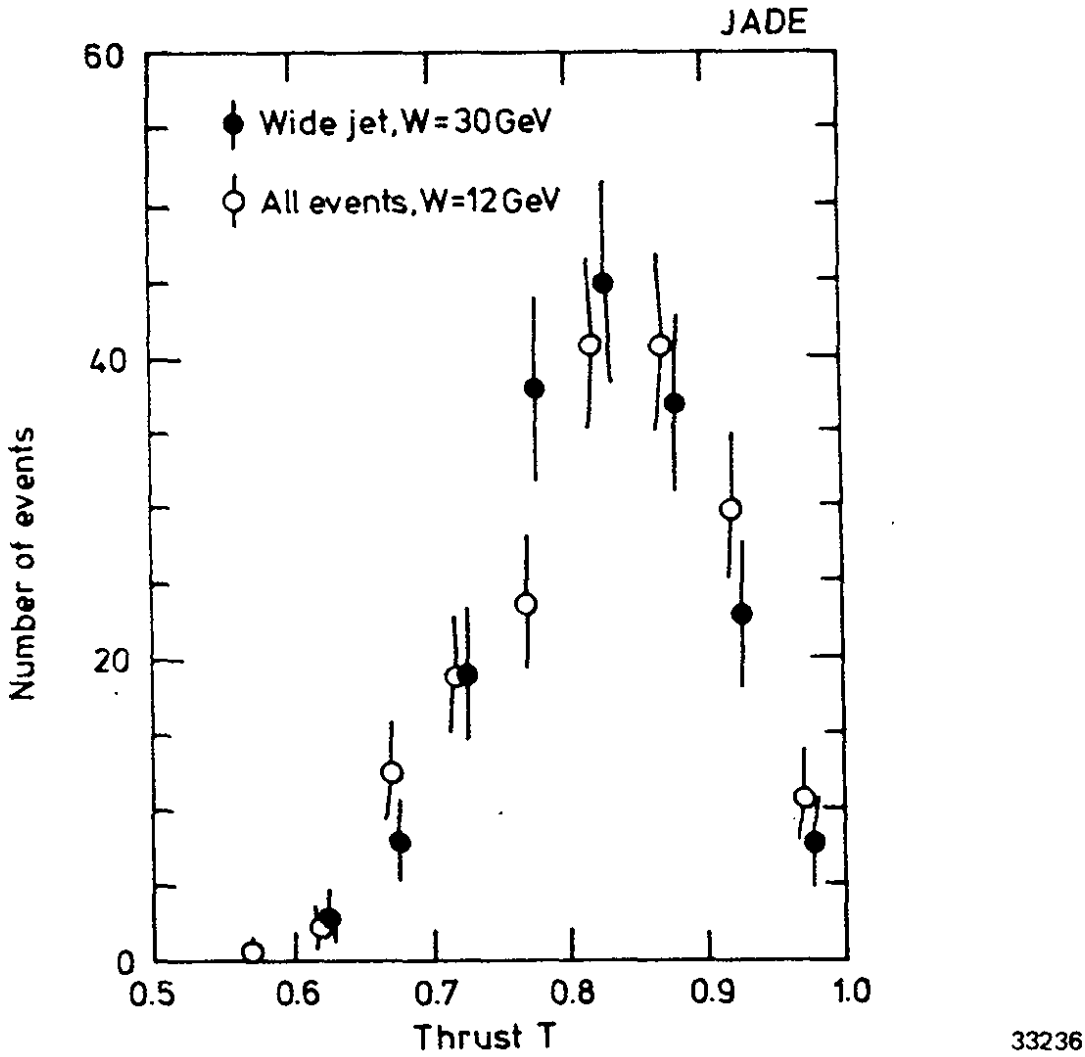

Fig. 53 On the top, a procedure of studying the structure of the wide jet in planar events from the reaction $e^+e^- \rightarrow$ hadrons is shown. The lower part shows the comparison of event shapes measured by thrust (T = 1/2 for spherical, T = 1 for collinear states), i) for the wide jet (transformed to its rest system) of planar events at 30 GeV, and ii) for complete events at 12 GeV (nearly all being 2-jet events). From the JADE group (Bartel et al. 1980b).

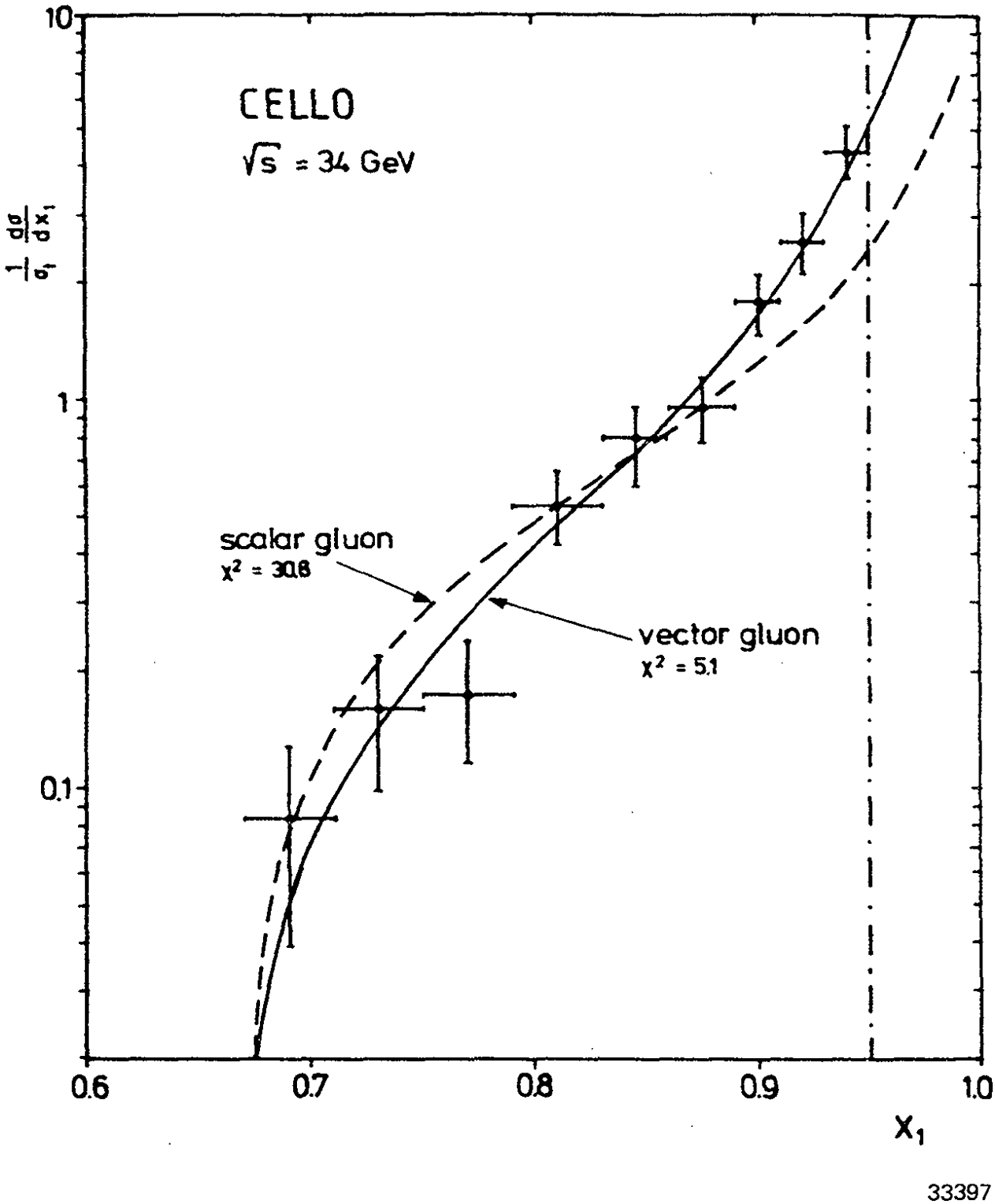

Fig. 54 Parton thrust distribution for three jet events as measured at W = 34 GeV by the CELLO group (Behrend et al. 1981). The curves show the QCD prediction for $\alpha_s = 0.1$ (solid line) and the prediction for scalar gluons (dashed line).

In the analysis of the TASSO group (Brandelik et al. 1980c) the angles θ_i were reconstructed from the jet axes determined from the charged particle vectors. From the angles the parton energies were determined and ordered such that $x_1 \geq x_2 \geq x_3$. Using Monte Carlo generated events it was ascertained that the x_i obtained by this approach agree closely with those of the parent partons. The resolution in x_1 is 6 % and systematic biases are very small (of the order of 1 %).

In order to avoid the problematic area near $x_1 = 1$ only events with $x_1 \leq 0.9$ were considered. A quantity particular sensitive to the question of vector or scalar gluons is the angle $\tilde{\theta}$ illustrated in Fig. 55b (Ellis & Karliner 1979). The $q\bar{q}g$ system is Lorentz boosted into the c.m. frame of partons 2 and 3 (one of which by virtue of the ordering of the x_i is more likely to be the gluon) and $\tilde{\theta}$ measures the angle between the 2, 3 axis and the parton 1. Assuming massless partons

$$\cos\tilde{\theta} = \frac{x_2 - x_3}{x_1} = \frac{\sin\theta_2 - \sin\theta_3}{\sin\theta_1} \qquad (45)$$

The measured distribution of $\cos\tilde{\theta}$ is shown in Fig. 56. The comparison with the vector gluon hypothesis (QCD) involves no free parameter since α_s has already been determined. The agreement between the data and QCD is perfect. The prediction for scalar gluons fails badly; the observed deviations correspond to 5 s.d. The scalar gluon hypothesis is inconsistent with the data (see also Berger et al. 1980b). This conclusion is strenghtened by the fact that the $\tilde{\theta}$ distribution predicted for scalar gluons at the parton level is hardly altered when fragmentation is included (see Fig. 56).

6.7 Alternative explanations of the three-jet events?

After the observation of three-jet events several models were proposed which maintain that the three jet events are not necessarily due to gluon bremsstrahlung but can be explained by a different mechanism. A detailed comparison of these models with experiment was recently presented by Söding (1981) using the TASSO data. In this comparison the most sensitive distributions were found to be the angular correlations between the jet axes, or equivalently, the distributions of the fractional energies x_i.

The jet Dalitz plot determined from the TASSO experiment for an average c.m. energy W = 33 GeV with 4945 events is shown in Fig. 57a. Collinear two-jet configurations (for which $x_1 = 1$) lie along the base line of the plot, symmetric three-star configurations at the top corner. The QCD prediction for $\alpha_s = 0.17$ predicts a very similar event distribution (Fig. 57b). The projection onto parton thrust x_1,

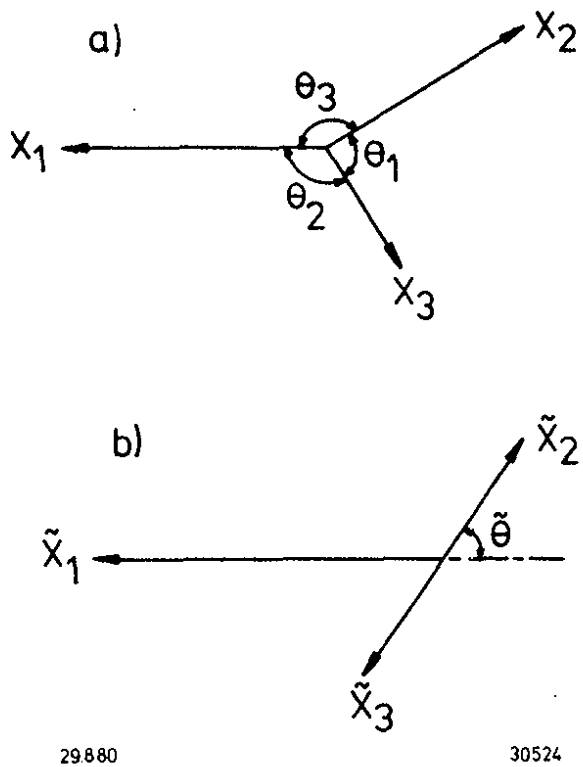

Fig. 55 (a) Momenta and angles of a $q\bar{q}g$ final state in the c.m. frame.
(b) The $q\bar{q}g$ final state transformed to the rest frame of particles 2 and 3.

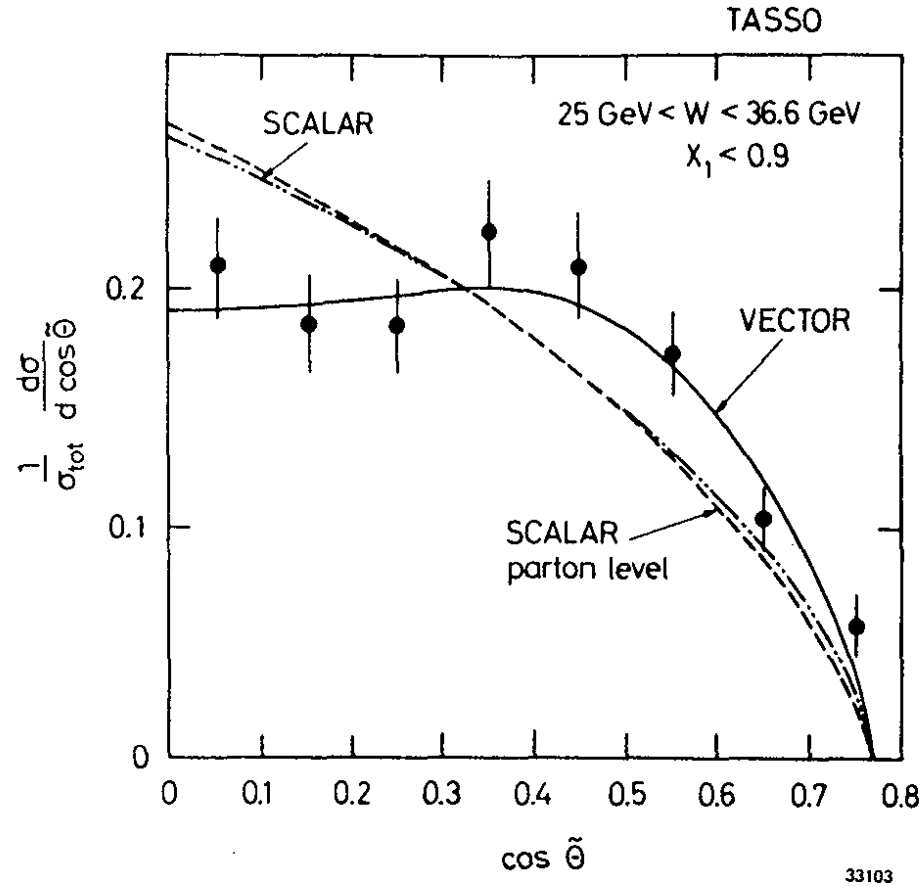

Fig. 56 Observed distribution of the Ellis-Karliner variable $\cos\tilde{\Theta}$ for events in the three-jet region defined by parton thrust $x_1 < 0.9$ for the reaction $e^+e^- \to$ hadrons at $\langle W \rangle = 33$ GeV (from the TASSO experiment Brandelik et al. 1980c). The full curve shows the QCD prediction to $o(\alpha_s)$ with $\alpha_s = 0.17$ (vector gluons), the dashed-dotted curve the prediction for scalar gluons. The dashed curve shows the scalar gluon prediction on the parton level, i.e. before correction for hadronization, radiative effects, and detector imperfections.

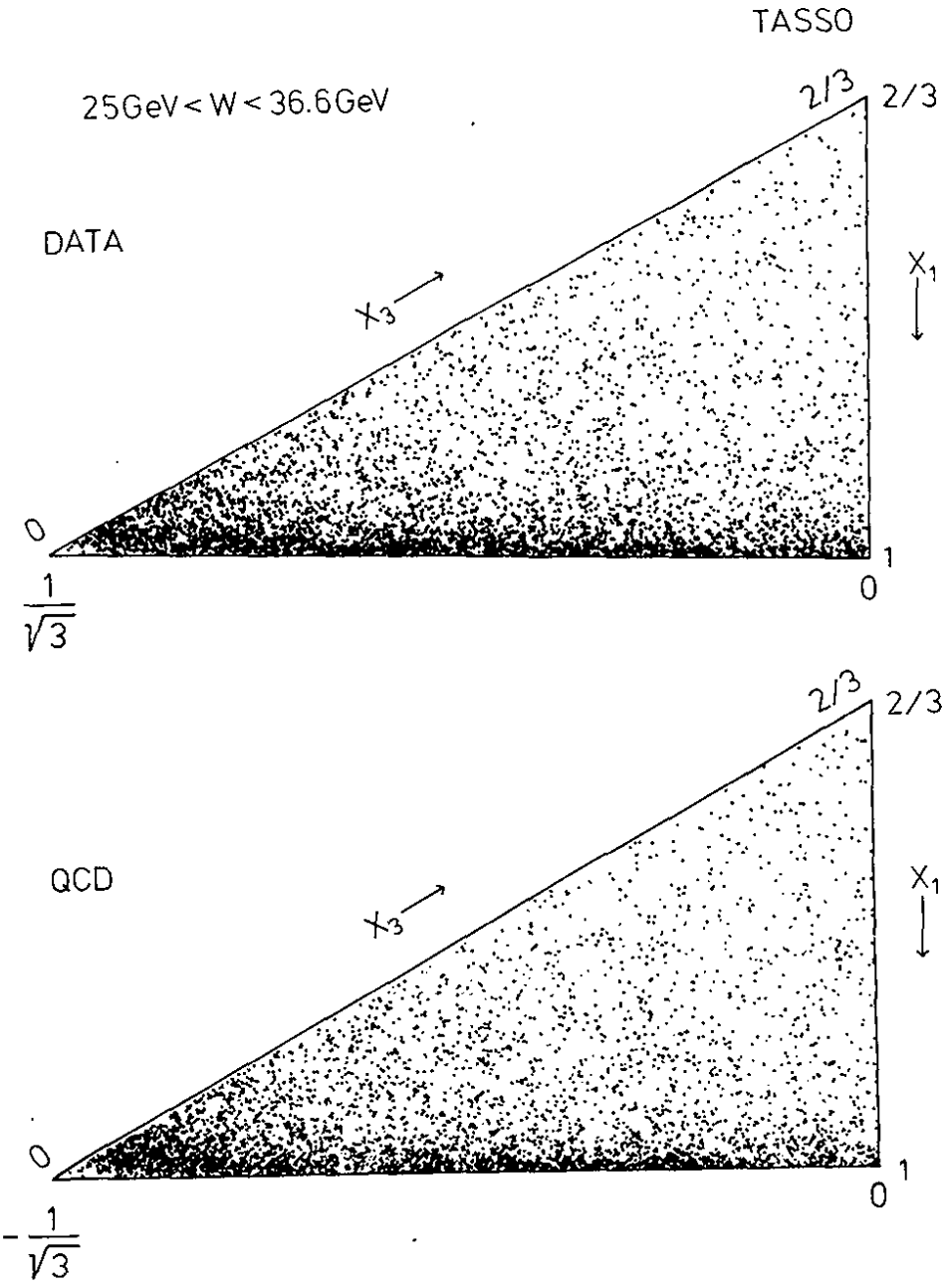

Fig. 57 Dalitz plot of the three reconstructed jet energies for the reaction e^+e^- → hadrons at <W> = 33 GeV, from the TASSO experiment (top plot). For comparison, the QCD prediction with α_s = 0.17 is shown using Monte Carlo simulations with the same number of events (bottom). From Söding (1981).

normalized to σ_{tot} is shown in Fig. 58. The QCD prediction agrees well with the data (solid curve).

We turn now to the comparison of the data with the alternative models. In the constituent interchange model (CIM) (T.A. De Grand et al. 1977) a hard (large p_T) meson or resonance is emitted instead of a gluon. This is a higher twist contribution. Extending an earlier analysis by the PLUTO group (Berger et al. 1980b) the TASSO data have been compared (Söding 1981) with the CIM making the conservative assumption that a whole spectrum of mesons can be emitted. The quark meson coupling strength has been adjusted such that the model fits the p_T^2 distribution at W = 12 GeV (Fig. 43). To describe the data at W = 33 GeV the coupling constant has to be increased by a factor of four (which means a factor of 16 in the cross section). Moreover the model fails to describe the parton thrust (x_1) distribution as shown by the dashed-dotted curve in Fig. 58. As a result no more than 5 % of the three-jet events can be attributed to higher twist effects.

A somewhat similar mechanism is suggested by the massive quark model (Preparata 1981). This model gives a good description of the p_T^2 distribution at W = 12 and 30 GeV. Whether the model can also account for the properties of the planar events such as the parton thrust (x_1) distribution or the distribution of p_T^2 with respect to the three jet axes has not yet been tested.

The emission of a large p_T meson from a quark in the process $e^+e^- \to q\bar{q} \to q\bar{q}M$ may also involve a contribution with the same W dependence as the leading process $e^+e^- \to q\bar{q}$ but with an intrinsic p_T^{-4} tail of the hadron distribution. For comparison, gluon bremsstrahlung (which is point-like) has a p_T^{-2} behaviour. On the other hand the most common assumption for hadronization is a gaussian p_T distribution as used e.g. in the Field-Feynman model (1978). It turns out that while it is possible to adjust the p_T^{-4} tail so as to reasonably fit the TASSO p_T^2 distribution (Fig. 43) e.g. at W = 12 GeV the strong W dependence of the p_T^2 distribution is not reproduced. Furthermore, the model predicts too few three-jet events with large angles between them (i.e. close to the symmetric three-star configuration).

The large tail of the p_T^2 distribution at high W could also be due to the fragmentation of the heavy quarks c and b which might impart a much larger intrinsic p_T^2 to their fragmentation products than light quarks do. In other words, the intrinsic transverse momentum q_T distribution could have two terms:

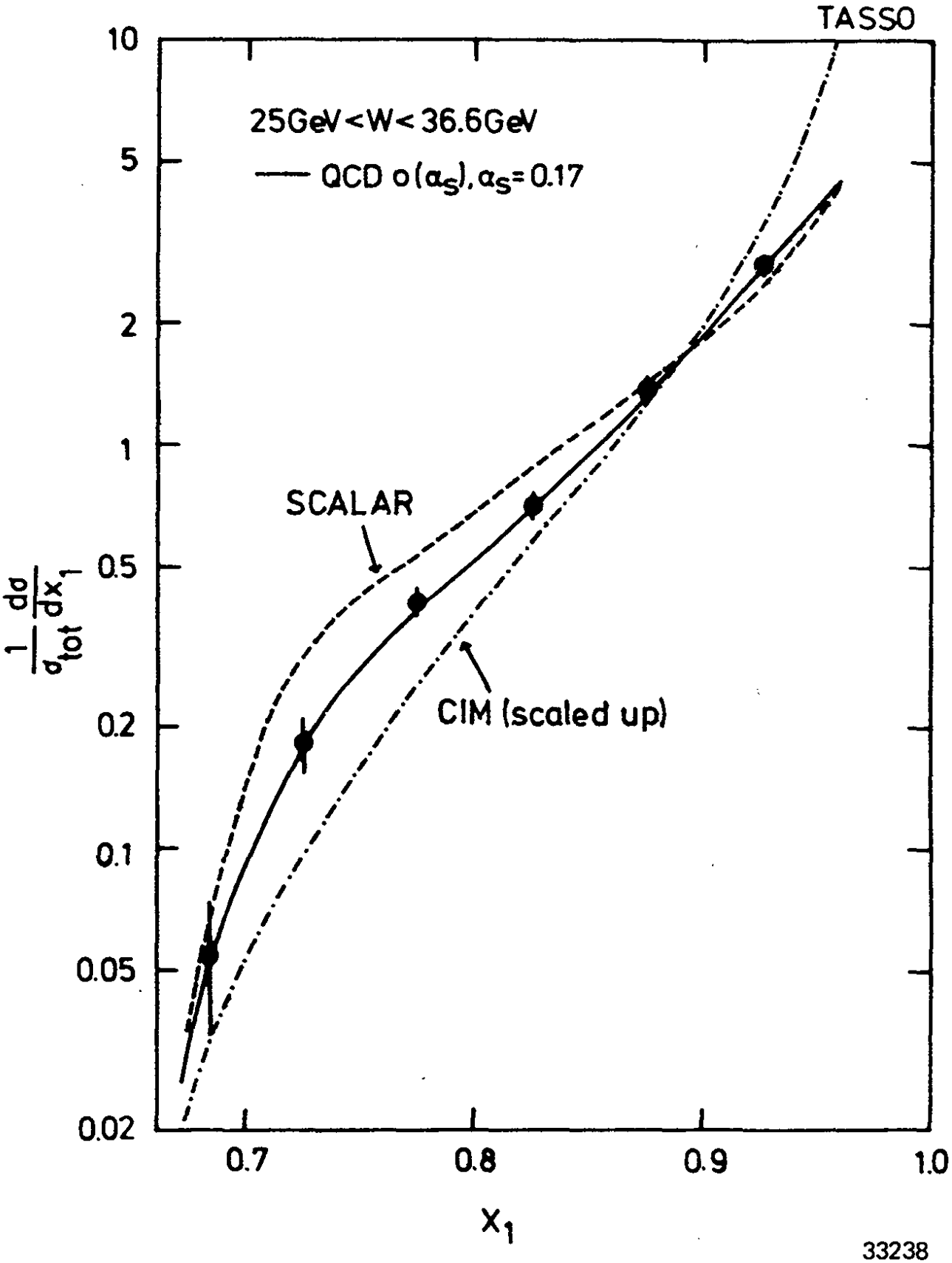

Fig. 58 Distribution of the maximum reconstructed jet energy x_1 (= parton thrust for three-jet events) in the reaction e^+e^- → hadrons at <W> = 33 GeV, from the TASSO experiment. The full curve shows the QCD prediction to $o(\alpha_s)$ with $\alpha_s = 0.17$, the dashed curve the prediction for scalar gluons (with the coupling $\alpha_s = 1.6$ optimized to furnish the best overall description of a number of event variables). The dashed-dotted curve is the prediction from the constituent interchange model with a scaled-up coupling constant such as to fit the p_T^2 distribution at the same energy. From Söding (1981).

$$\frac{dp}{dq_T^2} \sim A\, e^{-q_T^2/2\sigma_q^2} + B\, e^{-q_T^2/2\sigma_Q^2}$$

where the first is due to the light quarks (u,d,s), the second is due to c and b quarks, and $\sigma_Q >> \sigma_q$. In order to reproduce the observed p_T^2 distribution σ_Q has to be rather large (σ_Q = 0.8 GeV/c compared to σ_q = 0.3 GeV/c). This has the consequence that planar events from this model show a much weaker collimation around the three jet axes than the data shown in Fig. 46.

In conclusion none of the models which have been proposed as alternatives to QCD can describe all features of three jet prodcution. Whether the massive quark model is more successful remains to be seen.

6.8 The value of α_s and the next to leading order corrections

The number of three-jet events is directly related to the value of the quark gluon coupling strength α_s. The α_s values obtained at energies of 30 GeV are summarized in Table 6. Some of the results were determined in leading order (labelled α_s), some were obtained using the Ali et al. program which includes some of the next-to leading order diagrams (labelled some α_s^2).

Table 6. Determination of α_s from three-jet production near W = 30 GeV. First error is statistical, second systematic. From Braunschweig (1981).

Experiment	order in α_s	α_s
CELLO	α_s	0.15 ± 0.015 ± 0.03
JADE	α_s	0.18 ± 0.03 ± 0.03
MARK J	some α_s^2	0.17 ± 0.02
PLUTO	α_s	0.16 ± 0.02
TASSO	some α_s^2	0.17 ± 0.02 ± 0.03

All four experiments are seen to agree on the value of α_s, yielding an average of α_s = 0.17 ± 0.01 with a systematic uncertainty of 0.03.

A still open question is the effect of the complete second order corrections. An evaluation of all second order terms (which are displayed in Fig. 50) was recently made by three groups, R.K. Ellis et al. (1980), Fabricius et al. (1980)

and Vermaseren et al. (1980). Although working all in the $\overline{MS}$ renormalization scheme they arrived at apparently conflicting results which led to different conclusions. Fabricius et al. found that the $O(\alpha_s^2)$ corrections are comparatively small, while the two other groups concluded that the second order corrections to three-jet production are roughly 30 - 40 % of the first order contribution (Kunszt 1981, Ali 1981). All three groups found that the energy partition between the three jets and therefore the angular correlation between the jet axes is almost the same in $o(\alpha_s^2)$ as in $o(\alpha_s)$ which implies amongst other things that the conclusion on the gluon spin is unaffected by the second order corrections (see e.g. Kunszt 1981).

The reason for the discrepancy between the three theoretical analyses appears now to be understood (Buras 1981). It is due to different definitions of what is called a three-jet event and of thrust, the quantity directly compared with experiment. Fabricius et al. work with a Sterman-Weinberg (1977) type definition; a three-jet event is defined as an event which has all but a fraction $\varepsilon/2$ of its total energy distributed within three separated cones of full opening angle δ (see Fig. 59).

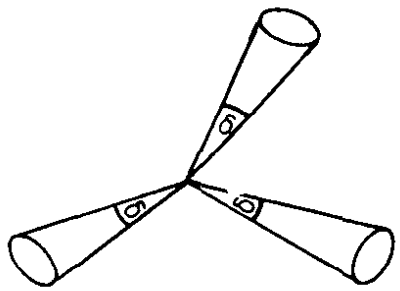

Fig. 59 Definition for a three-jet event used by Fabricius et al.

Values used for ε,δ in the calculation of Fabricius et al. were $\varepsilon = 0.2$, $\delta = 45^o$. The use of this type of jet definition is suggested by physics: If for a fixed W the angular separation of, say a quark and a gluon is below some minimum angle (defined by the hadronization process) it is impossible to separate the fragments from the two partons, and, consequently to observe two separate partons.

Now consider the diagram for two gluon emission, $e^+e^- \to q\bar{q}gg$, in Fig. 60.

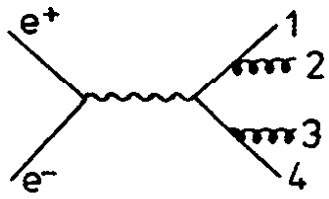

Fig. 60 QCD diagram for $e^+e^- \to q\bar{q}gg$

The effective mass squared of the parton system 1, 2 is given by the product of the four momentum vectors, $M_{12}^2 = 2p_1p_2$. Because of the cutoff in δ partons 1 and 2 are defined to be in one jet if $y_{12} \equiv 2p_1p_2/W^2 \geq 10^{-2}$. In the calculations of Ellis et al. and Vermaseren et al. the diagram shown in Fig. 60 is calculated on the parton level and is considered to represent a four-jet event down to extremely small y_{12} values ($y_{12} \approx 10^{-5}$). The differences between the α_s values extracted from the data at W = 30 GeV using one or the other approach are presently of the order of 20 %: Fabricius et al. find $\alpha_s = 0.17$ while Ali (1981) and Kunszt (1981) based on the work of Ellis et al. obtain $\alpha_s = 0.12 - 0.13$. These results should be considered as preliminary.

The comparison with QCD presented above dealt primarily with processes where a single hard gluon is emitted. Work has also started to search for effects of multiple, soft gluon emission which could affect, e.g. the two particle correlations. The conclusions from these tests are strongly model dependent since the effects are intimately related to the question of hadronization. Reference to these studies can be found e.g. in the review of Criegee and Knies (1981).

6.9 Summary of the QCD tests

The observation of three-jet events in high energy e^+e^- annihilation into hadrons may be considered a major triumph of the theory. QCD had predicted such events to occur as a result of hard gluon bremsstrahlung. Close examination of the details of three-jet production at PETRA shows consistency with QCD and confirms the vector nature of the gluon. The rate of three-jet events yields in leading order of QCD $\alpha_s = 0.17 \pm 0.02$.

The observed topology of the direct decays of the Υ, $e^+e^- \to \Upsilon$ (9.4 GeV $\to$ hadrons (Brandt 1979, Berger et al. 1980a, Niczyporuk et al. 1981) which has not been discussed in this review - exclude colourless gluons (Walsh & Zerwas 1980).
In conclusion, the experimental results show a strong preference for a theory with coloured vector gluons - just what QCD is. Two important characteristics of QCD have not yet been verified by experiment, the existence of the three-gluon vertex, and asymptotic freedom, i.e. the decrease towards zero of α_s with increasing Q^2. The first is related to the existence of bound gluon states or glue balls. The first glue balls might have been observed recently in radiative decays of the J/ψ (Scharre 1981). The second point will require higher Q^2 than presently available or a study of "cleaner" processes such as $\gamma\gamma$ scattering at large Q^2.

7. Quark and Gluon fragmentation

As seen above the hadronic final states in high energy e^+e^- annihilation are a result of quark and gluon induced jet formation. By analysing the final states one can hope to piece the jet fragments together and reconstruct the properties of the primordial parton, such as charge, flavour etc. This section summarizes briefly what is known on the final states at high energies.

7.1 Energy carried by neutrals

The energy fraction ρ_γ carried by photons (either from π^o, η... decay or from direct production), and ρ_N by neutrals obtained by subtracting the charged particles energies,

$$\rho_\gamma = \sum E_{\gamma j}/W$$
$$\rho_N = 1 - \sum E_{CHI}/W \qquad (46)$$

is shown in Fig. 61. ρ_N includes the energy carried by K^o and Λ particles. The fraction of energy carried by photons and by neutrals appears to be energy independent. Roughly speaking, one third of the energy goes into neutrals.The difference $\rho_N - \rho_\gamma$ provides an upper limit on the fraction of energy ρ_ν taken up by neutrinos. The JADE group found $\rho_\nu < 10$ % (95 % C.L.) which disfavours the free quark model of Pati and Salam (1978) where $\rho_\nu = 18 - 28$ % was predicted.

7.2 Charged particle multiplicity

In Fig. 62 the average charged particle multiplicity* $\langle n_{CH}\rangle$ is plotted as a function of c.m. energy. Above ~7 GeV $\langle n_{CH}\rangle$ is seen to rise (logarithmically) faster than at lower energies. Phase space predicts $\langle n_{CH}\rangle \sim s^{1/4}$ which fits the data rather well (see curve B); it fails, however, to reproduce the dispersion of the multiplicity distribution, $D = \sqrt{\langle n_{CH}^2\rangle - \langle n_{CH}\rangle^2}$ which was found to increase with energy like $\langle n_{CH}\rangle$.
The simplest form of scaling of charged particle production leads to $\langle n_{CH}\rangle = a + b \ln s$. This is certainly at variance with the data if the full energy range is considered. The observed rise of $\langle n_{CH}\rangle$ cannot be attributed to the onset of $b\bar{b}$ production which is found to yield an increase by ~0.2 units. In QCD an increase of $\langle n_{CH}\rangle$ over the scaling curve is predicted due to the additional contribution from gluon fragmentation. The exact form of the resulting energy dependence is not yet clear. If the result for infinitely heavy

---

* $\langle n_{CH}\rangle$ includes the $\pi^\pm$ coming from $K^o_S \to \pi^+\pi^-$ decay. This contribution amounts to 0.4 units at 7.4 GeV, 0.6 at 12 GeV and 1 unit at 30 GeV.

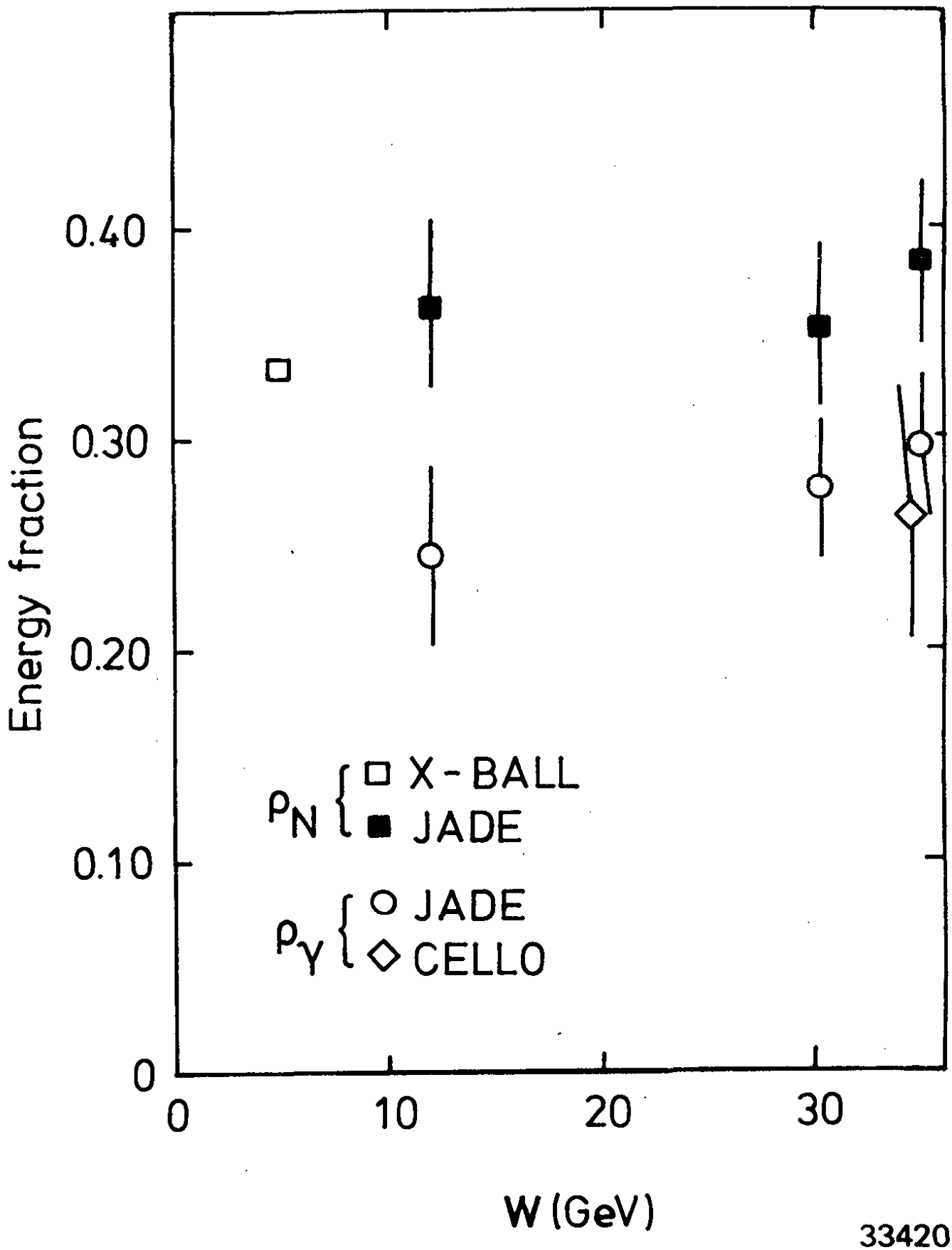

Fig. 61 The energy fractions carried by photons (ρ_γ) and by neutrals (ρ_N).

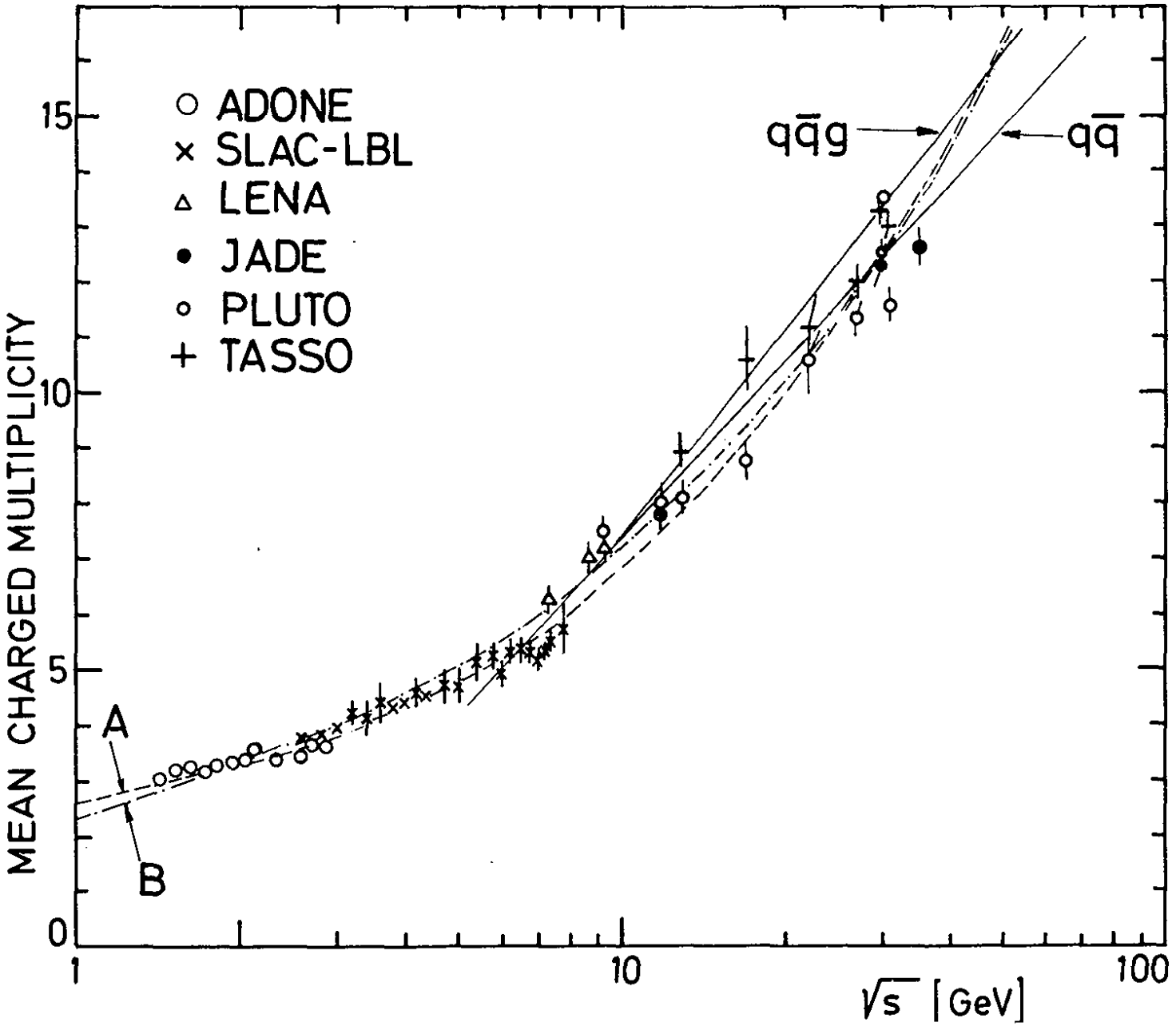

33263

Fig. 62 Mean charged multiplicity versus center-of-mass energy. The straight line labelled $q\bar{q}$ is a typical prediction for $q\bar{q}$ production with subsequent fragmentation of quarks into mesons. The line labelled $q\bar{q}g$ includes gluon bremsstrahlung. The curve labelled (A) is the best fit of the form $\langle N_{ch} \rangle = N_o + a \cdot \exp(b\sqrt{\ell n(s/\Lambda^2)})$ described in the text. Curve (B) shows the dependence $\langle N_{ch} \rangle = 2.3 \cdot s^{1/4}$ (s in GeV^2).

quarks is taken for guidance, one expects $\langle n_{CH} \rangle$ to grow like (Ellis 1980, Furmanski et al. 1979)

$$n_{CH} = n_o + a \exp(b\sqrt{\ell n(s/\Lambda^2)}) .$$

Fits of this form with $\Lambda = 0.3$ GeV yield $n_o = 2.0 \pm 0.2$, $a = 0.027 \pm 0.01$, $b = 1.9 \pm 0.2$ and reproduce the trend of the data (see curve A in Fig. 62). One may therefore be tempted to attribute the rapid rise to hard gluon effects. The solid lines in Fig. 62 compare the $\langle n_{CH} \rangle$ data with the $q\bar{q}$ model, $e^+e^- \to q\bar{q} \to$hadrons using the Field-Feynman fragmentation functions but <u>without</u> hard gluon contributions. The model accounts well for the rise seen above ~5 GeV*. The inclusion of hard gluon emission raises the prediction by a negligible amount below 10 GeV; at 35 GeV it adds 0.8 units. We conclude therefore that the rapid rise of $\langle n_{CH} \rangle$ is mostly due to the growing phase space: particle masses matter less as the energy increases.

In Fig. 63 the e^+e^- multiplicity distributions are compared in a KNO plot (Koba et al. 1972) with pp and $\bar{p}p$ data. Plotted is $P_{CH} \cdot \langle n_{CH} \rangle$ where P_{CH} is the probability for observing a final state with n_{CH} charged particles versus $n_{CH}/\langle n_{CH} \rangle$. The e^+e^- data obey KNO scaling between 9.4 and 35 GeV. They agree well with the $\bar{p}p$ data but disagree with the pp data which have a larger dispersion.

7.3 Inclusive particle spectra without particle identification

The differential cross section for producing a particle h with momentum and energy P, E and angle Θ relative to the beam axis can be expressed in terms of two structure functions $\bar{W}_1$ and $\bar{W}_2$ which are closely related to W_1 and W_2 measured in inelastic lepton hadron scattering (Drell and coworkers 1969)

$$\frac{d^2\sigma}{dx d\Omega} = \frac{\alpha^2}{s} \beta x \{ m\bar{W}_1 + \frac{1}{4} \beta^2 x \nu \bar{W}_2 \sin^2\Theta \} \qquad (47)$$

where m is the mass of h, $\beta = P/E$, $x = E/E_{beam} = 2E/\sqrt{s}$ and ν is the energy of the virtual photon as seen in the h rest system, $\nu = (E/m)\sqrt{s}$.

---

* At lower energies the model is presumably less reliable because of the approximations made for the fragmentation.

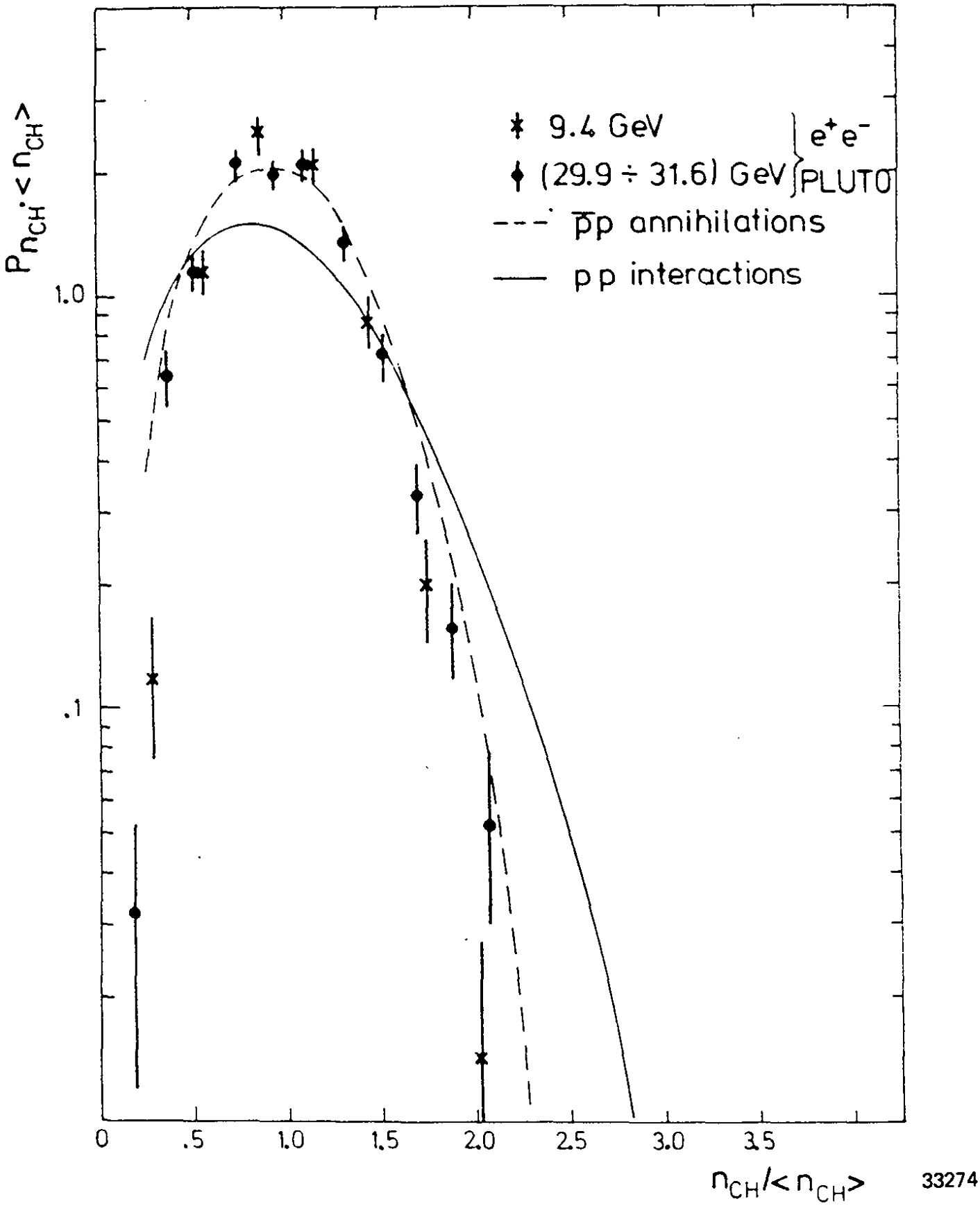

Fig. 63a KNO plot for charged particle multiplicites measured in e^+e^- annihilation. The dashed and solid curves show the results for $\bar{p}p$ annihilation and pp scattering. $P_{n_{CH}}$ is the probability of observing the charged multiplicity n_{CH}.

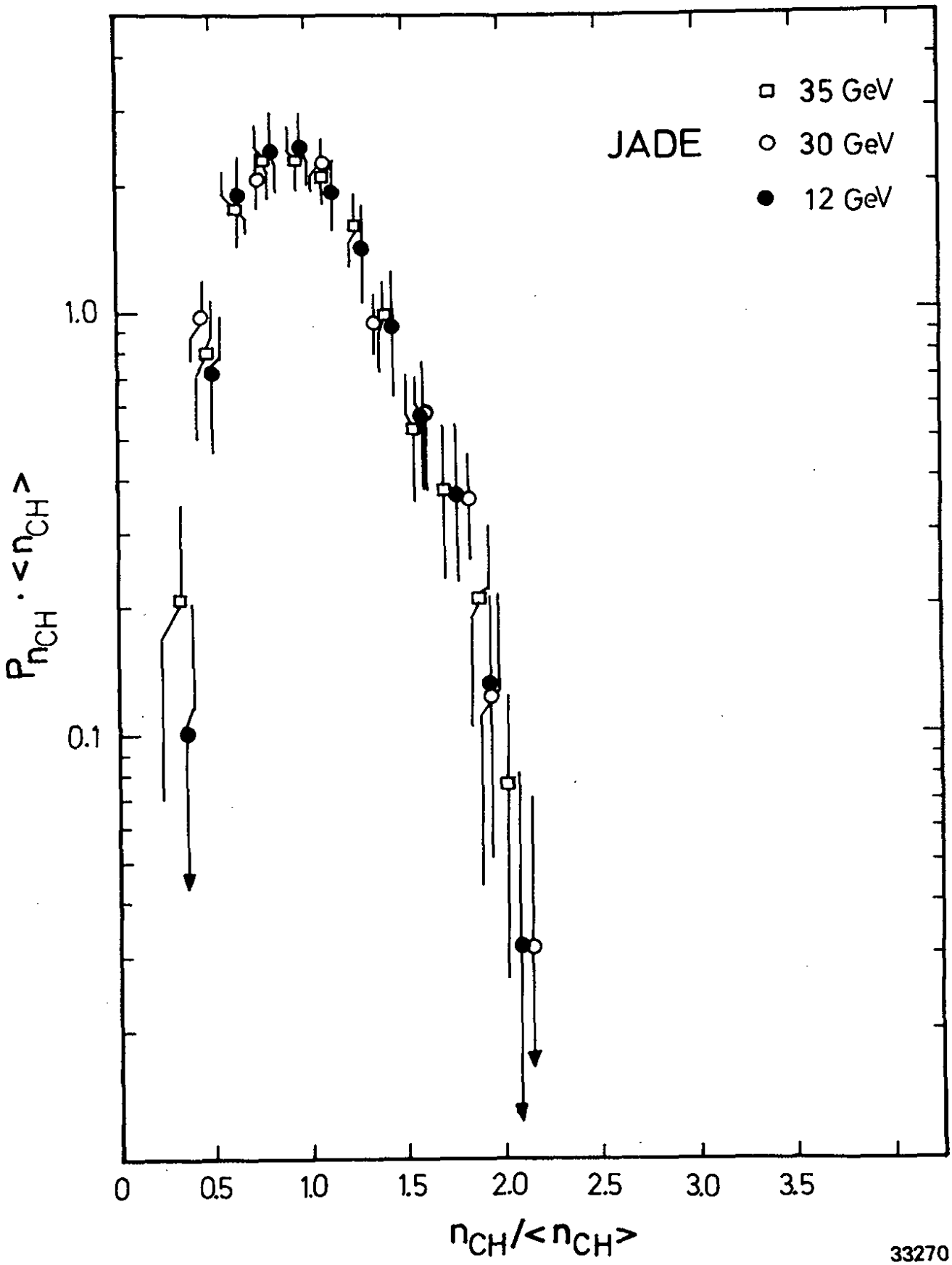

Fig. 63b Same as Fig. 63a

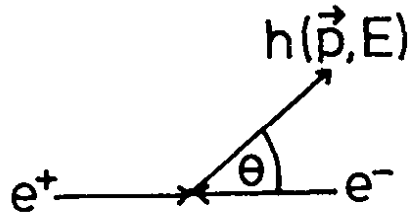

Diagram for inclusive particle production

At particle energies large enough that particle masses can be neglected, x can be replaced by the normalized momentum $x = P/E_{beam}$ and the scaled cross section reads

$$s d\sigma/dx \approx 4\pi\alpha^2 \times \{m\bar{W}_1 + \frac{1}{6} \times \nu\bar{W}_2\} \qquad (48)$$

The structure functions in general depend on two variables, e.g. x and s. If scale invariance holds $\bar{W}_1$ and $\nu\bar{W}_2$ are functions of x alone and $sd\sigma/dx$ is energy independent.

Scaling behaviour is e.g. expected in the quark parton model: at energies large enough that particle masses can be neglected, the number of hadrons h produced by a quark q with fractional energy x, $D_q^h(x)$, is independent of s. This leads to

$$\frac{d\sigma}{dx}(e^+e^- \to q\bar{q} \to h) = \sigma_{q\bar{q}} \cdot 2D_q^h(x) = \frac{8\pi\alpha^2}{s} e_q^2 D_q^h(x) \qquad (49)$$

Fig. 64 displays scaled cross sections not separated according to particle type. In this case the particle energy is unknown and x is defined as $x = 2p/W$. The data in Fig. 64 were measured at c.m. energies between 5 and 35 GeV. At low x values ($x < 0.15$) the particle yield shows a dramatic rise when the c.m. energy is increased from 5 to 35 GeV. This rise is related to the multiplicity growth seen above. At $x > 0.2$ only little energy dependence is observed; most of the variation with energy occurs between W = 5 and 12 GeV, with the low W data being higher. A similar behaviour is seen by MARK II comparing data taken at SPEAR and PEP (Hollebeek 1981). This type of scale breaking is expected in QCD where at high W gluon emission depletes the particle yield at large x and increases it at small x. However, scale breaking effects are better studied with the cross sections for specific particle types (π,k,p...) rather than with the unseparated cross sections which at lower energies are strongly affected by mass effects. For instance, proton production passes its phase space maximum only at a momentum of 1 GeV/c (see below) which corresponds to an x_p value of 0.4 at W = 5 GeV.

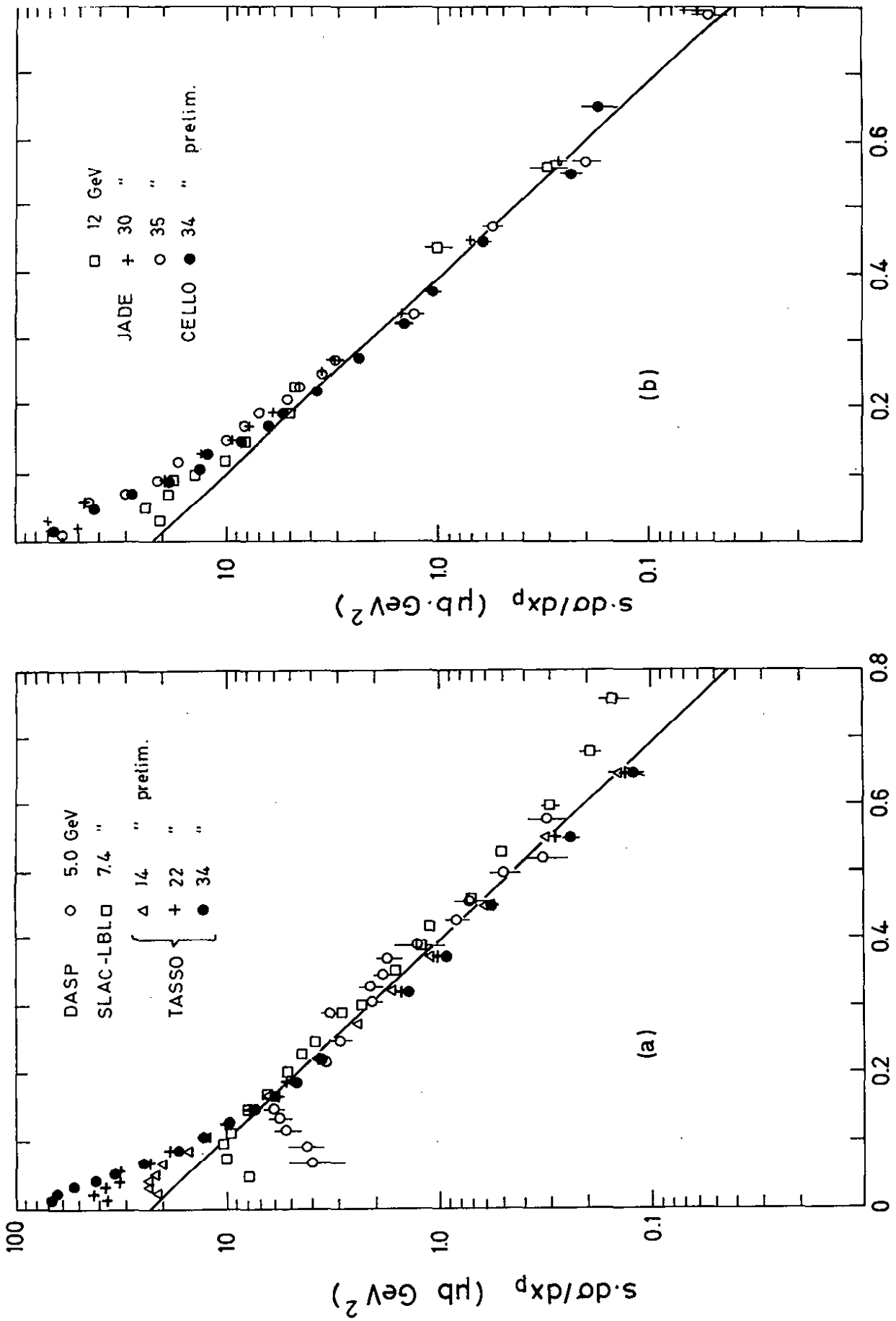

Fig. 64 Inclusive spectrum $s \cdot d\sigma/dx_p$ of charged particles. (a) shows the data of TASSO together with results from SLAC-LBL and DASP at lower energies. (b) shows the data from CELLO and JADE. The full lines are drawn to guide the eye and correspond to $s \cdot d\sigma/dx_p = 23 \cdot \exp(-8 \cdot x_p)$ μb GeV^2. From Felst (1981).

Fig. 65 shows the rapidity distributions normalized to the total cross section as measured by TASSO between 13 and 31.6 GeV. The thrust axis was taken as the jet axis since in this way the corrections for the y-axis relative to the true axis were found to be smaller at large y than if the sphericity axis had been chosen. To compute y, the particles were assumed to be pions. Also plotted in Fig. 65 are the data from SLAC-LBL measured at low energies (4.8 and 7.4 GeV). They were determined with respect to the sphericity axis. One observes a plateau near y = 0 that broadens with increasing c.m. energy. The height of the plateau is not constant but rises with increasing energy (see insert in Fig. 65). In the fragmentation region (y close to $y_{max} \approx 0.5 \ln(s/m^2)$) the particle yield is a steeply descending function of y. The width of the fragmentation region is roughly one unit, which is similar to what has been observed in hadron-hadron scattering.

The energy dependences of the plateau and fragmentation regions show that the faster than logarithmic growth of the average multiplcity at high energies is correlated with a rise of the plateau which is due to low energy particles. The same effect was observed in PP collisions (see e.g. Giacomelli & Jacob 1979).

7.4 Particle separated cross sections

Inclusive cross sections were measured for a variety of particles: $\pi^{\pm},\pi^{o},K^{\pm},K^{o}$, P,Λ. Table 7 lists the techniques used and the momentum range covered by various experiments.

We start with a discussion of the differential cross sections $d\sigma/dp$. Fig. 66 summarizes the cross sections near W = 30 GeV for the 6 particle species. The curves are drawn to guide the reader. Within errors there are twice as many $\pi^{\pm}$ as π^{o}. Pions are by far the most abundant type of particle which does not come as a surprise. At momenta below 1 GeV/c one finds large differences between the π yields and those for the heavier particles. As the momentum increases these differences become gradually smaller. The ratio $\pi^{\pm} : K^{o},\bar{K}^{o} : \Lambda,\bar{\Lambda}$ is of the order 100 : 10 : 1 near p = 0.5 GeV/c and 4 : 2 : 1 at 10 GeV/c. All cross sections rise at low momentum, go through a maximum and drop off towards higher momenta. The position of the maximum increases with the particle mass; it appears to be below 0.4 GeV/c for pions, around 0.7 GeV/c for kaons and near 1 GeV/c for lambdas. Most of this turn-on phenomenon at low momenta is an artifact of phase space. Consider the Lorentz-invariant phase space cross section $\frac{E}{4\pi p^2}\frac{d\sigma}{dp}$

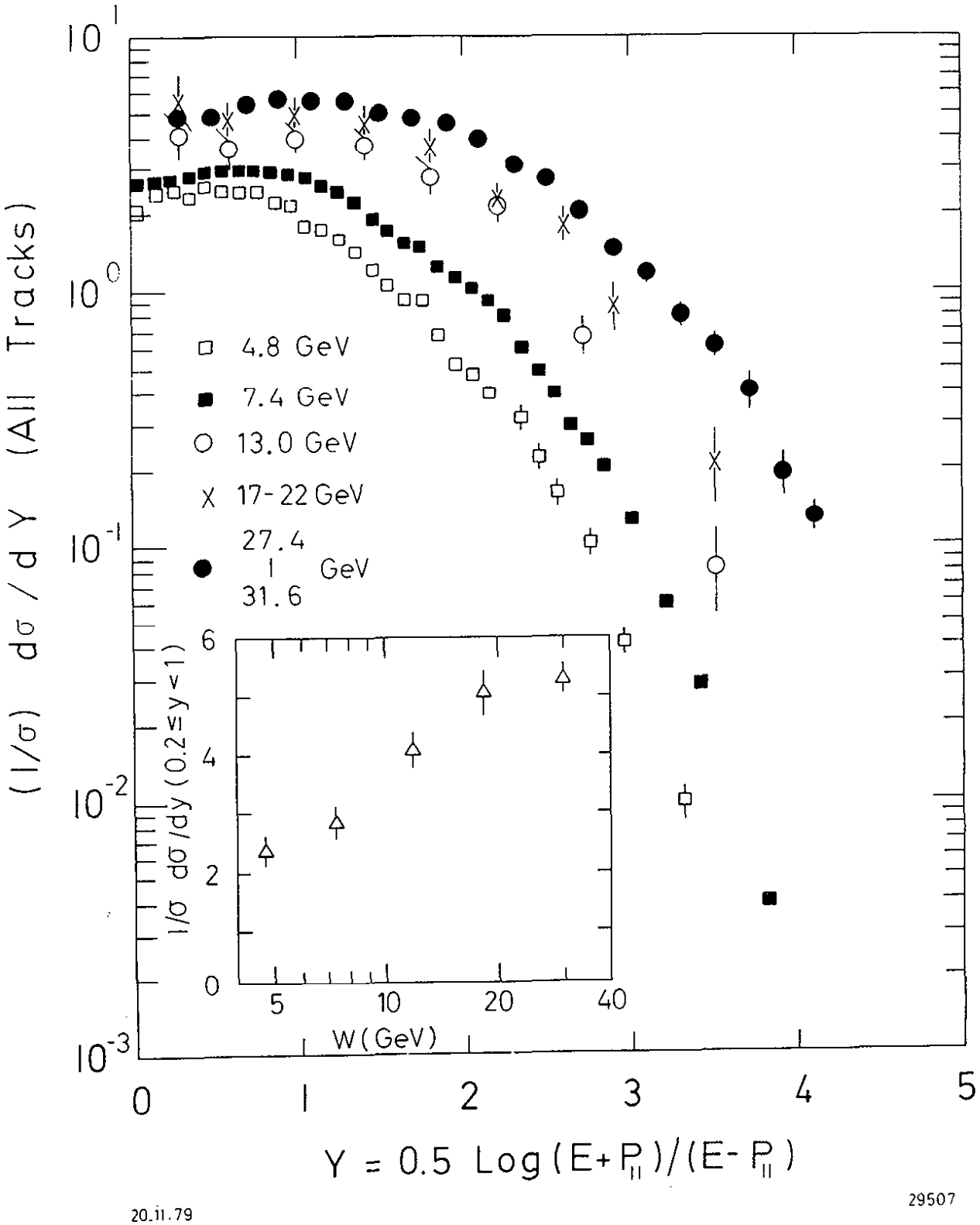

Fig. 65 Rapidity distributions $1/\sigma_{tot}$ $d\sigma/dy$ for charged particles (assuming the mass to be the pion mass) measured by SLAC-LBL at 4.8 and 7.4 GeV (Hanson 1978) and by TASSO between 13 and 31.6 GeV (Brandelik et al. 1980a). SLAC-LBL used the sphericity axis, TASSO the thrust axis. The insert shows $1/\sigma_{tot}$ $d\sigma/dy$ averaged over $0.2 < y < 1$ as a function of the c.m. energy.

Table 7. Experiments measuring particle separated cross sections

type of particle	experiment	technique	momentum range (GeV/c)	remark
$\pi^{\pm}$	TASSO[1]	TOF Cerenkov	0.4 - 10	
	JADE	dE/dx	<0.7, 2-7	preliminary
π^{o}	TASSO[2]	liquid Argon	0.5 - 4	
$K^{\pm}$	TASSO[1]	TOF	<1.1	
	JADE	dE/dx	<0.7	preliminary
$K^{o},\bar{K}^{o}$	TASSO[3]	$K^{o}_{s} \rightarrow \pi^{+}\pi^{-}$	all P	
	PLUTO[4]	"	"	
	JADE	"	"	preliminary
	MARK II	"	"	preliminary
$p,\bar{p}$	TASSO[1]	TOF	0.5 - 2.2	
	JADE	dE/dx	0.3 - 0.9	preliminary
	MARK II	TOF	0.5 - 2.0	preliminary
$\Lambda,\bar{\Lambda}$	JADE[5]	$\bar{\Lambda} \rightarrow \bar{p}\pi^{+}$ + dE/dx	0.4 - 1.1	
	TASSO[6]	$\Lambda \rightarrow p\pi^{-}$	1 - 10	
	MARK II	"		preliminary

1 Brandelik et al. (1980d) and (1981d)
2 Brandelik et al. (1981e)
3 Brandelik et al. (1980e) and (1981f)
4 Berger et al. (1981c)
5 Bartel et al. (1981c)
6 Brandelik et al. (1981f)

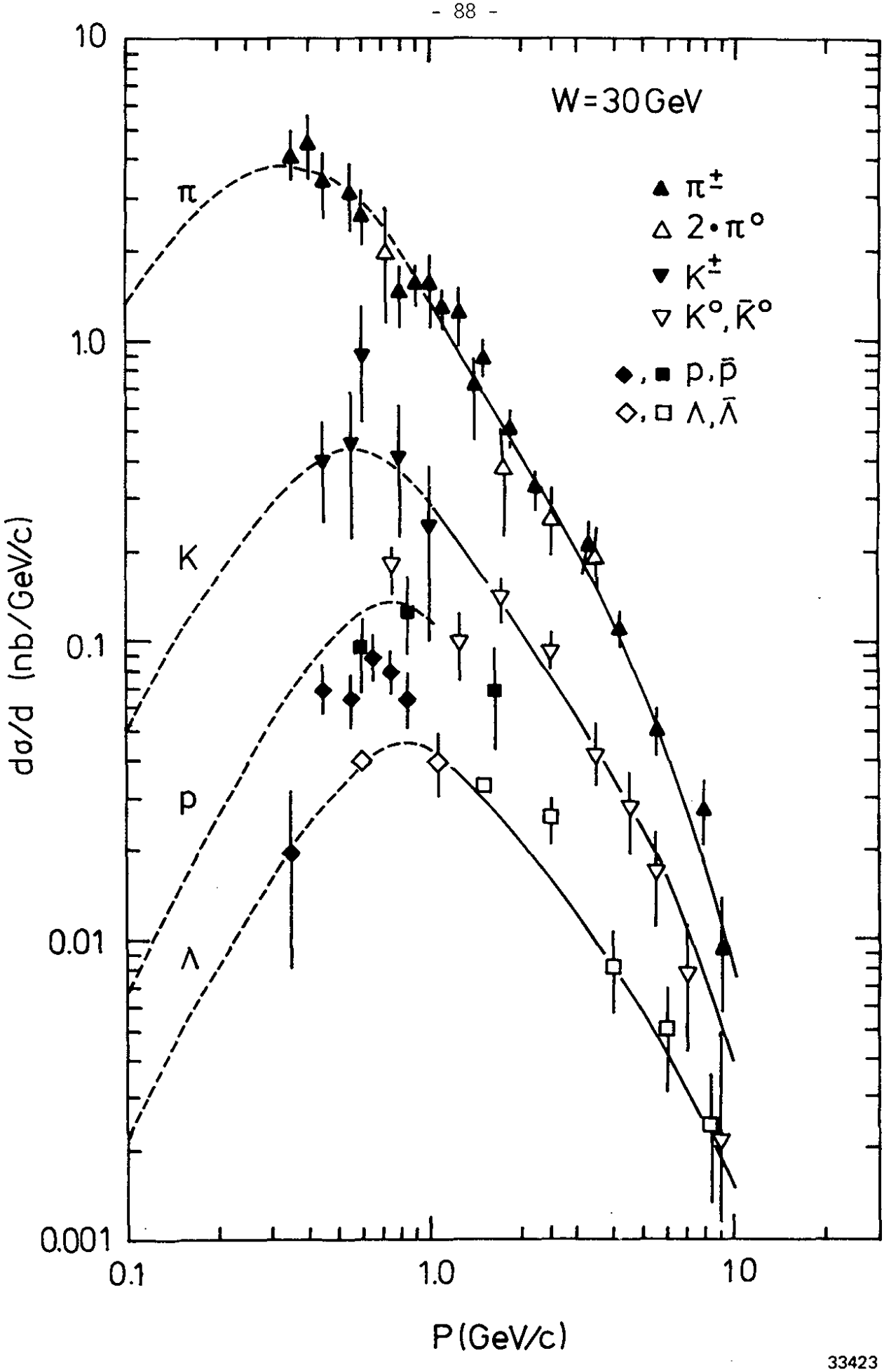

Fig. 66 Differential cross sections $d\sigma/dp$ for inclusive particle production $e^+e^- \to hX$ for $\pi^\pm\pi^-$ (TASSO, preliminary), $2\pi^\circ$ (TASSO), $K^+ + K^-$ (TASSO), $K^\circ + \overline{K^\circ}$ (TASSO), $p + \bar{p}$ (JADE, TASSO), $\Lambda + \bar{\Lambda}$ (JADE, TASSO). The dashed curves are of the form $E/p^2\ d\sigma/dp \sim \exp(-bE)$ with $b = 3.6\ \text{GeV}^{-1}$. The solid curves are handdrawn to follow the data.

and assume some momentum dependence C(P) for it:

$$\frac{E}{p^2}\frac{d\sigma}{dp} = C(P) \qquad (50)$$

or

$$\frac{d\sigma}{dp} = \frac{P^2}{E} C(P) \approx \frac{P^2}{m} C(p) \text{ for } p << m \qquad (51)$$

The low c.m. energy data (W = 4 - 5 GeV, Brandelik et al. 1979a) are well described by an exponential,

$$\frac{E}{p^2}\frac{d\sigma}{dp} = C \exp(-bE)$$

with b around 5 GeV^{-1}. This form describes also the high energy data up to particle energies around 1 GeV if b = 3.6 GeV is chosen (see dashed curves in Fig.66). The relative fractions of $\pi^{\pm}$, $K^{\pm}$ and $p,\bar{p}$ as a function of particle momentum p at W = 30 GeV are shown in Fig. 67. An average event at this energy has approximately 11 $\pi^{\pm}$, 5.5 π^{o}, 1.4 $K^{o},\overline{K^{o}}$, 1.4 $K^{\pm}$, $\gtrsim$0.4 $p,\bar{p}$ and 0.3 $\Lambda,\bar{\Lambda}$ in the final state. The number of K^{o}, $\overline{K^{o}}$ is a factor of 3 larger than observed in pp final states: at a c.m. energy of 27.6 GeV there are 0.46 ± 0.02 K^{o}, $\overline{K^{o}}$ per event (Kichimi et al. 1979). Whether the excess of kaons in $e^{+}e^{-}$ annihilation is due to the c and b quark contributions is not clear (see below).

The W dependence of the inclusive cross sections for K^{o} and Λ production are shown in Figs. 68 and 69. The K^{o} yield rises from W = 5 to W = 30 GeV at about the same rate as the average charge multiplicity does while for lambdas the rise could even be faster (see curves).

7.5 The scaled particle cross sections

The scaled cross sections $s/\beta\, d\sigma/dx$ ($x = 2E/W$) for π, K, p, Λ are shown in Figs. 70 - 72. All particles exhibit similar features: the cross section falls exponentially with a break in slope around x = 0.1. For $\pi^{\pm}$, K^{o},K^{o} and $\Lambda,\bar{\Lambda}$ which were all measured up to large x values the same x dependence is observed for $x \gtrsim 0.15$, $s/\beta\, d\sigma/dx \sim \exp(-8x)$ (see Fig. 72). For the π^{o} data the cross sections measured at energies below W = 8 GeV are systematically higher than those measured above 12 GeV which suggests the presence of scale breaking effects. Qualitatively, they seem to be of the magnitude predicted by QCD (Baier et al. 1979, Frazer & Gunion 1979) but a quantitative comparison has not yet been made.

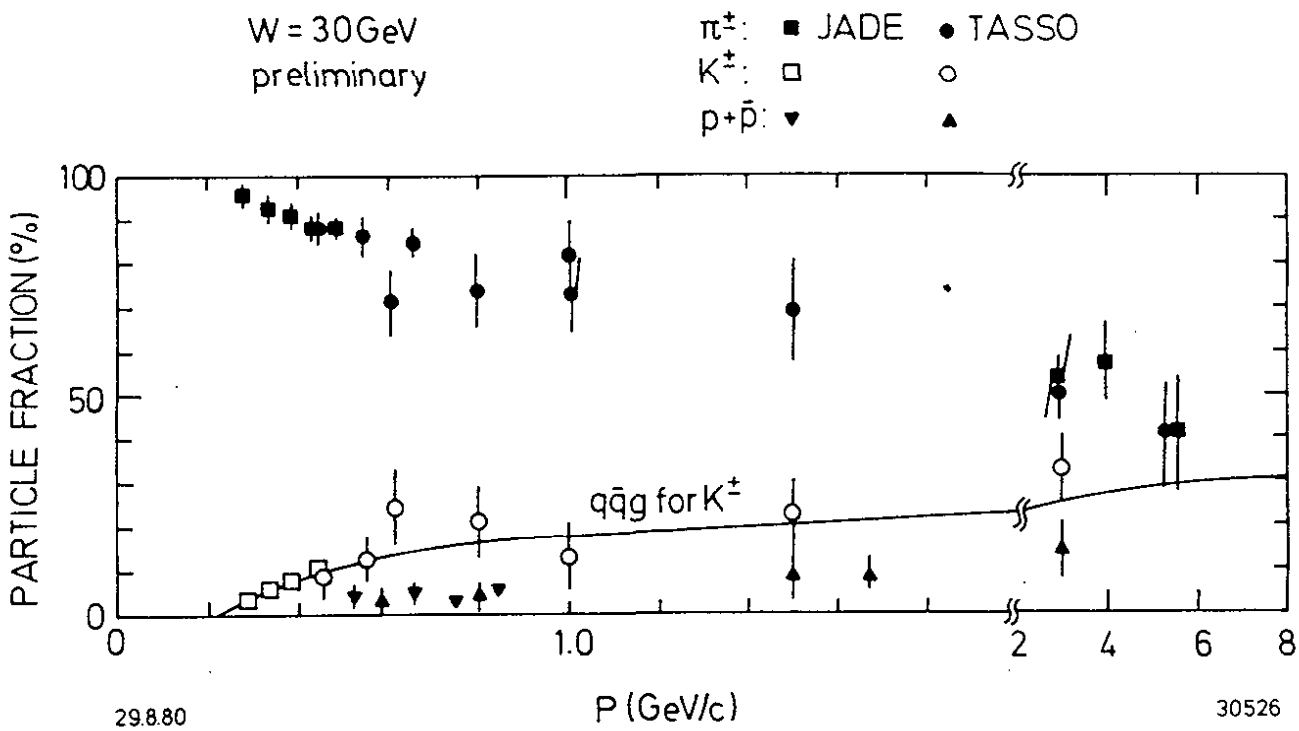

Fig. 67 Charged particle fractions as a function of momentum. From Pandoulas (1980).

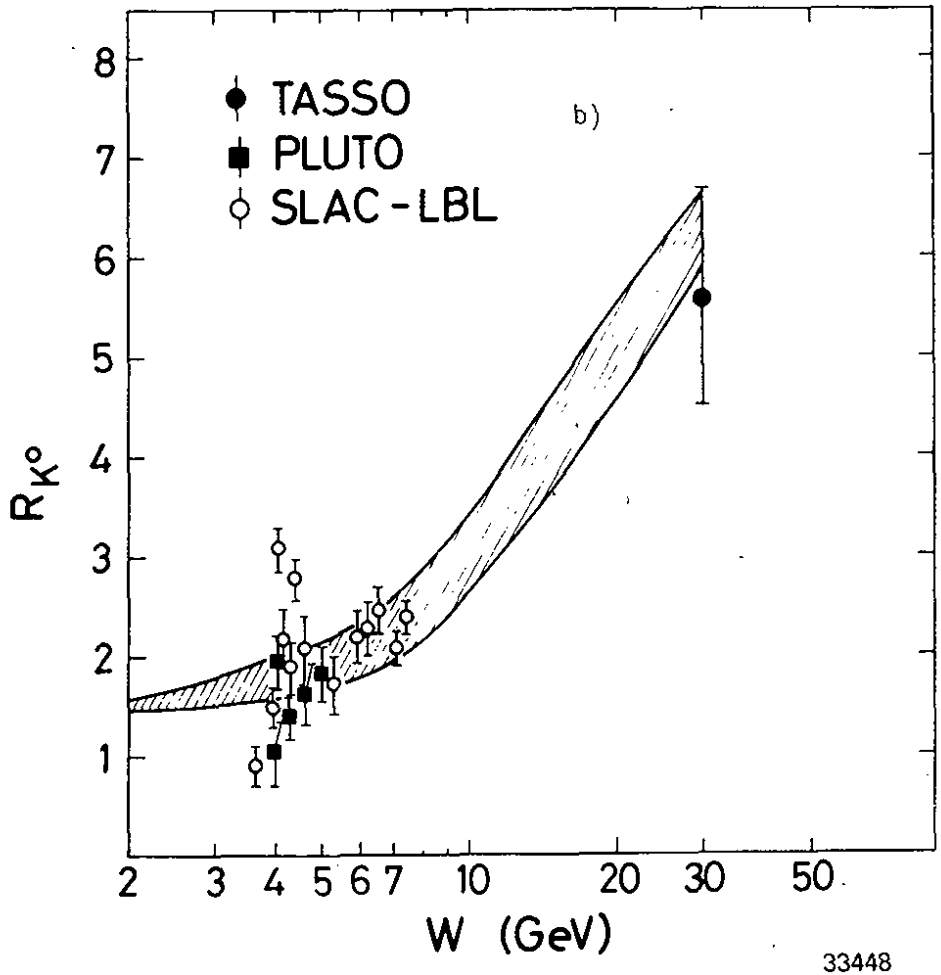

Fig. 68 The total cross section for inclusive $K^0 + \overline{K^0}$ production relative to the μ pair cross section, $R_{K^0} = (\sigma(K^0X) + \sigma(\overline{K^0}X))/\sigma_{\mu\mu}$.

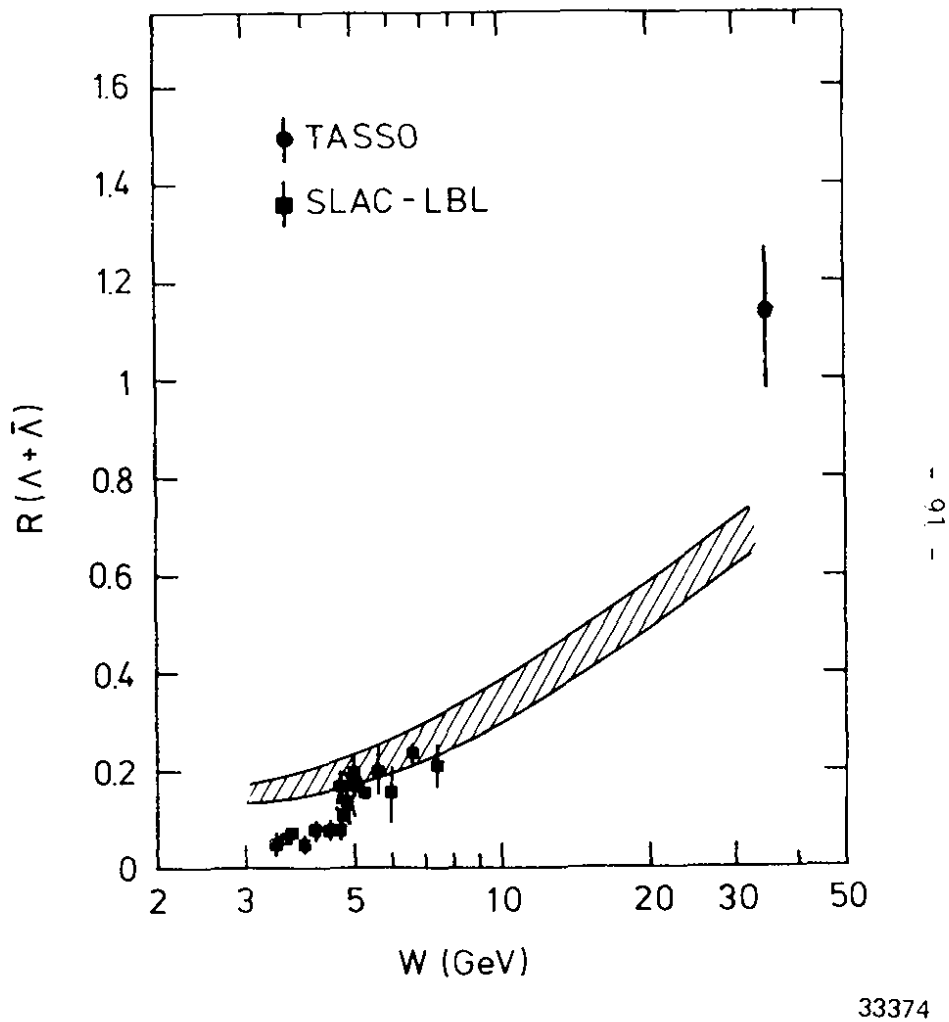

Fig. 69 The total cross section for inclusive $\Lambda + \bar{\Lambda}$ production relative to the μ pair cross section, $R_A = (\sigma(\Lambda X) + \sigma(\bar{\Lambda}X))/\sigma_{\mu\mu}$.

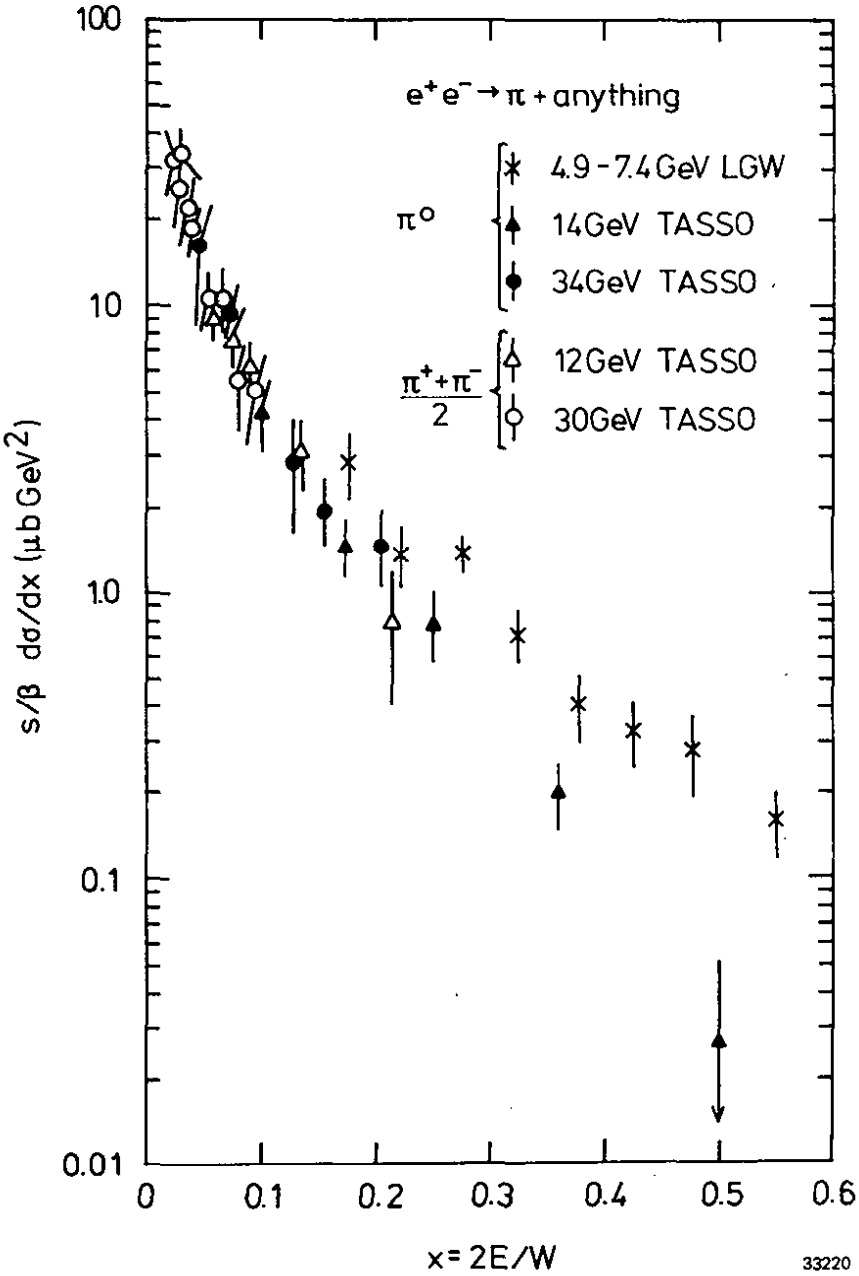

Fig. 70 The scaled cross section $s/\beta\ d\sigma/dx$ for π^0 and $(\pi^+ + \pi^-)/2$ production. From Brandelik et al. (1981c)

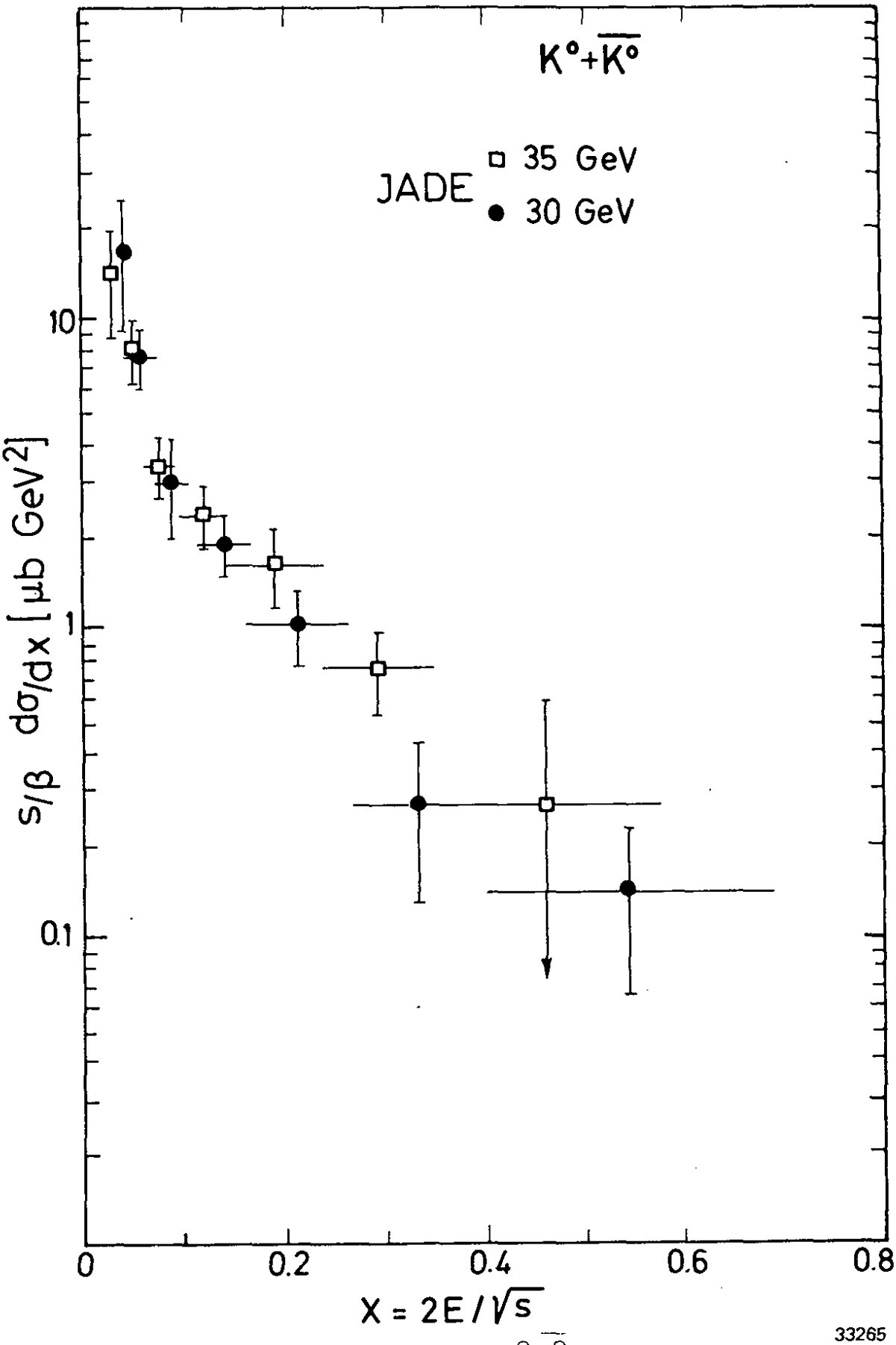

Fig. 71 The scaled cross sections for $K^{O}, \overline{K^{O}}$ production

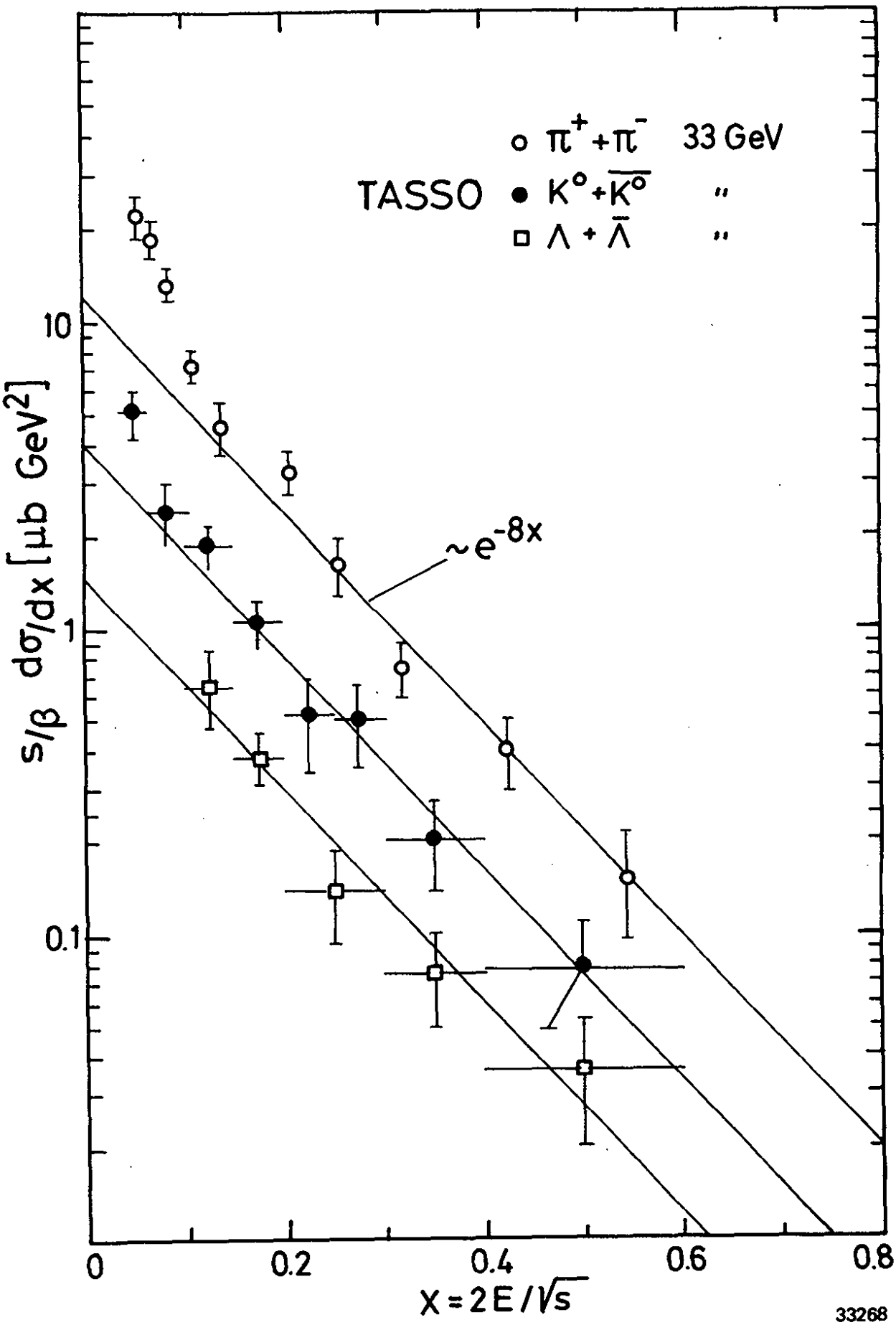

Fig. 72 The scaled cross sections for $\pi^+ + \pi^-$, $K^\circ + \overline{K^\circ}$ and $\Lambda + \bar{\Lambda}$ production.

We turn now to the large K yield observed in e^+e^- annihilation as compared e.g. to that for pp collisions. At first sight it would seem natural to assume the strange quark in the kaons to be either primary produced or to originate from the weak decay of c or b quark. By generating Monte Carlo events according to $e^+e^- \to q\bar{q}$, $q\bar{q}g$ and using a Field-Feynman type fragmentation one can study where the kaons are coming from (Holder 1981). Fig. 73 shows the comparison between the calculation and the data. The sum of all contributions gives a good description of the data. The curves labelled s, c + b show the amount of K^o production by primary s, c or b quarks. They are seen to account only for a about one third of the produced kaons. For the majority of the kaons the s quark is picked up from the sea. It is surprising to see that this is true even at x values as large as 0.4.

7.6 Where are all the baryons from?

The most surprising result of the inclusive measurements is the large yield of baryons* and their x dependence which is very similar to that for mesons. Very roughly, every other event contains a baryon-antibaryon pair. There is a long standing prediction by Drell and coworkers (1969) that nucleon production will not vanish at high energies, i.e. $R_{(p+\bar{p})} \sim W^{-2}$ (although the cross section for the exclusive channel, $e^+e^- \to p\bar{p}$, disappears presumably like W^{-10} as a result of the dipole behaviour of the nucleon form factor). The prediction is based on the assumption that if scaling holds proton production in e^+e^- annihilation,

$$e^+e^- \to \bar{p}X \tag{52}$$

can be related by crossing with inelastic electron proton scattering,

$$e\,p \to eX \tag{53}$$

Strictly speaking, the crossing relation holds only at $x \equiv 2E/W = 1$ (Gatto and coworkers 1972) but the hope was that it could also be applied in the region close to x = 1. Gribov and Lipatov (1971) related the structure functions for the two processes using a field theoretic model. This permits to express the cross section for the annihilation process in terms of the proton structure functions F_1 and F_2 determined from (53) at $\omega = \frac{1}{x}$:

$$\frac{s}{\beta}\,\frac{d\sigma}{dx}\,(e^+e^- \to \bar{p}X) = \frac{4\pi\alpha^2}{x}\,\{xF_1(\omega = \tfrac{1}{x}) - \tfrac{1}{6}\,\beta^2\,F_2(\omega = \tfrac{1}{x})\} \tag{54}$$

---

* A probably related phenomenon is the large yield of forward produced protons in μp scattering observed by EMC (Aubert et al. 1981c).

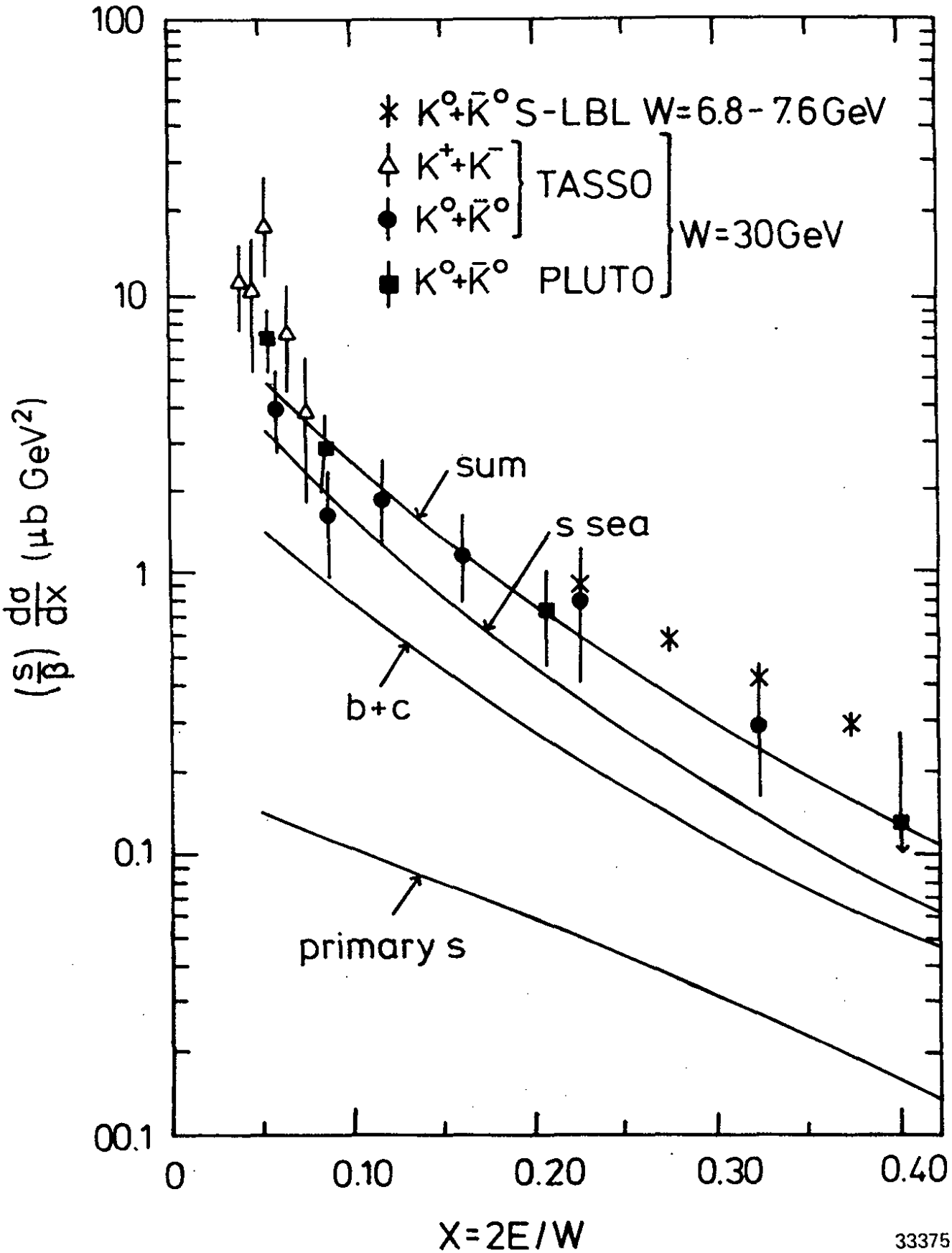

Fig. 73 K^{O} production cross sections. The lines show the origin of the strange quark in K^{O} according to a cascade model. The curves labelled s and b + c show the contributions from primary s, c and b quarks. The curve labelled sea shows the amount of K^{O} production with s quarks from the sea. From Holder (1981).

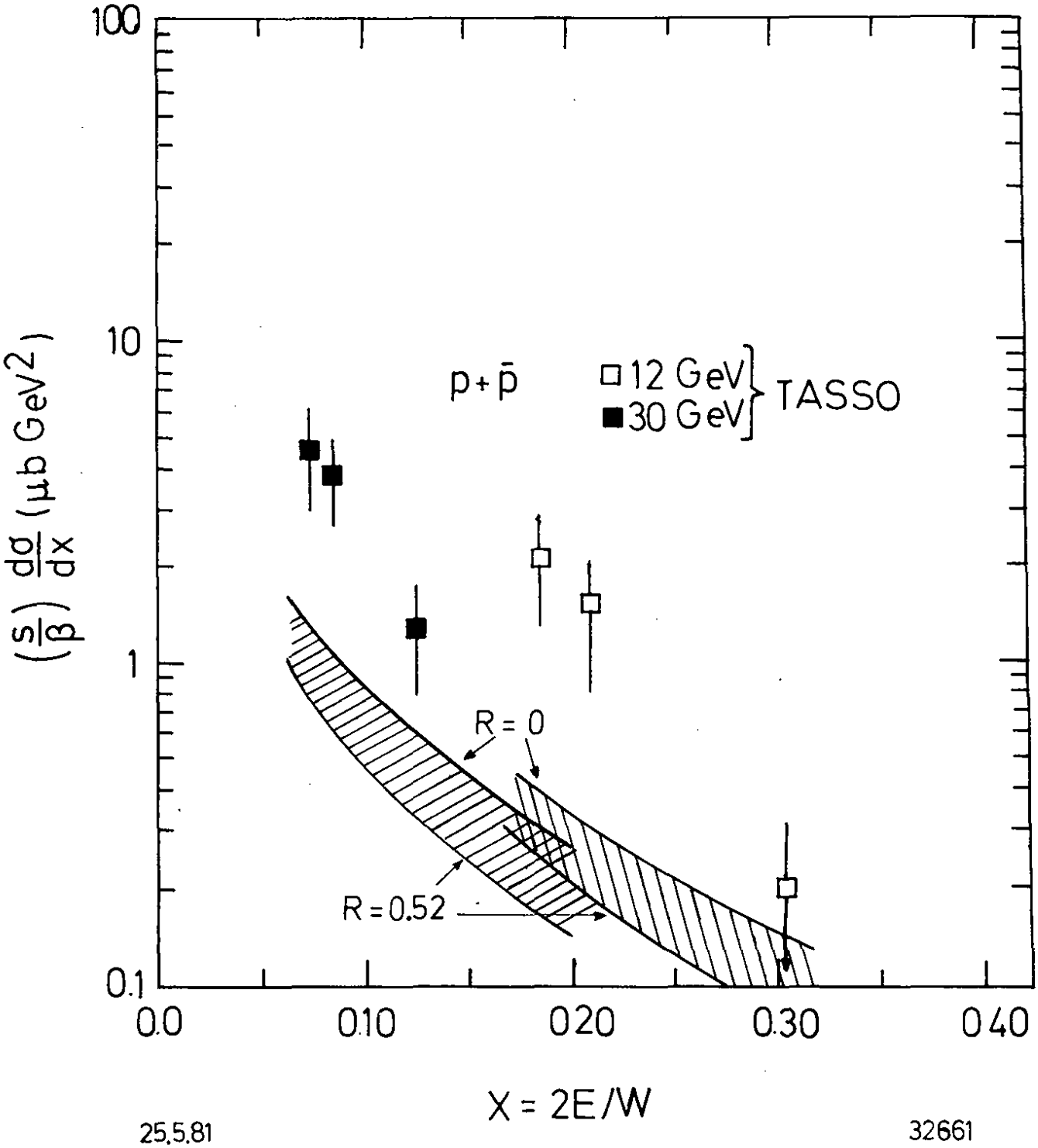

Fig. 74 The scaled cross sections for $p + \bar{p}$ production at W = 12 and 30 GeV compared to the Gribov-Lipatov prediction.

Fig. 74 compares the Gribov Lipatov prediction (shaded bands) with the data at W = 12 and 30 GeV. Like at lower energies (W = 4 - 4.5 GeV, Brandelik et al. 1979a) the theoretical prediction is below the data. Part of the discrepancy - if not all - may have to be attributed to contributions of the type

$$e^+e^- \to hX,\ h = \bar{\Lambda}\ (\to \bar{p}\pi),\ \bar{\Sigma}\ (\to \bar{p}X),\ \text{etc}$$

which should be excluded from the e^+e^- data before making the comparison (Schierholz & Schmidt 1975).

Several models were recently proposed which incorporate baryon production in the fragmentation (see e.g. Ilgenfritz et al. 1978, Casher et al. 1979, Ritter & Ranft 1980, Andersson et al. 1981, Hofmann 1981, Meyer 1981, Schierholz & Teper 1981, Bowler 1981). The simplest approach assumes that a quark can not only pull a $q\bar{q}$ but also a diquark-diantiquark $(qq,\bar{q}\bar{q})$ out of the vacuum (see Fig. 75).

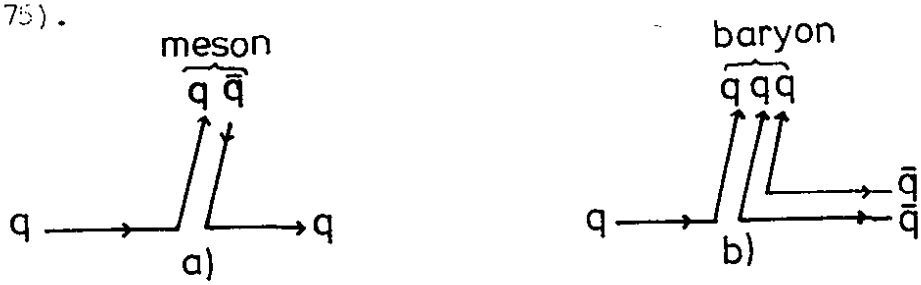

Fig. 75 Quark fragmentation into a meson (a) and a baryon (b)

A good fit to the $p,\bar{p}$ and $\Lambda,\bar{\Lambda}$ data is obtained if the relative probability for picking up a diquark, $P(qq)/P(q)$ is determined from the data and all other fragmentation parameters for baryons are assumed to be same as for mesons (T. Meyer 1981). Fig. 76 shows a comparison with the $p,\bar{p}$ and $\Lambda,\bar{\Lambda}$ data for $P(qq)/P(q) = 0.075$. Both data sets are represented well by the model. A more detailed description of baryon production, starting also from diquarks, was developed in the string model (Andersson et al.1981, Bowler 1981). The dashed curves in Fig. 76 show the result of the first group. The p data which had been used to fix the parameters of the model are reproduced. The model fails for the Λ data where the predicted cross sections are a factor of 2 - 3 too small. The model appears to be flexible enough to resolve this discrepancy.

The requirement of diquark-antidiquark states in the vacuum runs into a problem with R: if diquarks are pointlike R will receive a large contribution from diquark pair production, $e^+e^- \to (qq)(\bar{q}\bar{q})$. This is excluded by the data A wayout is to assume the diquarks to be extended objects with a size of order GeV^{-1}.

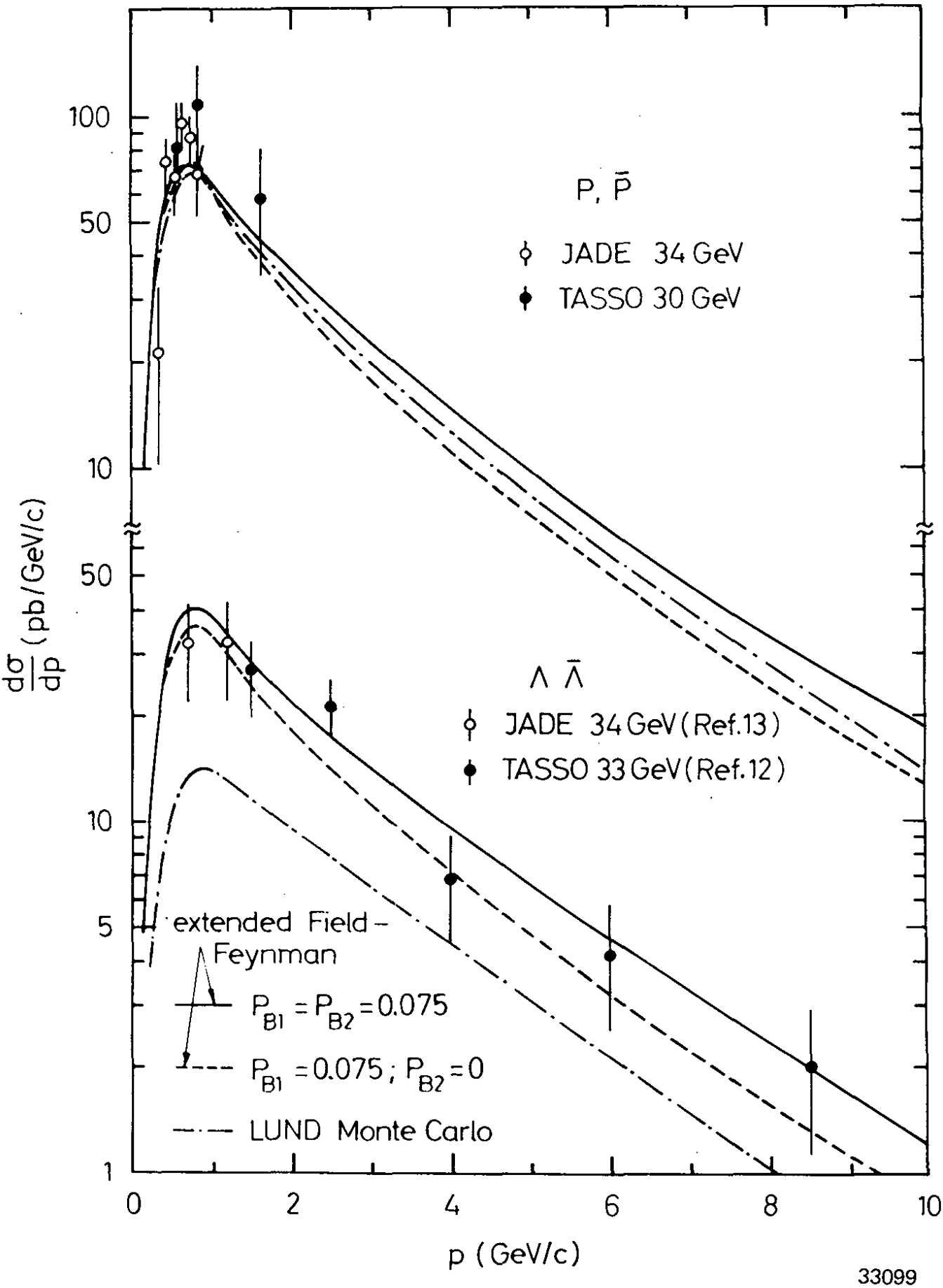

Fig. 76 Inclusive production of $p + \bar{p}$ and $\Lambda + \bar{\Lambda}$ at W = 30 - 34 GeV. The solid and dashed curves show the prediction of the model by Meyer. The dashed-dotted curves show the prediction of the Lund model. From S.L.Wu (1981).

In conclusion, the question asked at the beginning on how baryons are formed, is still open. It remains to be seen whether the diquark concept can be substantiated by other data. A far less exciting alternative is to assume that a quark pulls only $q\bar{q}$ states out of the vacuum; however, quarks and antiquarks from several of the fragmentation steps are so close in phase space that they rearrange into mesons or baryons in a statistical manner.

7.7 Gluon fragmentation

Three-jet events interpreted as hard-gluon bremsstrahlung offer the possibility to compare directly quark and gluon fragmentation. It is generally expected that gluon jets will yield a higher multiplicity and a softer hadron spectrum as well as larger jet cone angles than quark jets of the same characteristic momentum (see e.d. Konishi et al. 1979). The reason is the larger colour charge of gluons which leads to a larger parton multiplicity in their evolution.

In gluon bremsstrahlung ($e^+e^- \to q\bar{q}g$) the gluon has on average, a lower energy than quark or antiquark. However, in practice the identification of the gluon amongst the three jets sofar has been possible on a statistical basis only. An attempt to compare gluon and quark fragmentation has been presented by the JADE group (Bartel et al.1981). In planar events the slim jet (q) and the two subjets which together form the broad jet were identified. The subjet with the smaller angle relative to the slim jet was called the "gluon" jet (g), the other the "quark" jet (q). Monte Carlo studies indicated that in 50% of the events the gluon is correctly identified. The particle yield is plotted in Fig. 77 as a function of the fractional angle Θ/Θ_{max} between the particle and the q direction (a) for the region between q and $\bar{q}$ and (b) between q and g. One finds that in the center region, $\Theta/\Theta_{max} \approx 0.5$, the particle angular density in the region between q and g is considerably larger than between q and $\bar{q}$. It is unclear whether this difference is due to higher order effects in QCD or whether it indicates a difference between quark and gluon fragmentation. The string model approach to $q\bar{q}g$ has predicted such a difference (Andersson et al. 1980).

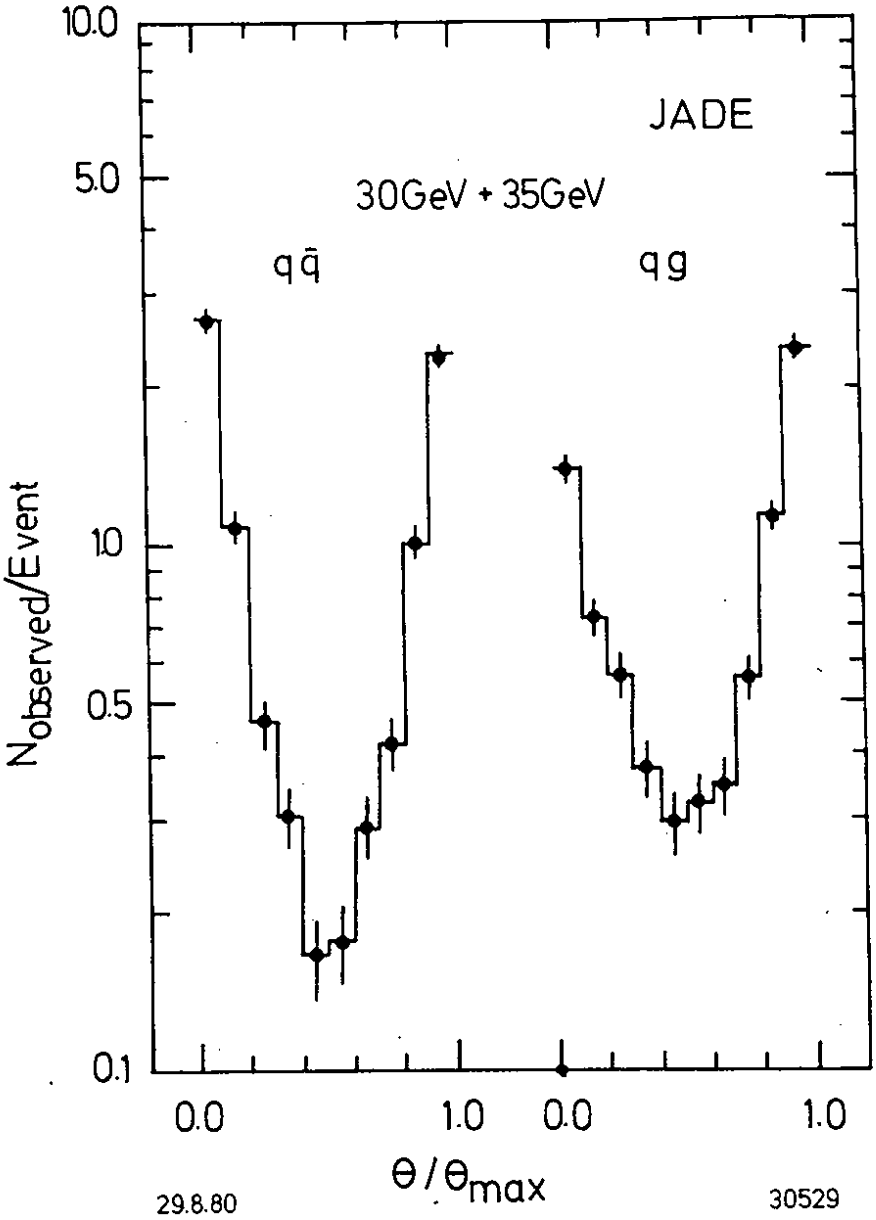

Fig. 77 Angular distribution Θ/Θ_{max} of particles in the $q\bar{q}$ and qg regions (defined in the text) as measured by the JADE group at W = 30 - 35 GeV.

Acknowledgements

It is a pleasure to acknowledge the stimulating atmosphere provided by the organizers of the schools, in particular by Profs. D. Speiser, J. Weyers and M. Nikolic. I have profitted from many discussions with my colleagues from TASSO, in particular Dr. W. Koch, and Profs. P. Söding and S.L.Wu. I am very grateful to Mrs. E. Hell for her special efforts to get the manuscript ready and to Mrs. H. Siegner for her help with the drawings.

LITERATURE CITED

Ali, A. et al. 1979. Z. Physik C2:33; Phys. Lett. 83B:375

Ali, A. et al. 1980. Phys. Lett. 93B:155; Nucl. Phys. B168:409

Ali, A. et al. 1981. DESY Report 81/59

Andersson, B., Gustafson, G., Sjöstrand, T. 1980. Phys. Lett. 94B:211 and references quoted therein

Andersson, B., Gustafson, G., Sjöstrand, T. 1981. Lund Report TP 81-3, TP 81-6, TP 81-7

Aubert, J. J. et al. 1981. Phys. Lett. 103B:388

Barber, D. P. et al. 1979. Phys. Rev. Lett. 43:830

Barber, D. P. et al. 1980a. MIT Report LNS 113

Barber, D. P. et al. 1981a. Phys. Rev. Lett. 46:1663

Barber, D. P. et al. 1981b. MIT LNS Report 115

Bartel, W. et al. 1980a. Z. Phys. C6:295

Bartel, W. et al. 1980b. Phys. Lett. 91B:142

Bartel, W. et al. 1981a. DESY Report 81/72

Bartel, W. et al. 1981b. Phys. Lett. 101B:361

Bartel, W. et al. 1981c. Phys. Lett. 104B:325

Bartel, W. et al. 1981d. Phys. Lett.

Behrend, H.-J. et al. 1981. DESY-Report 81/80

Berends, F., Kleiss, R. 1981. Nucl. Phys. 178:141

Berends, F., Gaemers, K. F. J., Gastmans, R. 1973. Nucl. Phys. B63:381

Berger, Ch. et al. 1979. Phys. Lett. 86B:418

Berger, Ch. et al. 1980a. DESY Report 80/117

Berger, Ch. et al. 1980b. Phys. Lett. 97B:459

Berger, Ch. et al. 1981a. Phys. Lett. 99B:489

Berger, Ch. et al.1981b. DESY Report 81/54

Berger, Ch. et al. 1981c. Phys. Lett. 104B:79

Berger, Ch. 1981. EPS Int. Conf. on High Energy Physics, Lisbon

Bjorken, J. D., Brodsky, S. J. 1970. Phys. Rev. D1:1416

Bjorken, J. D., Llewellyn Smith, Ch. 1973. Phys. Rev. D7:887

Bletzacker, F., Nieh, H. T. 1977. Phys. Rev. D16:2115

Bowler, M. 1981. Oxford Univ. Report 76-81

Brandelik, R. et al. 1979. Phys. Lett. 86B:243

Brandelik, R. et al. 1979.Nucl. Phys. B148:189

Brandelik, R. et al. 1980a. Phys. Lett. 92B:199

Brandelik, R. et al. 1980b. Phys. Lett. 94B:437

Brandelik, R. et al. 1980c. Phys. Lett. 97B:453

Brandelik, R. et al. 1980d. Phys. Lett. 94B:444

Brandelik, R. et al. 1980e. Phys. Lett. 94B:91

Brandelik, R. et al. 1981a. Phys. Lett. 99B:163

Brandelik, R. et al. 1981b. Phys. Lett. 100B:357

Brandelik, R. et al. 1981c. DESY Report

Brandelik, R. et al. 1981d. DESY Report

Brandelik, R. et al. 1981e. DESY Report 81/69

Brandelik, R. et al. 1981f. Phys. Lett. 105:75

Brandt, S. et al. 1964. Phys. Lett. 12:57

Brandt, S. 1979. Proc. Int. Conf. High Energy Physics, Geneva, p. 338

Branson, J. G. 1981. Int. Symp. on Lepton and Photon Interactions at High Energies, Bonn
and DESY Report 81/73

Braunschweig, W. 1981. Int. Symp. on Lepton and Photon Interactions at High Energies, Bonn

Bürger, J. 1981. Int. Symp. on Lepton and Photon Interactions at High Energies, Bonn

Buras, A. J. 1981. Int. Symp. on Leptons and Photon Interactions at High Energies, Bonn
and Fermilab Report 81/69

Casher, A., Neuberger, H. Nussinov, S. 1979. Phys. Rev. D20:179

Celmaster, W., Gonsalves, R. J. 1979. Phys. Rev. Lett. 44:560

Chetyrkin, K. G., Kataev, A. L., Tkachev, F. V. 1979. Phys. Lett. 85B:277

Cords, D. 1980. Proc. XXth Int. Conf. on High Energy Physics, Madison, Wisc.; DESY Report 80/92

Criegee, L., Knies, G. 1981. DESY Report 81/44 and Physics Reports

de Grand, T. A., Ng, Y. G., Tye, S. H. H. 1977. Phys. Rev. D16:3251

Dine, M., Sapirstein, J. 1979. Phys. Rev. Lett. 43:668

Dittmann, P., Hepp, V. 1981. Z. Physik. C10:283

Drell, S. D., Levy, D., Yan, T. M. 1969. Phys. Rev. 187:2159; 1970 Phys. Rev. D1:1035:1617:2402

Drijard, D. et al.1979. Nucl. Phys. B155:269; 1980 Nucl. Phys. B166:233

Duinker, P. 1981. Int. Conf. on High Energy Physics, Lisbon

Eidelman, S. I., Kurdadze, L. M., Vainstein, A. I. 1979. Phys. Lett. 82B:278

Ellis, J., Gaillard, M. K., Ross, G. G. 1976. Nucl. Phys. B111:253; (E.B130:516)

Ellis, J. 1980. private communication

Ellis, R. K., Ross, D. A., Terrano, A. E. 1980. Phys. Rev. Lett. 45:1226; 1981. Nucl. Phys. B178:421

Fabricius, K. et al. 1980 Phys. Lett. 97B:431; DESY Report 81/35

Fahri, E. 1977. Phys. Rev. Lett. 39:1587

Farrar, G. 1978. Proc. Int. School of Subnuclear Physics, Erice

Farrar, G., Fayet, P. 1980. Phys.Lett. 89B:191

Fayet, P., Ferrara, S. 1977. Phys. Reports 32C:249

Felst, R. 1981. Int. Symp. on Lepton and Photon Interactions at High Energies, Bonn

Field, R. D., Feynman, R. P. 1978. Nucl. Phys. B136:1

Fournier, D. 1981. Int. Symp. on Lepton and Photon Interactions at High Energies, Bonn

Fritzsch, H., Gell-Mann, M. 1972. Proc. XVI Int. Conf. on High Energy Physics, Chicago, Vol. 2, p. 135

Fritzsch, H., Gell-Mann, M., Leutwyler, H. 1973. Phys. Lett. 47B:365

Furmanski, W., Petronzio, R., Pokorski, S. 1979. Nucl. Phys. B155:253

Gatto, R., Menotti, P., Vendramin, I. 1972. Nuovo Cim. Lett. 4:79

Gatto, R., Preparata, G. 1972. Nucl. Phys. B47:313

Georgi, H., Politzer, H. D. 1974. Phys. Rev. D9:416

Giacomelli, G., Jacob, M. 1979. Physics Reports 55:1

Glashow, S. L. 1961. Nucl. Phys. 22:579; 1980. Rev. Mod. Phys. 52:539

Gol'fan, Yu. A., Likhtman, E. P. 1971. JETP Letters 13:323

Gribov, V. N., Lipatov, L. N. 1971. Phys. Lett. 37B:78

Gross, D. J., Wilczek, F. 1973. Phys. Rev. Lett. 30:1343;
Phys. Rev. D8:3633; also 1974. Phys. Rev. D9:980

Hanson, G. G. et al. 1975. Phys. Rev. Lett. 35:1609

Harari, H. 1977. Weizmann Inst. Report WIS 77/56
and 1978. Physics Reports 42:235

Hofmann, W. 1981. Z. Physik C10:351

Holder, M. 1981. Int. Conf. on High Energy Physics, Lisbon

Hollebeek, R. J. 1981. Int. Symp. on Lepton and Photon Interactions at High Energies, Bonn

Hoyer, P. et al. 1979. Nucl. Phys. B161:349

Ilgenfritz, E. M., Kripfganz, J., Schiller, A. 1978. Acta Phys. Pol. B9:881

Kichimi et al. 1979.

Koba, Z., Nielsen, H. B. Olesen, P. 1972. Nucl. Phys. B40:317

Kobayashi, M., Maskawa, T. 1973. Progr. Theor. Phys. 49:652

Kogut, J. B., Susskind, L. 1974. Phys. Rev. D9:697; D9:3391

Kramer, G., Schierholz, G., Willrodt, J. 1978. Phys. Lett. 79B:249

Kramer, G., Schierholz, G. 1979. Phys. Lett. 82B:102

Kramer, G., Schierholz, G., Willrodt, J. 1980. Z. Physik C4:149

Litke, A. 1981. Int. Symp. on Lepton and Photon Interactions at High Energies, Bonn

Marshall, R. 1981. EPS Int. Conf. on High Energy Physics, Lisbon

Meyer, T. 1981. DESY Report 81-46

Nambu, Y. 1966. Preludes in Theoretical Physics (Amsterdam), p. 133

Niczyporuk, B. et al. 1981. DESY Report 81/008

Pati, J. C., Salam, A. 1978. Nucl. Phys. B144:445

Polyakov, A. M. 1975. Proc. 7th Int. Symp. Lepton and Photon Interactions at High Energies, Stanford, p. 855

Preparata, G. 1981. Univ. of Bari Report GT:81-13

Renard, F. 1981. Basics of Electron - Positron Collisions, Editions Frontières, Vol. 32

Ritter, S., Ranft, J. 1980. Acta Phys. Pol. B11:259

Salam, A. 1962. Phys. Rev. 127:331; 1980 Rev. Mod. Phys. 52:525

Scharre, S. 1981. Berkely Report LBL-13018

Schierholz, G. Teper, M. 1981. DESY Report 81/41

Schwitters, R. F. et al. 1975. Phys. Rev. Lett. 35:1320

Söding, P. Wolf, G. 1981. DESY Report 81/13 and Ann. Rev. Nucl. Sci. Vol 31

Söding, P. 1981. DESY Report 81/70

Spitzer, H. 1980. Proc. 15th Rencontre de Moriond, 1980, Vol.II, p. 157 and DESY Report 80/43

Sterman, E. Weinberg, S. 1977. Phys. Rev. Lett. 39:1436

Vermaseren, J. A. M., Gaemers, K. J. F., Oldham, S. J.1981. Nucl. Phys. B187:301

Walsh, T. F., Zerwas, P. M. 1980 Phys. Lett. 93B:53

Wedemeyer, R. 1981 Int. Symp. on Lepton and Photon Interactions at High Energies, Bonn

Weinberg, S. 1967. Phys. Rev. Lett. 19:1264; 1980. Rev. Mod. Phys. 52:515

Weinberg, S. 1973. Phys. Rev. Lett. 31:494

Weiss, J. M. et al. 1981. Phys. Lett. 101B:439

Wess, J., Zumino, B. 1974. Nucl. Phys. B70:39

Wiik, B. H., Wolf, G. 1979. Electron-Positron Interactions, Springer Tracts in Modern Physics, Vol. 86

Wolf, G. 1980. DESY Report 80/13

Woodworth, Ph. 1981. EPS Int. Conf. High Energy Physics, Lisbon

Wu, S.L. DESY-Report 81/71

Yamada, S. 1980. Proc. XX Int. Conf. on High Energy Physics, Madison, Wisconsin; Univ. Tokyo Rep.